Analysis of undrained soil behaviour of Dutch organic clay in K_0-consolidated triaxial tests

MSc thesis Applied Earth Sciences

T.G. Wegman

Witteveen+Bos
TU Delft Delft University of Technology
Deltares Enabling Delta Life

Analysis of undrained soil behaviour of Dutch organic clay in K_0-consolidated triaxial tests

MSc thesis Applied Earth Sciences

T.G. Wegman

Student number: 4304721

Thesis committee:

Dr. Ir. P. J. Vardon,	TU Delft, chair of thesis committee
Ir. H. J. Lengkeek,	Witteveen+Bos/TU Delft
Dr. Ir. C. Zwanenburg,	Deltares/TU Delft
Ir. K. Reinders,	TU Delft

Witteveen + Bos

TU Delft Delft University of Technology

Deltares Enabling Delta Life

Abstract

In 2017 new guidelines concerning macro stability calculations were implemented by the Dutch Ministry of Infrastructure and Environment. These guidelines are formulated in “Wettelijk Beoordelingsinstrumentarium” (WBI). The largest difference with the previous version of the guidelines concerns the material model that is prescribed to determine shear strength parameters. In triaxial tests shear strength parameters are to be determined at ultimate state (25% axial strain), which is assumed to be a good representation of critical state. Critical state is a concept from Critical State Soil Mechanics (CSSM) and assumed to be a good representation of the state reached after large deformations induced by macro instability. Another fundamental assumption in the WBI is the use of the SHANSEP method. This method encompasses a laboratory procedure and a normalisation method. CSSM was originally defined and elaborated under isotropic stress conditions while in engineering practice anisotropic conditions are mostly used.

The goal of this thesis is to investigate the undrained soil behaviour of organic clay in triaxial tests following the SHANSEP procedure and compare the results to the CSSM framework. In order to do so a series of eight K_0-consolidated triaxial tests is executed using silty organic Oostvaarders plassen clay, which is assumed to be representative for a typical Dutch soil. A large range of over consolidation ratios is applied (1-20). Both compression and extension tests are executed. The triaxial tests are complemented by two K_0-CRS tests and an isotropic compression test to determine relevant soil properties. The results are compared to the CSSM. The qualitative soil behaviour is analysed as well as the actual predicted undrained shear strength S_u. Parameter relationships as described by CSSM are tried to be established from the data. The undrained shear strength is predicted by using numerical and analytical formulations of the Modified Cam Clay model, which is the most basic implementation of CSSM.

From the data a clear failure line could be determined in $p' - q$ space. In the triaxial compression tests failure at ultimate state gave very consistent result, a failure line could precisely be determined. In extension failure at peak strength showed the most consistent results. Ultimate state could not be reached under representative stresses because the formation of large shear bands and necking during shearing. A unique $p' - e$ relation was much harder to establish. The general trend as described by the CSSM was clearly visible but the uncertainty was rather large. Several factors contributed to the uncertainty. Among which the void ratio determination method that was used to determine the void ratio after the triaxial test, which is prone to errors. The MCC model was not able to model the stress path correctly and p' at failure was not correctly predicted resulting in incorrect S_u prediction. The MCC model overestimated S_u in compression tests. In extension, however, S_u is well predicted by the MCC model. The SHANSEP method turned out to be a very convenient way to normalise the undrained shear strength of the triaxial tests, both in compression and extension. Only at very large OCR S_u/σ'_{v0} is slightly overestimated.

Preface

This thesis forms the fulfilment of my university education and the end of my time as a student in Delft. During my bachelor Applied Earth Sciences I developed a rather broad basis of knowledge and insights to eventually continue with a masters programme in Geo-Engineering. During the masters programme I deepened my knowledge, I hope to continue this trend during my professional career.
I would like to thank all the supervisors that guided me through the completion of this thesis. First of all Dr. ir. Phil Vardon as the chair of the thesis committee. Phil's sharp comments and feedback were always very to the point. I would also like to thank ir. Arny Lengkeek for forming the link between Witteveen+Bos and me and arranging a working place at the Rotterdam office. Arny's enthusiastic attitude towards basically any progress that I showed formed a great motivation. I would also like to express my gratitude to Dr. ir. Cor Zwanenburg. First of all Cor made it possible to do laboratory tests at Deltares on which this thesis is based. Cor's knowledge on the topic is incredible, I could always ask for help, input or advice.Furthermore Cor really took time to read my preliminary reports in detail to give elaborate feedback on the contents as well as on readability and writing. The last supervisor I would like to thank is ir. Kristina Reinders for complementing the thesis committee on such short notice.

Besides the supervisors I would also like to thank the laboratory staff at the geotechnical laboratory of Deltares. In particular Max Zuidhoek, as triaxial test specialist Max executed the triaxial tests. I could always discuss and ask for advice on certain matters. Max really showed to be interessted in the topic as well.

My colleagues, both fellow students and employees, at Witteveen+Bos made life a bit more pleasant during my thesis. The lunch break walks were always a highlight of the working day. I would like to thank them for that.

Last but not least I would like to thank my brother Rik. We could always discuss about anything. Particularly complaining to each other about our theses and relating matters, often was a great release.

Tiemen Wegman
Delft, January 2020

Contents

Nomenclature

Abbreviations

CSL	Critical State Line
CSSM	Critical State Soil Mechanics
DSS	Direct Simple Shear
ESP	Effective Stress Path
FEM	Finite Element Method
K_0-CL	K_0-Consolidation Line
LEM	Limit Equilibrium Method
MCC	Modified Cam Clay
NC	Normally Consolidated
NCL	Normal Consolidation Line
OC	Over consolidated
OCR	Over Consolidation Ratio
POV(M)	Project Overstijgende Verkenning (Macrostabiliteit)
SHANSEP	Stress History And Normalized Soil Engineering Properties
TRX	Triaxial
TSP	Total Stress Path
WBI	Wettelijk Beoordelings Instrumentarium

Symbols

C_c	Compression index [e /log(σ'_v)]
C_r	Unload/Reload index [e /log(σ'_v)]
CR	Compression index [ϵ/log(σ'_v)]
RR	Unload/Reload index [ϵ/log(σ'_v)]
λ	Compression index [e/ln(p')]
κ	Unload/Reload index [e/ln(p')]
Δu	Excess pore pressure [kPa]
e	Void ratio [-]
ϵ	Strain [-]
Γ	Intersection between CSL and p'-axis in $p' - v$-space
K	Horizontal to vertical stress ratio [-]
Λ	Plastic volumetrix strain ratio [-]
m	Strength increase exponent [-]
M_c	Slope of failure line in $p' - q$-space in compression
M_e	Slope of failure line in $p' - q$-space in extension
N	Intersection between NCL and p'-axis in $p' - v$-space
N_0	Intersection between K_0-CL and p'-axis in $p' - v$-space
ν	Poisson's ratio [-]
p	Mean stress [kPa]
ϕ	Friction angle [°]
q	Deviator stress [kPa]
R_0	Over consolidation ratio in terms of p' [-]
r	Spacing ratio [-]
S	S_u/σ'_{v0} under normally consolidated conditions [-]
S_u	Undrained shear strength [-]
σ	Stress [kPa]
v	Specific volume [-]

Subscripts

$_0$	Initial i.e. at start of test or at start of shearing
$_c$	Pre-consolidation i.e. maximum stress that is reached
$_f$	At failure
$_h$	Horizontal component
$_{ie}$	Isotropic equivalent
$_{ur}$	Unload/Reload
$_v$	Vertical component

Superscripts

$'$	Effective

1

Introduction

The Netherlands has a rich history in the field of water defences. Throughout the years the Dutch became specialists in building dikes and other water defences. In the realm of dikes in the Netherlands much is going on recently. Guidelines need to be adapted to rising seawater levels, more intense storms and other consequences of climate change. In 2017 a new standard has been implemented by the Dutch Ministry of Infrastructure and Environment, which all Dutch dikes have to meet. The approach has been shifted from a design based on the probability of occurrence of normative conditions, i.e. water levels and wave heights during a severe storm, towards risk of flooding, thus including the consequences, of the hinterland instead. As a result an expected 1900 km of the 3500 km of primary flood defences in The Netherlands has to be reinforced during the coming years [25]. In the Netherlands several failure mechanisms are assessed, among which macro stability. Macro (in)stability entails formation of a usually circular slip plane along which the dike body (partly) slides down. Traditionally macro-stability is assured by applying new earth materials at the toe of the existing dike. The Netherlands is, however, a densely populated country, therefore in many places there is not sufficient space to accommodate traditional dike enforcement. In the framework of “projectoverstijgende verkenning macrostabiliteit” (POVM) new techniques are developed to make dike reinforcement better, faster and cheaper [25]. One of the techniques that is investigated is the installation of structural elements, such as sheet piles, in the dike. Conventional Limit Equilibrium Methods (LEM) that are used to assess the strength of dikes are not able to integrate structural elements in the calculation accurately. LEM neither are capable of computing deformations in the dike, which are important for the determination of stresses that act on the sheet piles. Instead Finite Element Methods (FEM) are more suitable. Key in a realistic representation of the soil behaviour and thus undrained shear strength determination, is the underlying constitutive soil model that is implemented in the FEM analysis. Consensus about the importance of undrained shear strength of poorly permeable soil layers in macro stability assessment prevails among researchers and engineers. Also the guidelines, formulated in the "Wettelijk beoordelingsinstrumentarium" (WBI)[16], aligns with that idea and has been altered accordingly. This means that Critical State Soil Mechanics (CSSM) has to be used in the assessment of the macro stability of a dike, in the new standard. Another fundamental assumption in the WBI is the use of the SHANSEP method, as explained by Ladd and Foott [14].

1.1. Problem statement

The WBI 2017 prescribes a different material model for the description of soil behaviour compared to the previous version. The WBI prescribes the CSSM theory or framework for the determination of strength parameters from the laboratory data and description of the material behaviour of the soil. Ultimate state is assumed to be a good approximation of critical state, the WBI therefor prescribes strength parameter determination at ultimate state. CSSM is originally defined under isotropic stress conditions. Besides a new material model ,the WBI does also prescribe the use of the SHANSEP method. The SHANSEP method is a normalisation method to normalise the undrained shear strength and schematise the S_u profile of soil bodies. The SHANSEP method also includes a laboratory procedure for assessment of undrained shear strength. The SHANSEP method prescribes anisotropic consolida-

tions and generally the vertical effective stress σ'_v is used as state parameter. Anisotropic conditions are a realistic representation of real soil conditions and does connect well to the daily engineering practice. The SHANSEP procedure and CSSM framework are both prescribed for an undrained strength assessment, according to the WBI. There is a difference in underlying theoretical and experimental basis which can cause incorrect interpretation and calculation of undrained shear strength.

1.2. Objective and research questions

The main purpose of this thesis is formulated in the following objective:

Investigate undrained material behaviour of Dutch organic clay in triaxial tests following the SHANSEP procedure as prescribed in the WBI and compare to the CSSM framework.

The process to reach this objective is guided by the following research questions:

1. How well does CSSM describe the undrained soil behaviour in anisotropically consolidated triaxial tests?
2. How well does the triaxial test data fit in the SHANSEP equation?
3. Can isotropic and anisotropic unload/reload soil parameters be recalculated from each other correctly?
4. What is the definition of undrained shear strength according to different theories and how do these definitions fit in the CSSM framework?
5. What is the difference in undrained shear strength s_u between isotropically and K_0-consolidated triaxial tests in numerical simulations of the Modified Cam Clay model?

Secondary objectives that arose during the planning and execution of the laboratory work is to find out the maximum consolidation rate without failing the sample before reaching the desired pre-consolidation pressure. Besides that the effect of sampling direction on the soil behaviour of remoulded clay is investigated. Additional benefit of the execution of the laboratory work is extension of the database that is available within the POVM framework.

1.3. Methodology

Large part of this thesis consists of laboratory work and analysis and interpretation of the data. A series of eight triaxial tests is executed complemented by two K_0-CRS tests and an isotropic consolidation test. The tests are performed in the laboratory of Deltares in Delft on reconstituted Oostvaardersplassen (OVP) clay. The SHANSEP procedure is followed as prescribed by the WBI. Which means application of anisotropic consolidation untill a predefined consolidation pressure well over the in-situ consolidation pressure. Resulting in different precisely determined consolidation pressures and over consolidation ratios. The triaxial test data is placed in the CSSM framework, i.e. an analysis of the qualitative behaviour and analysis of the undrained shear strength predicted by the Modified Cam-Clay model. The Modified Cam-Clay model is used because it is assumed to be the most basic and common application of CSSM. Analytical equations derived from the Modified Cam-Clay model are used to compute undrained shear strength. Complementary, the parameters that are found are be used in Plaxis software to run single element analyses. Besides CSSM the data is compared to the SHANSEP equation as well. Results of earlier tests on OVP clay are looked into and form a reference of the gathered laboratory data.

1.4. Scope

CSSM is a very broad concept that covers a wide range of soil behaviour for different engineering applications. The fundamentals are described by several relationships linking stress state and void ratio. A very large number of new relationships can be derived from these original relationships. To limit the scope of this thesis a limited number of relationships are investigated in this thesis. These relationships are outlined in the theoretical background. This thesis focuses on macro stability for which undrained

shear strength s_u is the most important characteristic. Soil however exhibits strength anisotropy which means that s_u also depends on the loading conditions. To cover the full range of undrained shear strength values of a soil, triaxial tests in compression and extension as well as direct simple shear (DSS) tests are necessary. Within the scope of this thesis only triaxial tests are conducted. Soil behaviour in laboratory testing is always subject to boundary conditions induced by the test that influence the soil behaviour. To eliminate the boundary effects as much as possible, the effects are identified, described and eventually corrected for.

2

Theoretical Background

This chapter explains the theoretical background of this thesis. In order to understand the research a general explanation of macro stability evaluation and the current practice concerning macro stability is given. Throughout the chapter more detail and explanation of soil behaviour and the CSSM and SHANSEP theory is provided.

2.1. Macro (in)stability

Macro stability is resistance of a dike against sliding of dike material causing a (partial) loss of the water retaining function of the dike. A schematisation of this failure mechanism is shown in Figure 2.1. Instability can occur due to differences in pore pressure and thus in effective stresses in the soil which in turn effects the shear strength of the soil. pore pressure differences can be the result of water level fluctuations or (extreme) precipitation. Macrostability can occur both inwards towards the hinterland as well as outwards towards the water body. Outwards macro instability is often the result of a rapid draw-down of the water body. Undrained shear strength determined at critical state is a good measure of mobilised resistance against sliding along the sliding plane, according to international literature [26]. Hence it is adopted in guidelines of assessment of particularly dike stability.

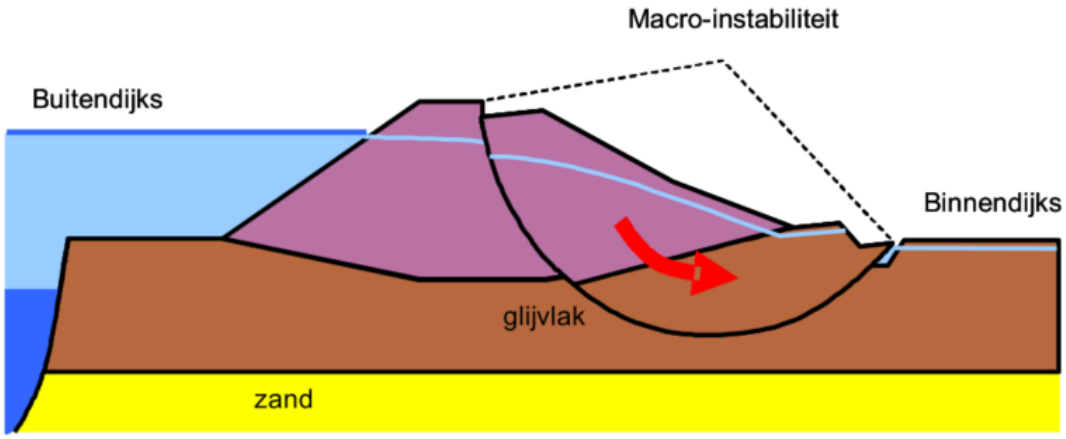

Figure 2.1: Schematisation of macro instability (from [16])

Many methods have been developed throughout the years to assess macro stability. Several analytic Limit Equilibrium Methods are available such as: Bischip, LiftVan and Spencer-Van der Meij. These calculations are basically equilibrium models where driving forces and resisting forces are analysed on an assumed sliding plane. Often a factor of safety is determined which is defined as follows:

$$FoS = \frac{resisting\ forces}{driving\ forces} \tag{2.1}$$

Recent developments in dike designs in the Netherlands cause a growing demand for Finite Element Methods. Because of limited space availability in The Netherlands alternatives to traditional dike reinforcement, which is application of more dike material, have to be found. Experiments using structural elements, e.g. sheet piles, in dike design are being investigated. LEM's are however not suitable for stability calculation including sheet piles. FEM's are suitable when using the right underlying constitutive model appropriate for the soil conditions.

2.2. Current practice

As mentioned before new guidelines have been implemented concerning water safety of the Netherlands, in 2017. The design of flood defences used to be based on the probability of occurrence of normative conditions, i.e. it should be able to withstand a storm that statistically occurs once every several thousand years. The approach has been shifted towards a design based on the risk of flooding of the hinterland instead, thus including the consequences of flooding. Design and engineering methods as well as safety factors and parameter values are documented in the "Wettelijk beoordelingsinstrumentarium" (WBI) provided by the ministry of infrastructure and environment. Every aspect of flood protection is covered in a separate section of the WBI. In this thesis there is focused on the dike failure mechanism macro(in)stability, which is documented in "Schematiseringshandleiding macrostabiliteit" [16]. A major difference compared to previous versions of the WBI is the differentiation between drained and undrained analysis. Two fundamental ideas that are adopted in the guidelines are investigated in this thesis. The application of the Critical State Soil Mechanics (CSSM) model and SHANSEP (Stress History And Normalised Soil Engineering Properties) method for characterisation of soil behaviour. Another point that is adopted is the definition of strength of the soil. Instead of strength at small strain (2 tot 5% axial strain in triaxial testing) now ultimate state strength has to be used for calculations. For clay samples ultimate state is 25% axial strain in a triaxial test. For peat ultimate state is defined at 40% strain in a DSS test. Ultimate state is assumed to be equal to critical state. Undrained shear strength at critical state is assumed to be a good measure of the average mobilised shear strength mobilised along a slip surface. Also guidelines regarding laboratory testing are provided in the WBI. In the CSSM framework a differentiation between drained and undrained conditions has been distinguished. Drained conditions occur in soil layers with a large permeability in comparison to the deformation rate. Excess pore pressures are not developed and the shear strength of the soil only depends on the friction angle of the soil. Undrained shear strength is however a complex phenomenon. Due to low permeability excess pore pressures develop upon loading and completely different soil behaviour is observed. Undrained shear strength is not a soil parameter, S_u depends on several factors such as the stress history of the soil, friction angle and the current stress conditions.

2.3. Undrained shear strength

The general definition of undrained shear strength is the maximum internal resistance to applied shearing forces under undrained conditions for specific stress conditions and load history. Undrained shear strength of a soil can be determined from e.g. triaxial tests and is defined as one-half of the deviator stress q at failure. Failure can however be interpreted differently, in this thesis the strength is analysed at:

- 25% strain (ultimate state)
- maximum deviator stress (peak strength)
- maximum deviator stress to mean effective stress ratio q/p'

Ultimate state strength is assumed to be a good approximation of critical state and is prescribed by the WBI. According to CSSM theory p', q and e do not change with continuous shearing when critical

state is reached, this is explained more elaborately in Chapter 2.4.S_u at maximum deviator stress, also called peak strength, is the most general and intuitive definition of undrained shear strength. Critical state is rather hard to determine unambiguously. According to the definition as displayed in Section 2.4 is critical state a state in which the soil continuously shears without any change in p', q and e. In order to determine critical state from triaxial data p', q and also for example Δu during shearing can be looked at. Perfect behaviour is however not expected.s_u determined at maximum q/p' ratio gives a better indication of the normalised behaviour of the soil. The deviator stress at maximum q/p' is equal to the deviator stress at maximum σ'_v/σ'_h.

Another factor in determination of s_u of soils is strength anisotropy. Ladd and DeGroot, (2003) show the difference in maximum strength and at which strain level for different test types. This is shown in Figure 2.2. The Figure also shows that the normalised values converge at large strains under plane-strain condtions. As a result of strength anisotropy is S_u of a soil best represented by a combination of several lab test, as Bjerrum illustrated nicely in Figure2.3.

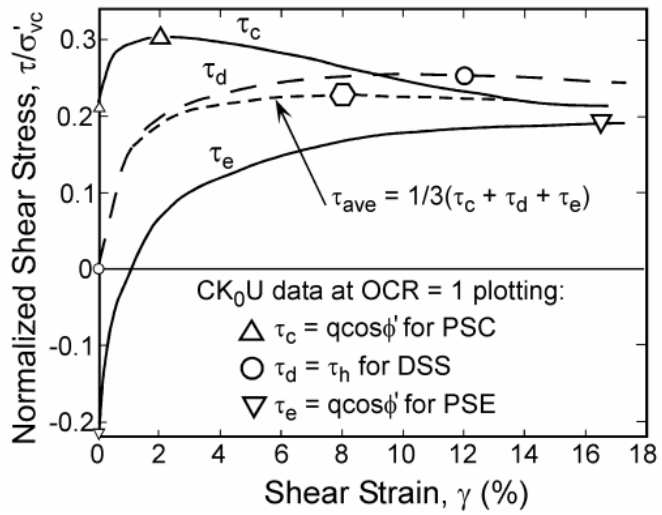

Figure 2.2: Normalised shear stress with increasing strain for plane strain compression(PSC), plane strain extension (PSE) and direct simple shear (DSS)

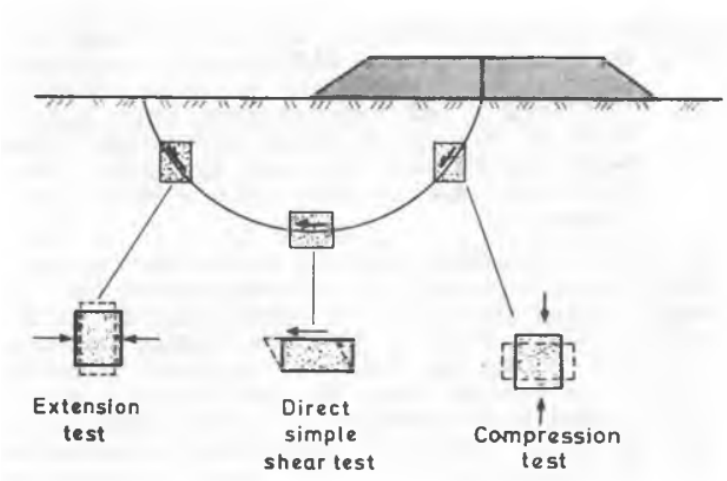

Figure 2.3: Representative lab test for stress situation in an embankment (from [1])

Different types of anisotropy can be observed in natural soils. The most apparent types is the so-called structural anisotropy. Which is caused by the sedimentation process of the soil. Clay particles, for example, are flat platy particles that are mostly deposited in the horizontal plane. It is then to be expected that e.g. the stiffness along the plane differs from the stiffness perpendicular to the plane. Anisotropy can be found in all types of soil properties, such as strength, stiffness and permeability. Peat is another soil type that is prone to anisotropy. The extent of the anisotropy depends on the degree of humification and the amount and dimension of fibres in the organic matter that makes up the fabric of the peat [30]. This also applies to organic matter that is possibly present in clay.Besides anisotropy resulting from the structure and fabric of the soil, anisotropy can be induced by the stress history of the soil. When a soil is loaded asymmetrically, which is call pre-shearing, an anisotropic stiffness develops in the soil.

2.4. Critical State Soil Mechanics

In the 50's of last century developments in lab testing equipment and the results it produced, caused the demand for a more thorough understanding of soil behaviour and hence for new theories and explanation. Material models that were conventionally applied to soil mechanics were not able to explain many features in the material behaviour of soils that was observed in lab tests. Roscoe et al. (1958) wrote the first publication on the critical state concept. A study on the yielding of soils based on extensive soil test data on clay deposited by river Cam. In the years after the Cam-clay model was defined, which was the first implementation of calculations that support the CSSM philosophy. In the years after the model was improved to the Modified Cam-clay model (MCC).The basis of the theory is an observed logarithmic relationship between the change in void ratio e and mean effective stress p'. Instead of void ratio specific volume v is used in the Cam-clay model, v is defined as $1+e$. For primary compression the slope of the line in $p' - e$ space is determined by the isotropic compression index λ. For unloading/reloading the isotropic swelling index κ is used. This is clarified in Figure2.4.

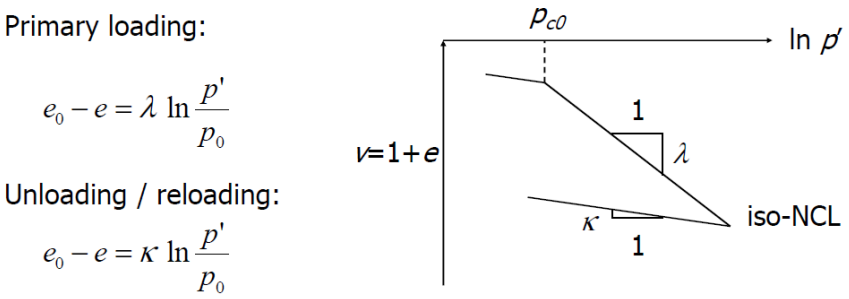

Figure 2.4: p'-v plot of isotropic compression of normally consolidated soil (from [2])

Roscoe and Burland [20] suggested that a soil element undergoing shear eventually reaches a condition, i.e. critical state, in which the soil can continue to deform without further change of void ratio or stress invariants p' and q. Or in other words a state in between dilation and contraction of the soil. This means theoretically that excess pore water pressure does not change anymore when critical state is reached in e.g. laboratory tests. Critical state is synonymous for failure. This can be visualised in by a curved plane in $p' - q - e$ space as shown in Figure 2.6. Where p' is mean effective stress and q is deviatoric stress as defined in Equations 2.4 and 2.5 respectively. Basically the soil starts to flow like a frictional fluid when it reaches critical state. In p'-q space such states are represented by a straight line of equation:

$$q = M \cdot p' \tag{2.2}$$

The critical state line can also be plotted in $p' - v$ space and results in a straight line described by:

$$\nu = \Gamma - \lambda \cdot ln(p') \tag{2.3}$$

Where:

$$p' = \frac{\sigma'_1 + \sigma'_2 + \sigma'_3}{3} = \frac{\sigma'_1 + 2\sigma'_3}{3} \; (\sigma'_2 = \sigma'_3 \; in \; triaxial \; testing) \tag{2.4}$$

$$q = \sigma_1 - \sigma_3 \tag{2.5}$$

$\lambda = compression\ index$

$\Gamma = intersection\ of\ CSL\ with\ v - axis\ in\ p' - v\ space$

$M = slope\ of\ the\ CSL\ in\ p' - q\ space$

The CSL, isotropic compression line and K_0CL consolidation line are shown in Figure2.5. The ICL and and K_0CL are parallel to the CSL when a constant K_0 ratio is applied, and can be described by a similar line. Γ is however replaced by N and N_0 respectively. In [7] a method to relate Γ , N and N_0 is provided that assumes the state boundary surface of the Modified Cam-Clay model. A more detailed description of the MCC model follows in Chapter 2.7.

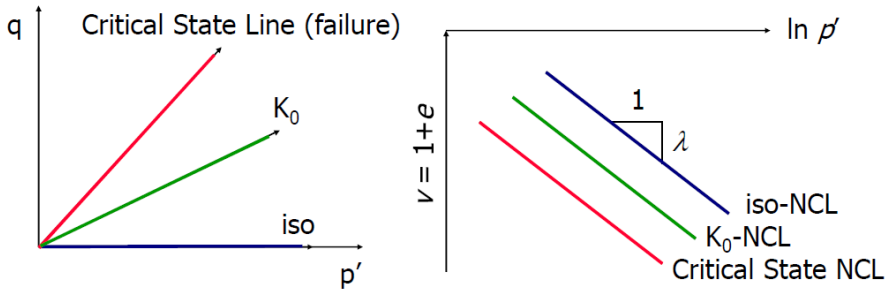

Figure 2.5: CSL, isotropic compression line and K_0 consolidation line shown in p'-q space and p'-v space (from [2])

In 2.5 the unique relationship between p', q and void ratio is represented.

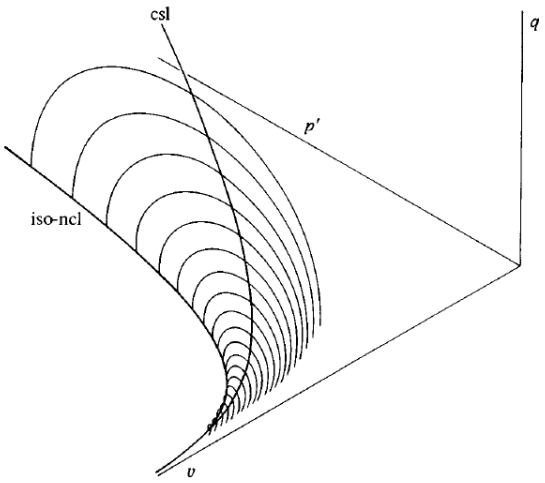

Figure 2.6: Critical state line plotted in p'-q-e space (from [28])

Under undrained conditions the net volume change is zero. Therefore the void ratio cannot change during undrained shearing. This means that during shearing the stress path is represented by a horizontal line in the right image of Figure 2.5. Consequently the following equation is valid:

$$e_f = e_\Gamma - \lambda \cdot ln(p'_f) \tag{2.6}$$

Rearranging Equation 2.6 gives:

$$p'_f = exp(\frac{\Gamma - e_0}{\lambda}) \tag{2.7}$$

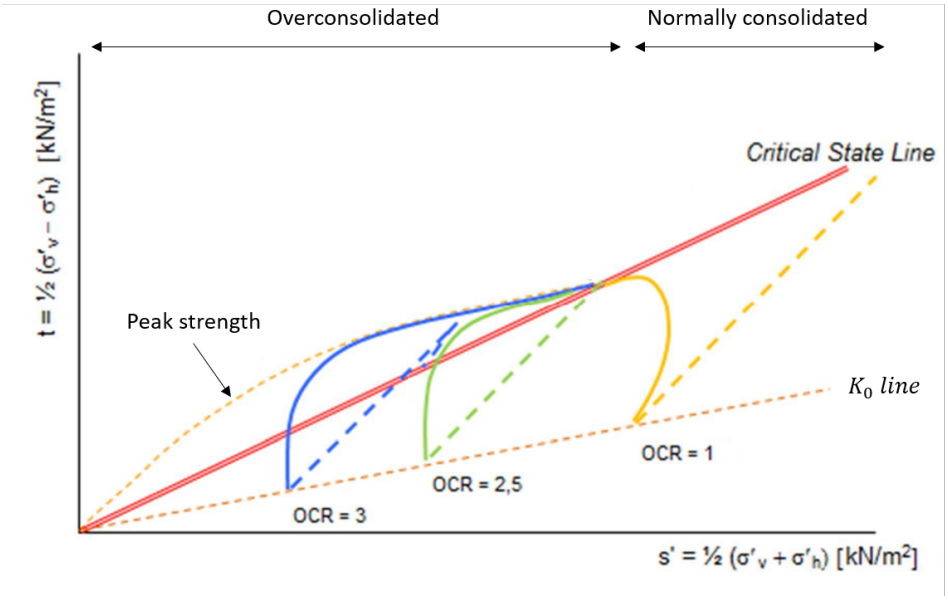

Figure 2.7: Drained and undrained behaviour as defined by CSSM (adapted from [16])

Because $q_f = M \cdot p'_f$:

$$q_f = M \cdot exp(\frac{\Gamma - e_0}{\lambda}) \tag{2.8}$$

Undrained shear strength S_u is defined as one half of the deviator stress at failure. This finally results in the following equation:

$$s_u = \frac{M}{2} \cdot exp(\frac{\Gamma - e_0}{\lambda}) \tag{2.9}$$

Which is only valid for normally consolidated soils [3]. From Equation 2.9 can be concluded that S_u is only dependent of the void ratio at the start of shearing. Parameters M, λ and e_0 are constants for a certain soil.

2.5. CSSM and undrained shear strength

CSSM is assumed to be suitable for (macro) stability analyses of mainly poorly permeable soil layers. Which makes it very applicable to Dutch soil conditions. According to international literature is the critical state strength a good measure of resistance against macro instability of dikes or embankments [26]. The CSSM-framework differentiates between peak and critical state undrained shear strength of the soil and, as mentioned before, between NC and OC soils. In Figure2.7 this is shown in s'-t space. The dashed lines shows the effective stress paths that represent drained behaviour. The solid lines represent undrained behaviour and show completely different stress paths. The stress paths start at a consolidation pressure s' and mobilise a shear strength t. For NC and lightly OC (<1.5) soils show contractive behaviour and is represented by the yellow line. While OC soils show dilatant behaviour and is represented by the blue and green lines. Contraction causes excess pore pressure to occur while dilation causes the opposite, namely underpressure. According to Terzaghi's effective stress principle is the total stress equal to the sum of effective stress and pore pressure[8]. Therefore the pore pressure is represented by the difference in effective (solid lines) and total (dashed line) stresses. As a result of excess pore water pressure the effective stress is lower than the total stress and therefore the mobilised shear strength is limited and much smaller than drained shear strength for the same consolidation pressure. Pore water under-pressure causes a higher effective stress than the total stress. As a result is the mobilised undrained shear strength of an overconsolidated sample larger than the drained shear strength of an equally consolidated sample.

2.6. Yield surface

The yield surface is a general principle to model plasticity and indicate the transition form elastic to plastic behaviour. The yield surface or contour can be visualised in $p' - q$ space as a ellipse in the MCC model. The exact shape is still subject to discussion and differs for different constitutive models. All stress increments in $p' - q$ space that are within the yield surface are considered to cause elastic strains, i.e. fully recoverable strains when the stress is released. When the applied stress path reaches the yield surface, yielding starts. Yielding comprises of a combination of elastic and plastic, i.e. non-recoverable, straining. Failure is eventually reached when the stress path reaches the critical state line (CSL). Failure always occurs after yielding. Yielding can cause the yield surface to expand or to shrink.

Expansion of the yield surface causes strain hardening of the soil which is directly related to contraction of the soil. This occurs when the stress path is located below the CSL i.e. NC soils. When the soil contracts stress increase and pore water is expelled from the soil which makes it appear to be wet. This is why it is called the “wet” side of the diagram. This is shown in Figure2.8.

Shrinkage of the yield surface can also occur: when the stress path reaches the yield surface left of the CSL this results in strain softening which is directly associated with dilation. As a result the deviator stress decreases and the stress path moves downward in the $p' - q$ diagram towards the CSL. The yield surface shrinks following the stress path until failure is reached at the CSL. Dilation causes a stress relieve resulting in a pore volume increase. Consequently water is sucked into the pores which makes the soil appear to be dry. Hence the area above the CSL is called the “dry” side. This is shown in Figure2.9. A more detailed explanation is given below on the basis of two situations from [3]. The shape of the yield surface assumed in the MCC model is an ellipse. The yield surface intersects the M_c-line at one half of the mean effective stress at the pre-consolidation pressure. Indicated by p'_{ie} in Figure2.10. The ratio of p'_{ie} and p' at the top of the yield surface is equal to the spacing ratio r, which is 2 in the MCC model, this is explained in Chapter 2.7.

2.6.1. Undrained Triaxial test on normally consolidated sample

An important assumption is that there are no volume changes under undrained conditions. This results in a horizontal line in graph b as shown in Figure2.8. Instead of volume change pore pressure is generated upon loading. A distinction between total stress path (TSP) and effective stress path (ESP) is made. Within the yield surface, i.e. fully elastic soil response, the ESP forms a straight vertical line. Upon loading the soil wants to contract but this is prevented under undrained conditions. The complete stress increment is carried by the pore water and hence p' does not change. When the ESP reaches the yield contour plastic strains are generated, compaction on the wet side and contraction on the dry side (see Figure2.9). These plastic volumetric strains need to be compensated by elastic straining. According to the elastic part of the model, elastic expansion is associated with a reduction of mean effective stress, which explains why the ESP bends towards the left at the wet side of the CSL. The hardening process continues until the the ESP reaches the CSL. Failure is only reached when the ESP reaches the CSL, failure is thus independent of the TSP in undrained conditions.

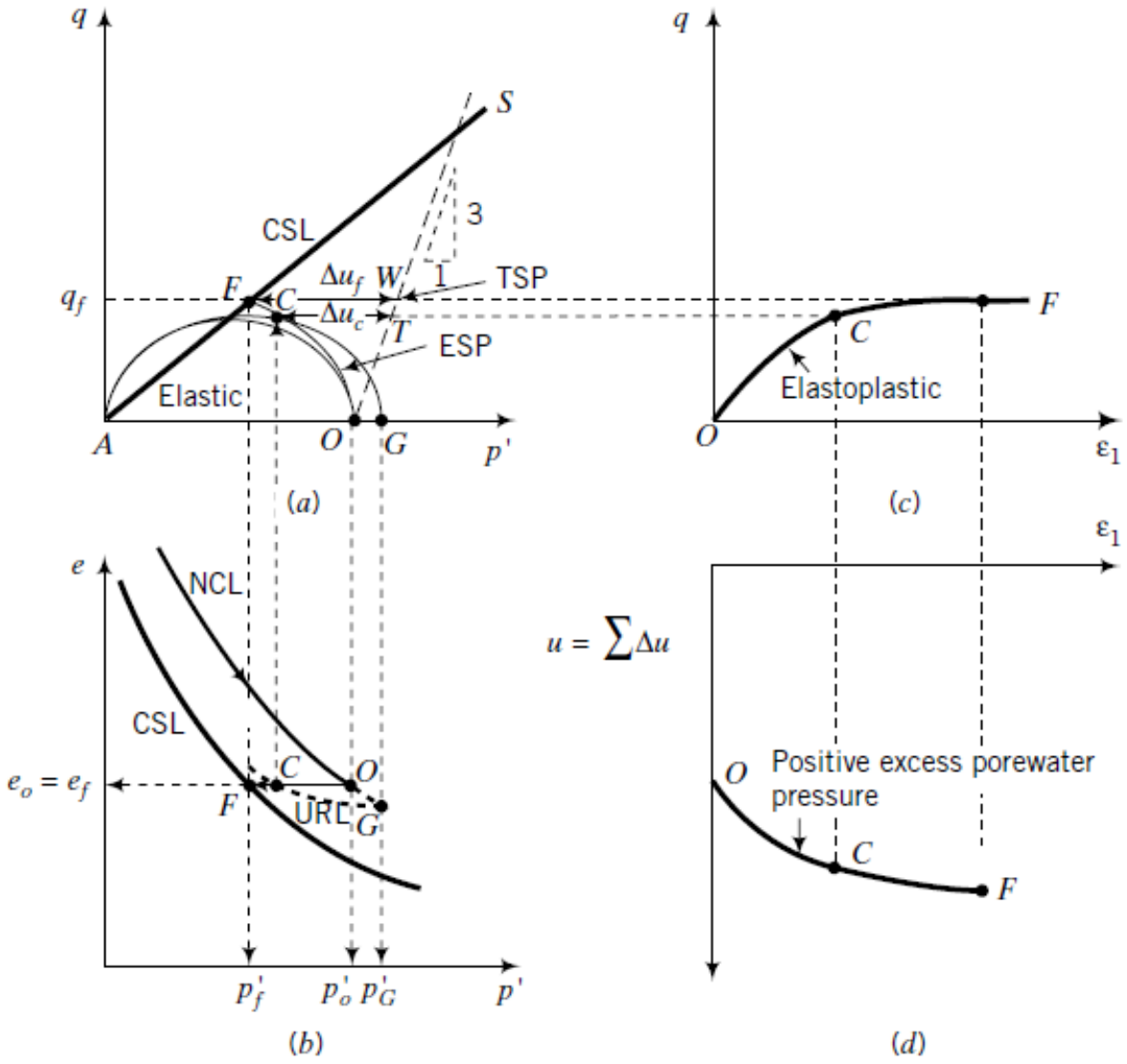

Figure 2.8: Example results of CU triaxial test on a normally consolidated sample (from [3])

2.6.2. Undrained Triaxial test on overconsolidated sample

The starting point now again lies within the yield surface, as shown in 2.9, which means initially elastic response upon loading. As explained before does the ESP form a vertical line within the yield surface. As soon as the yield surface is reached, the soil wants to dilate plastically, since the ESP is at the dry side now. Again this plastic strain needs to be compensated but now with elastic compaction. Elastic compaction is associated with increase in effective stress. Therefore the ESP now bends towards the right until the CSL is reached.

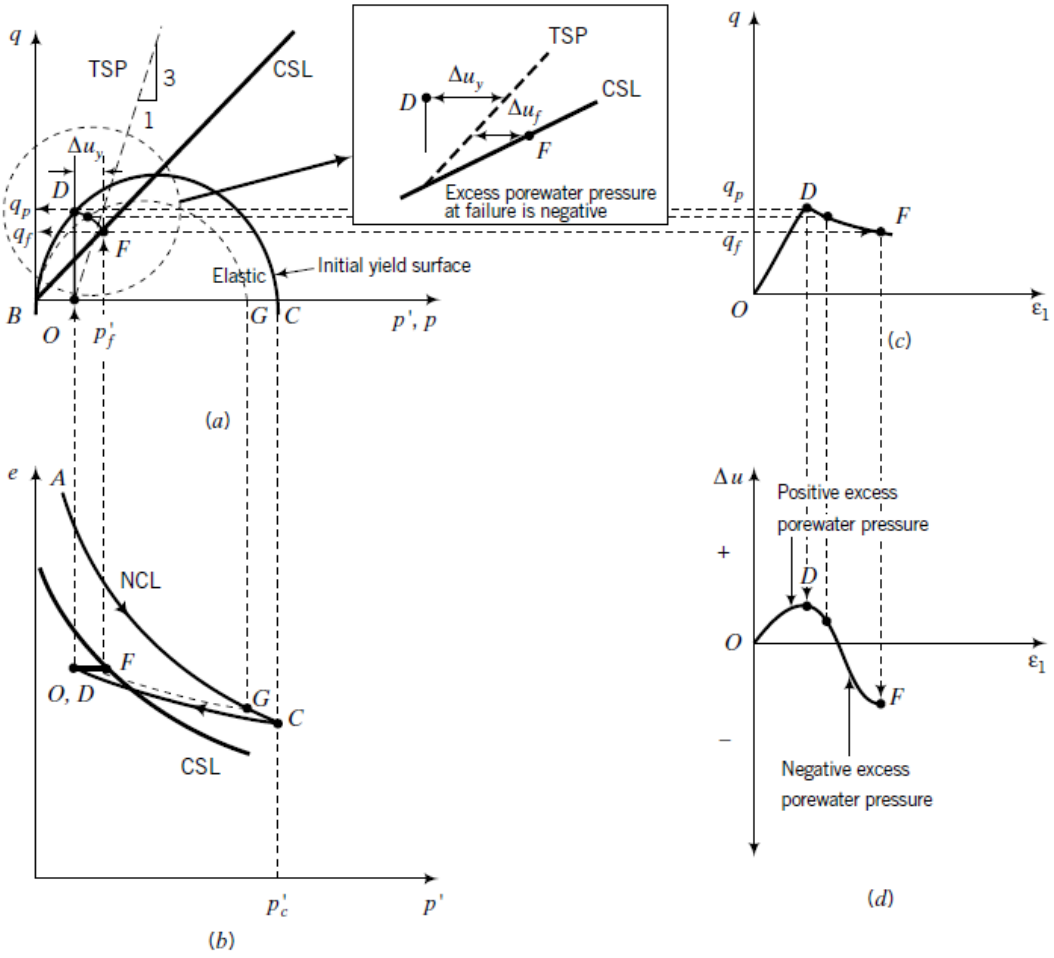

Figure 2.9: Example results of CU triaxial test on a over consolidated sample (from [3])

2.7. Modified Cam clay model

The Cam-Clay (CC) and Modified Cam-Clay (MCC) models are elastic plastic strain hardening models that are based on Critical State theory. The two models are assumed to be the most direct implementations of CSSM. The behaviour as described in Section 2.4 is assumed. MCC is an enhanced version of the original CC model, the most important difference is the yield function. The yield function of the MCC model can be described by the following Equation ([15]):

$$f = \frac{q^2}{M^2} + p'(p' - p_{ie}) \tag{2.10}$$

Useful equations to calculate s_u can be derived from the Modified Cam-clay model. An example is based on the proportions between p' at failure, p'_f, and p' at the start of shearing , p'_0. Which lie on the critical state line and (K_0)consolidation line respectively. The ratio between the two is equal to the ratio of OCR in terms of isotropic stress, R_0, and the spacing ratio, r , raised to the power Λ. The spacing ratio is defined as p'_c over p' at the intersection of the unloading line and the critical state line. In the MCC model $r = 2$. The equation is shown below in Equation 2.11 The complete derivation of this equation can be found in e.g. [29].

$$\frac{p'_f}{p'_0} = (\frac{R_0}{r})^{\Lambda} \tag{2.11}$$

$$R_0 = \frac{p'_c}{p'_0} \tag{2.12}$$

Λ is the plastic volumetric strain ratio. This is the ratio of the plastic component to the total component of the volumetric strain increment in normal consolidation. This ratio can be calculated by Equation 2.13.

$$\Lambda = \frac{\lambda - \kappa}{\lambda} \tag{2.13}$$

Combining the above equations results in:

$$s_u = \frac{q_f}{2} = \frac{M \cdot p'_f}{2} = \frac{M \cdot p'_0}{2} \cdot (\frac{R_0}{2})^{\Lambda} \tag{2.14}$$

Equation 2.14 is however only valid for isotropically consolidated samples. An extension to 1D or K_0 consolidated conditions of the above equation has been presented in [29]. p' is expressed in terms of σ'_v and M expressed in terms of ϕ by applying Jaky's formula (Equation 2.22))

$$p' = \frac{1}{3}(\sigma'_v + 2 \cdot K_0 \cdot \sigma'_v) \tag{2.15}$$

For normally consolidated conditions Equation 2.14 can be expressed as (from [29]):

$$\frac{s_u}{\sigma'_{v0}} = \frac{sin(\phi)}{2a} \cdot (\frac{a^2 + 1}{2})^{\Lambda} \tag{2.16}$$

Where

$$a = \frac{3 - sin(\phi)}{2(3 - 2sin(\phi))} \tag{2.17}$$

Including Jaky's formula limits the freedom of implementing K_0 and ϕ values that not satisfy Jaky's formula. Therefore Equation 2.16 is rewritten to exclude Jaky's formula and express the equation in terms of K_0 and M, the full derivation of Equation 2.18 is shown in Appendix D. This becomes:

$$\frac{s_u}{\sigma'_{v0}} = \frac{M}{2} \cdot (\frac{\eta_0^2 + M^2}{2M^2})^{\Lambda} \cdot \frac{1 + 2K_0}{3} \tag{2.18}$$

Where η is the ratio of q and p'.
Further extension of the work of Wroth has been presented in [4]. An extension of Equation 2.14 includes the relation of OCR to R_0 by the ratio α_R . Equation 2.20 does however not include Jaky's formula and thus leaves more freedom for the choice of parameters.

$$\alpha_R = \frac{R_0}{OCR} = \frac{9(1-K_{0nc})^2 + M^2(1+2K_{0nc})^2}{M^2(1+2K_0)(1+2K_{0nc})} \tag{2.19}$$

Where K_{0nc} is a soil parameter and K_0 is a state parameter. Substitution of Equations 2.15 and 2.19 in Equation 2.14 results in :

$$\frac{S_u}{\sigma'_{v0}} = \frac{1}{6} \cdot M(1+2K_0)(\frac{\alpha_R \cdot OCR}{2})^{\Lambda} \tag{2.20}$$

Equation 2.19 calculates links over consolidation ratio and isotropic over consolidation ratio. But p'_{ie} is calculated instead of p'_0. p'_{ie} is the equivalent isotropic stress. p'_{ie} is the isotropic stress at the tip of the yield surface. This concept is clarified below in Figure 2.10. The figure shows compression to point A and unloading to point B. The equivalent isotropic pressure is represented by p'_{ie}. $p'_{ie} = p'_0$ when isotropic consolidation is applied.

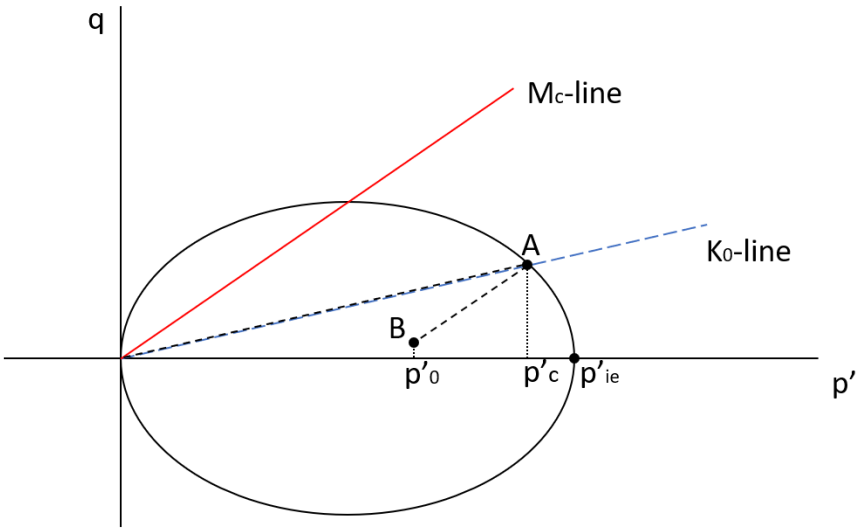

Figure 2.10: Difference p'_c and p'_{ie}, adapted from [4]

2.8. Stress History And Normalized Soil Engineering Properties

Another pillar on which the current guidelines are based is the so-called Stress History And Normalized Soil Engineering Properties (SHANSEP) method, developed by Ladd and Foott, e.g. [12] or [14]. As the name suggests is this method is based on observed normalised behaviour and it takes the stress history of the soil into account. Normalised behaviour in this case means that when S_u values of a soil are normalised by their preconsolidation pressure σ'_v. NC soils consolidated until different consolidation pressures theoretically result in equal normalised S_u values. For OC soils the ratio S_u/σ'_v increases with OCR. An example is shown in Figures 2.11 and 2.12 for a soil with a consolidation pressure of 75 kPa.

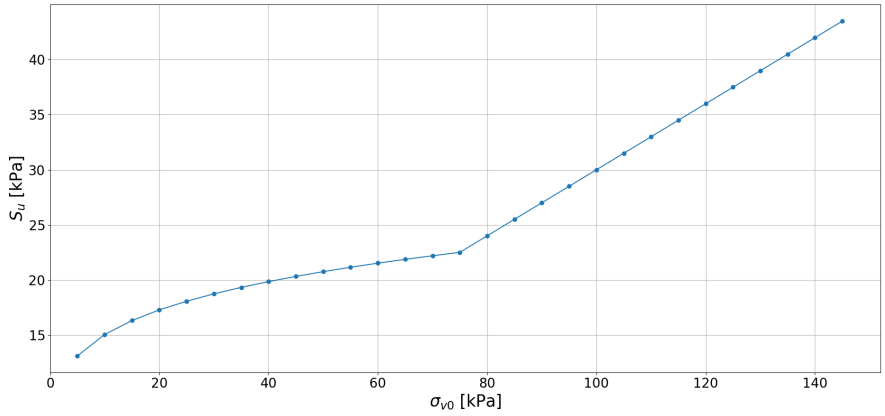

Figure 2.11: Relation of S_u and σ_{v0} according to Equation 2.21

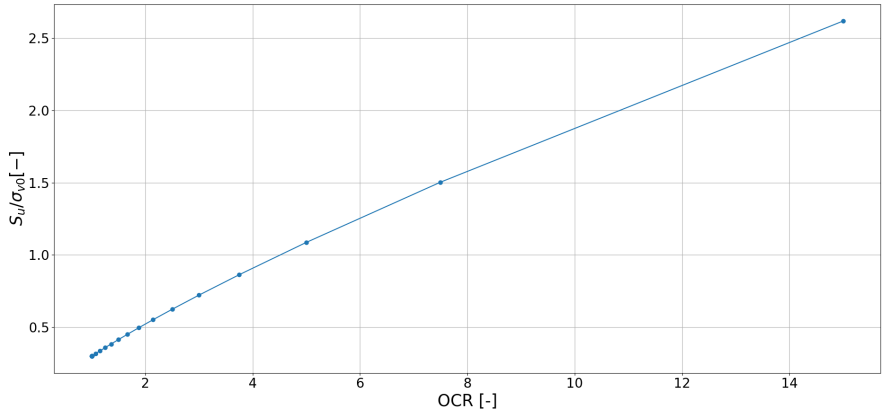

Figure 2.12: Relation of ratio S_u/σ'_v and OCR

The method is based on CSSM and is best suitable for undrained loading conditions. The undrained shear strength is determined as follows:

$$s_u = \sigma'_v \cdot S \cdot OCR^m \tag{2.21}$$

Where OCR is in terms of effective vertical stress. The strength ratio S is the ratio of undrained shear strength over consolidation effective vertical stress for normally consolidated conditions (s_u/σ'_{vc}). This parameter represents the assumption of normalized behaviour of soil. An example plot of Equation 2.21 is shown in Figure 2.11. S_u from different types of test (i.e. triaxial compression and extension and DSS) converge to a single value at large strain, under plane strain conditions. When calculating the shear resistance this value can be applied along the complete sliding plane. Parameter m represents the rate of strength increase with OCR.

Ladd and Foott provide a procedure that can be followed in order to determine the parameters of the SHANSEP method. Generally this means in practice that a set of triaxial tests is executed whereby the samples are consolidated well beyond the in-situ consolidation pressure of the sample. Part of the samples is then unloaded until a predefined consolidation pressure corresponding to a specific OCR. In fact Ladd and Foott provided a very specific list of steps, these steps are not exactly followed in this thesis. The steps are listed below:

1. Select samples and use one-dimensional consolidation testing, to calculate properly the preconsolidation pressure (σ'_p).
2. Using specimens from the same sample and anisotropically consolidate them with consolidation pressures 1.5, 2.5 and 4.0 times higher than the established σ'_p.
3. These tests should show a constant relationship between shear strength and consolidation pressure (S_u/σ'_{vc}). This should at least be true for the higher two pressures in the above steps. If not, the SHANSEP procedure does not apply and consequently, the SHANSEP equation can no longer be used to describe S_u in the field.
4. The pressure that shows a constant (S_u/σ'_{vc}) relationship is selected as the laboratory consolidation pressure σ'_{vm}.
5. The specimens are consolidated to the pressure equal to σ'_{vm} and then allowed to swell to the known over consolidation ratio (OCR). After shearing these specimens, the S can be obtained, which is a necessary parameter for the derivation of the m parameter through the S_u/σ'_{vc} versus OCR plot.

2.9. Comparison isotropic/anisotropic

As mentioned before are the SHANSEP procedure and CSSM theory originally not defined in the same stress space. In order to clarify the difference a comparison is made in this section. CSSM and the MCC model are expressed in terms of isotropic stress p', deviator stress q and void ratio e. These parameters are included in the fundamental CSSM relations, e.g. Equations 2.2 and 2.3. In order to compute p' and q horizontal stresses are needed. In daily engineering practice the horizontal stresses are often unknown and thus not considered. Vertical pressures, on the other hand, can be approximated well from the density of the soil complemented with pore pressures measurements. In the SHANSEP method the vertical effective stresses are used for normalisation of the undrained shear strength.

The ratio between between horizontal and vertical stress is called the lateral earth pressure K. K generally ranges approximately between 0.35 for sands and 0.70 for soft clays at rest [18]. K is dependent on the loading situation. K at rest can be approximated by Jaky's formula ([9]):

$$K_{nc} \approx 1 - sin(\phi) \tag{2.22}$$

In Figure 2.13 the difference between 1D and isotropic compression is shown as explained by Wroth ([29]).

In the MCC model isotropic and anisotropic consolidation until equal mean effective stress does not lead to an equal failure point. The best way of clarifiying the difference is to compare S_u/σ_{v0} of the two scenarios. In Figure 2.14 two triaxial tests are simulated. Both consolidated to the same vertical pressure σ_{v0}. Under isotropic conditions $p' = \sigma'_{v0}$, and under anisotropic conditions $p' < \sigma'_{v0}$. Isotropic consolidation always results in the highest possible p'_0 for a certain σ'_{v0}. In the MCC model p' at failure is directly linked to p' at the end of consolidation. The larger p'_0 the larger p'_f. As a result does isotropic consolidation always result in the highest possible value of S_u/σ'_{v0} for equal σ'_{v0}. The difference in S_u/σ'_{v0} depends on K_0, which determines the ratio between p' and σ'_{v0}. The nearer K_0 approaches 1 the nearer isotropic conditions are approached.

The same principle holds for over-consolidated samples; p'_0 determines the failure point. Isotropic unloading results in a small p' relative to σ_v. When unloading anisotropically, p' decreases more slowly

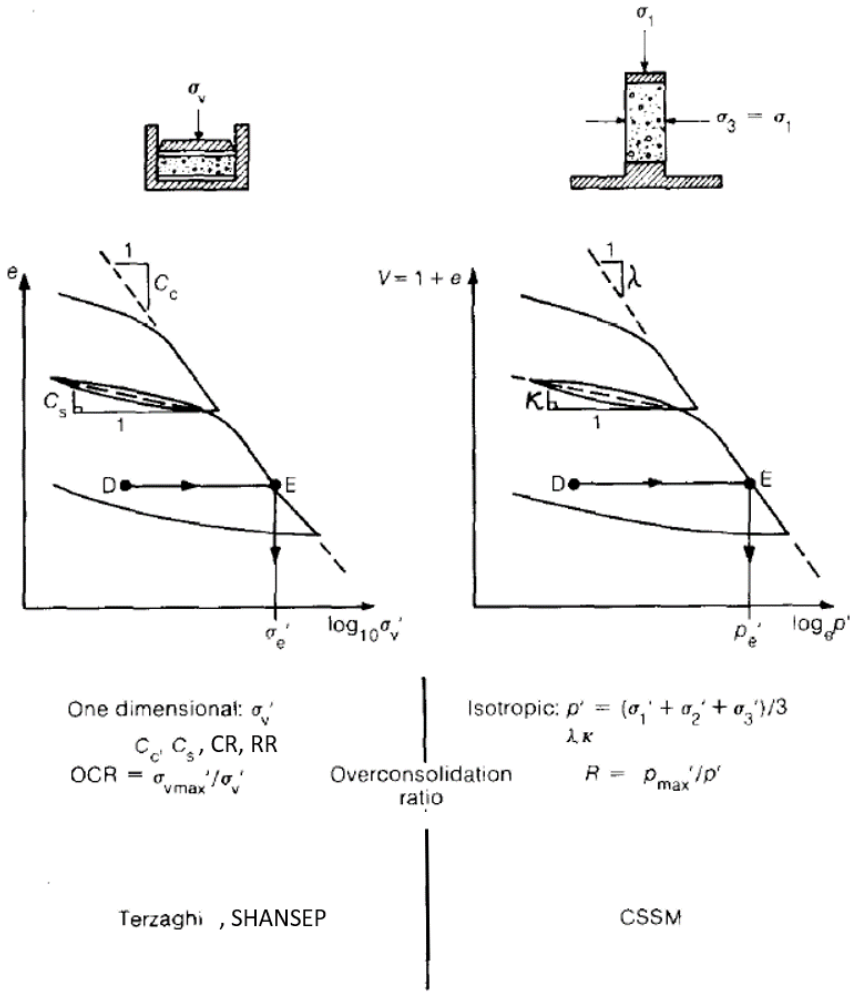

Figure 2.13: Comparison anisotropic and isotropic compression, adapted from [29]

compared to the decrease in σ_v. The exact ratio depends on K_0 and K_{ur} and the extent of unloading. For lightly over-consolidated samples generally S_u/σ_{v0} is larger for isotropically consolidated samples. At some point S_u/σ_{v0} for anisotropically consolidated samples becomes larger. In Figure 2.15 the development of p' during unloading is shown. Two samples both consolidated until $\sigma'_v = 100kPa$ are simulated. The Plaxis soil test module does not provide the possibility to define the loading stress path and unloading stress path exactly. Only the stress state at start of shearing and the vertical preconsolidation σ_{vc} can be defined. This means that p'_c is equal for isotropic and anisotropic unloading and true anisotropic loading and unloading stress path cannot be modeled in the Plaxis soil testing module.

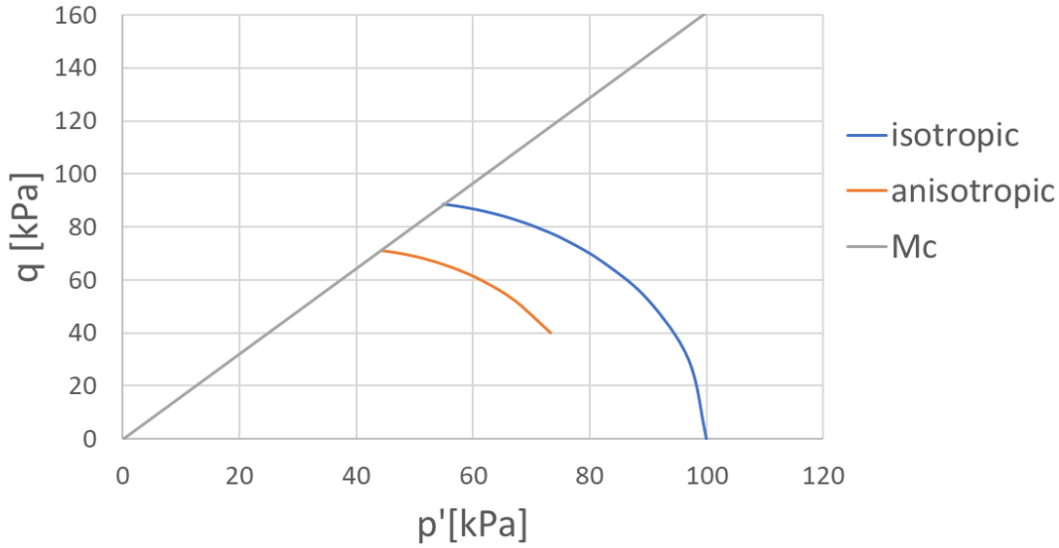

Figure 2.14: Comparison anisotropic and isotropic compression until $\sigma'_{v0} = 100kPa$ in MCC model, simulated in Plaxis

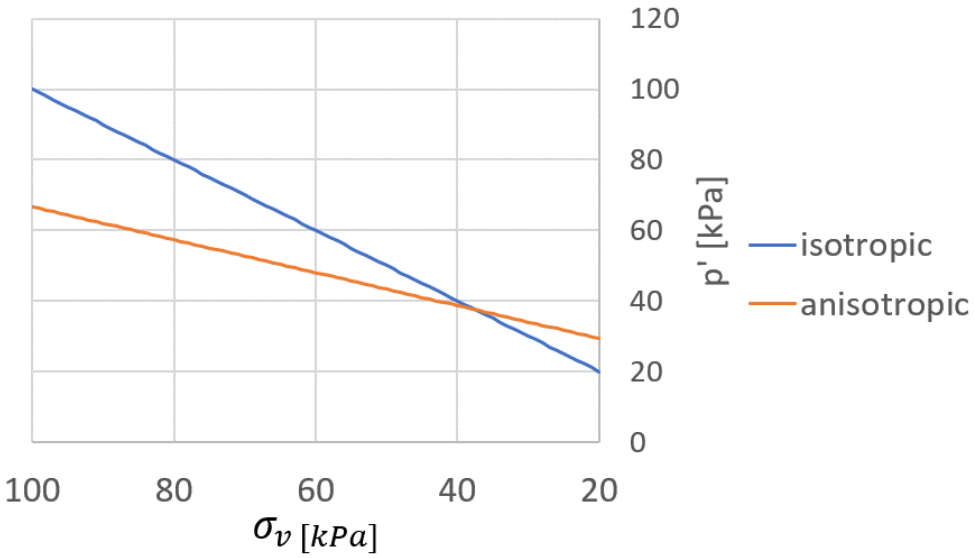

Figure 2.15: Development of p' during isotropic and anisotropic unloading. $K_0 = 0.5, K_{ur} = 0.2$

3

Laboratory Tests Description

In this chapter a description is provided of the lab tests that were executed for this thesis. First the material that is used is described. In the subsequent sections the individual tests and accessory phases and stress paths are explained. Also are the results presented, a elaborate analysis is however given in Chapter 4. A total of eight undrained triaxial tests, an isotropic compression test and two K_0-CRS tests are executed. Besides the lab tests, classification tests are executed as well to determine the material properties. In Table 3.1 an overview of the executed lab tests is shown. Earlier research executed on the same material is used as reference for certain choices in the execution of the laboratory work. The previous work is documented in [31].

3.1. Material

The material that was used in all the laboratory tests is remoulded Oostvaardersplassen clay. There is chosen to use reconstituted clay for this series of tests because the tests are meant to investigate intrinsic behaviour of clay. By remoulding clay it turns into a more or less homogeneous material. Less experimental issues are expected and the results are reproducible when using remoulded clay. OVP clay is used more often in different research projects at Deltares, e.g. POV-M research. The laboratory staff was therefore familiar with the material and much of the behaviour of the material was known. OVP clay is a lightly organic, strongly silty clay. According to Tigchelaar et al. 2001 does the clay consist of: 3% sand, 71% silt, 26% clay and has an organic matter content of 9.5%. OVP clay is assumed to be representative for Dutch organic soils. In the early 1990's the material was extracted in the Oostvaardersplassen, an area in the Netherlands. The material was located at a depth of 1.5 to 3 metres beneath surface level. In April 2017 a sample of about 100 kg was taken from the total sample and mixed in a vacuum mixer for four hours to remove air bubbles that were locked in the soil fabric. After addition of de-aired water the slurry was mixed for another ten hours. The mixture

Table 3.1: Overview of laboratory tests

Sample	Type of test	Cell number	initial void ratio [-]
CRS1	$K_0 - CRS$	2	2.51
CRS2	$K_0 - CRS$	2	2.52
ISO1	Isotropic compression	2	2.56
TRX1	Triaxial compression	2	2.51
TRX2	Triaxial compression	2	2.49
TRX3	Triaxial compression	1	2.58
TRX4	Triaxial compression	1	2.59
TRX5	Triaxial compression	2	2.60
TRX6	Triaxial compression	2	2.59
TRX7	Triaxial extension	2	2.54
TRX8	Triaxial extension	2	2.35

was then divided into two consolidation cells, from now on referred to as cell 1 and cell 2, to bring the water content down. The slurry was K_0-consolidated at a pressure of 40 kPa for 172 days. The resulting blocks of remoulded clay were sealed and stored in a climate controlled storage room. During the execution of other projects pieces were cut out of the blocks for sample extraction. This resulted eventually in an unclear collection of bits and pieces of clay. It was not always clear which cell the sample originated from. The cells numbers documented are therefore not completely certain. In Table 3.2 the Atterberg limits of the samples is shown. Per cell a sample from the top and from the bottom is taken.

Table 3.2: Atterberg limits of preconsolidated OVP samples, from [31]

Sample	Cell	Liquid limit [%]	Plastic limit [%]	Plasticity index [%]
Top	1	164.5	55.4	109.1
Bottom	1	166.5	56.0	110.5
Top	2	163.9	55.0	108.9
Bottom	2	167.0	55.6	111.3

Unfortunately there was not sufficient material left to retrieve the samples completely as desired. Therefore some of the samples are retrieved perpendicular to the pre-consolidation direction and not all the samples have the same initial void ratio. In order to avoid any effects on the results the stress levels are chosen in such a way that the pre-consolidation stress levels are well exceeded in both vertical as well as horizontal direction and the so-called virgin zone is reached. An extra K_0-CRS test is executed to map the effect of the sampling direction.

3.2. Triaxial tests

Monsters of approximately 130 mm height and a radius of 65 mm are tested tested. After consolidation the height was between approximately 90 and 110 mm. Since K_0-consolidation was applied, the radius was ideally still 65 mm after consolidation. In practice, however, the radius was between 62 and 65 mm. A membrane of 0.25 mm thickness is used to confine the sample. Furthermore five drainage strips are used to increase the consolidation rate. The strips are placed under an angle of 60°. This has least influence on the strength of the sample. The test results are corrected for strength effects of the membrane and the drainage strips conform [11]. In Figure 3.1 the sample preparation is shown.

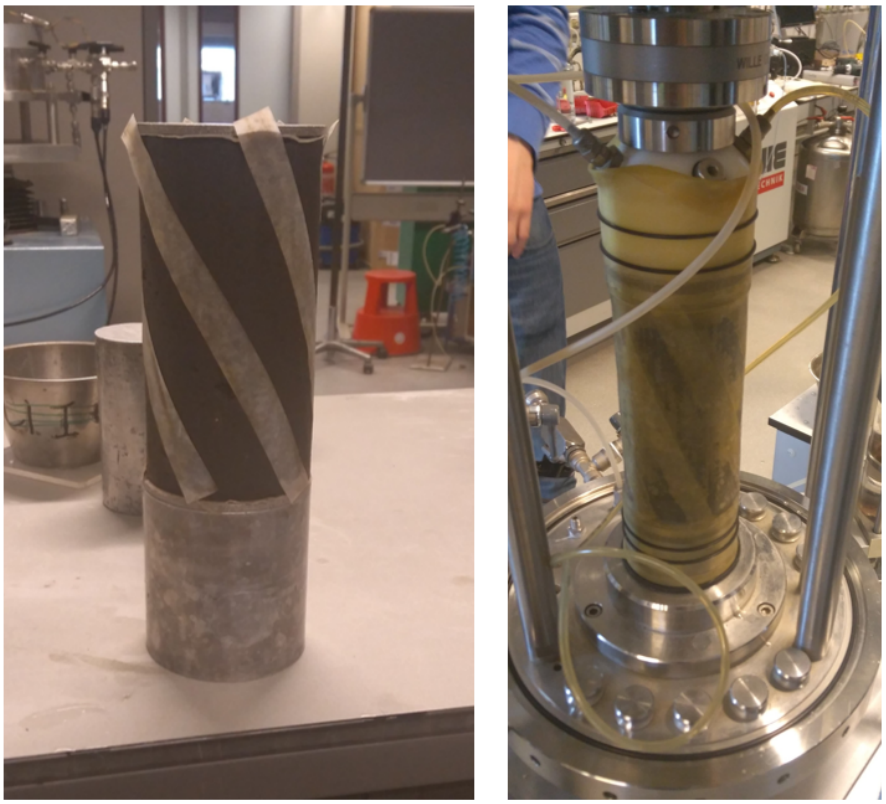

Figure 3.1: Left: drainage strips on the sample. Right: placement of the sample in triaxial apparatus

3.2.1. Consolidation phase

Key in the execution of triaxial tests is the stress path that is followed. The scope of the lab work is to investigate the undrained behaviour of the clay when applying the SHANSEP procedure and place the results in CSSM framework. During the execution of the laboratory work the planned stress paths had to be adapted several times due to unforeseen circumstances. According to CSSM,[20], the undrained shear strength of a soil is dependent on the void ratio. In order to verify this statement for K_0-consolidated soil the stress paths are chosen in such a way that a certain void ratio is reached following different stress paths. Theoretically the void ratio at the end of consolidation, i.e. the void ratio during shearing, can be predicted by using soil parameters λ and κ, or similar compression and swelling parameters. Also the void ratio can be monitored during the consolidation phase by using the water extrusion that is measured continuously during the test. However, the results of both methods did not agree with each other and neither with the void ratio that was measured after every tests conform international standards. A factor that contributes to this inconsistency are assumptions that are done on particle density. The difference resulting from assuming the maximum and minimum particle density of the range of values that was found during previous work on OVP clay, is a difference in void ratio of 0.03, which is a deviation of $\pm 0.5\%$. A difference in weight however has a much larger effect. A deviation of 1 gram results in a difference in void ratio of approximately 0.015 for the samples that were used. After shearing water is found in between the sample and the membrane. This water is extruded from the sample, thus theoretically not contributing to the void ratio. It is however measured because it sticks to the sample. Also small rock or shell fragments can have an effect on the calculated void ratio. Creep influences the void ratio as well.

Eventually the stress paths are chosen such that a spread in data points is obtained in terms of OCR, void ratio and preconsolidation stress. An overview of the executed lab tests is shown in Table 3.2. As can be seen in Table 3.3 rather high OCRS are chosen (up to 20). Such high OCRS can occur at the toe of the dike during uplift. These phenomena result in increasing pore pressures and hence the effective stress decreases which in turn results in a high OCR. Because this situation is best

represented by an extension test (as explained in Section 2.3) two extension tests are executed as well.

Table 3.3: Overview of triaxial tests

Test nr.	Type	Stress state	σ'_{v0} [kPa]	σ'_{vc}	OCR [-]	p'_0 [-]	p'_c [kPa]	R_0	K_0 [-]
TRX 1	compression	NC	100	100	1	62	62	1	0.43
TRX 2	compression	OC	20	121	6	20	75	3.8	0.98
TRX 3	compression	NC	200	200	1	123	123	1	0.43
TRX 4	compression	OC	10	200	20	31	123	4.0	4.18
TRX 5	compression	OC	50	150	3	41	92	2.2	0.74
TRX 6	compression	OC	12.5	150	12	22	92	4.2	2.12
TRX 7	extension	OC	50	150	3	41	92	2.2	0.74
TRX 8	extension	OC	12.5	150	12	22	92	4.2	2.12

The consolidation phase is executed in several steps. The first step is isotropic consolidation until approximately 20 kPa, which is well below the pre-consolidation pressure of the material. This step is included to move away from the failure line and make sure the samples do not fail yet at very low pressures already. Secondly the deviator stress is increased until the right ratio of horizontal to vertical stress (K_0) is reached. From this point onward K_0 is kept constant until the required pre-consolidation pressure is reached. After consolidation a waiting period is implemented, during which the pressures are kept constant, to make sure excess pore pressure developed in the sample could dissipate and the effective stress homogenises throughout the complete sample. Also should creep deformations be (near) zero. To check this condition the drains of the triaxial apparatus were temporarily closed. The pore pressure was thereafter allowed to increase 1 kPa in ten minutes. If the pore pressure increased, extra waiting time was implemented until a maximum of 48 hours. For normally consolidated samples shearing can be started. For over consolidated samples an extra unloading step is implemented. Now a new ratio of horizontal to vertical stress is applied (now called K_{ur}) which is often approximately one half of K_0. K_0 and K_{ur} are actually tangent values and not an absolute ratio of σ'_h and σ'_v. After unloading to the required pressure, a waiting period is applied again.

The first triaxial test is executed K_0-seeking, this is explained in more detail in Section 3.5. Based on the results and on previous test results on OVP clay the $K_0{}^{NC}$ is determined to be 0.43. TRX2 is unloaded K_0-seeking. This however gave unexpected results that did not agree with K_0-CRS results. The K_{ur} was namely equal to the $K_0{}^{NC}$. The reason for this unexpected behaviour is unclear. Therefore a K_{ur} of 0.27 is assumed eventually. Based on Section 3.5 a consolidation rate of 0.5 kPa/hr cell pressure increase is applied. The lab technician however did keep an eye on the sample area. Under K_0 conditions the sample area should be more or less constant. If this was not the case the loading rate was lowered.

In Figures 3.2 and 3.3 the consolidation phases of samples 1 to 4 is shown. In Figure 3.2 it is clearly visible that TRX1 is consolidated K_0 seeking. Also the crash of the control programme is visible. TRX2 and TRX4 are not completely following the stress path as planned, this is the result of execution in the laboratory. The stress path does however not deviate too much and does not come near the failure line, the effect is therefore assumed to be nil.
During the consolidation phase of the extension tests, TRX 7 and TRX 8, deviating consolidation behaviour was observed by the lab technician. The waiting time necessary to fulfill the condition of a maximum pore pressure increase of 1 kPa when closing the drainage valves, was much longer than the during the previous tests. The maximum waiting time needed for TRX 1 to 6 was maximum 48 hours. While after over 100 hours both TRX 7 and 8 did not meet the condition yet. Also was the back-pressure needed to reach a B-factor of 0.97 400 kPa, compared to 300 kPa for the samples 1 to 6. The most probable explanation is that the drainage of the sample was disturbed. Smooth end platens are used during the extension tests. This means that between the samples and the porous end platens a thin layer of grease and an extra membrane is placed. Possibly the porous plates became (partly) clogged by the grease. After a build-up of pressure the grease is released causing a "jump" in the wa-

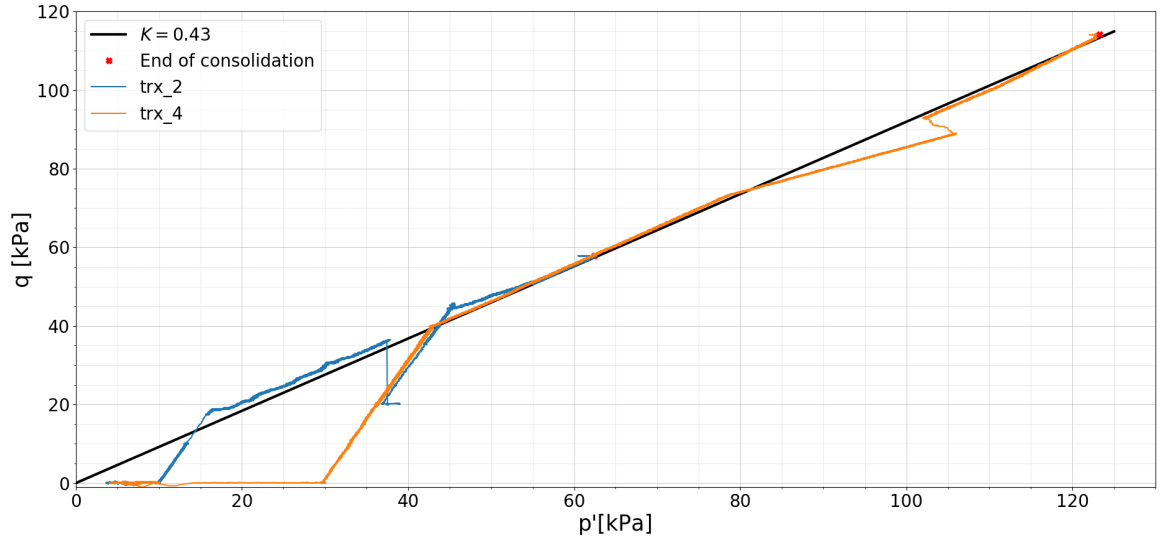

Figure 3.2: p'-q plot of consolidation phase normally consolidated samples

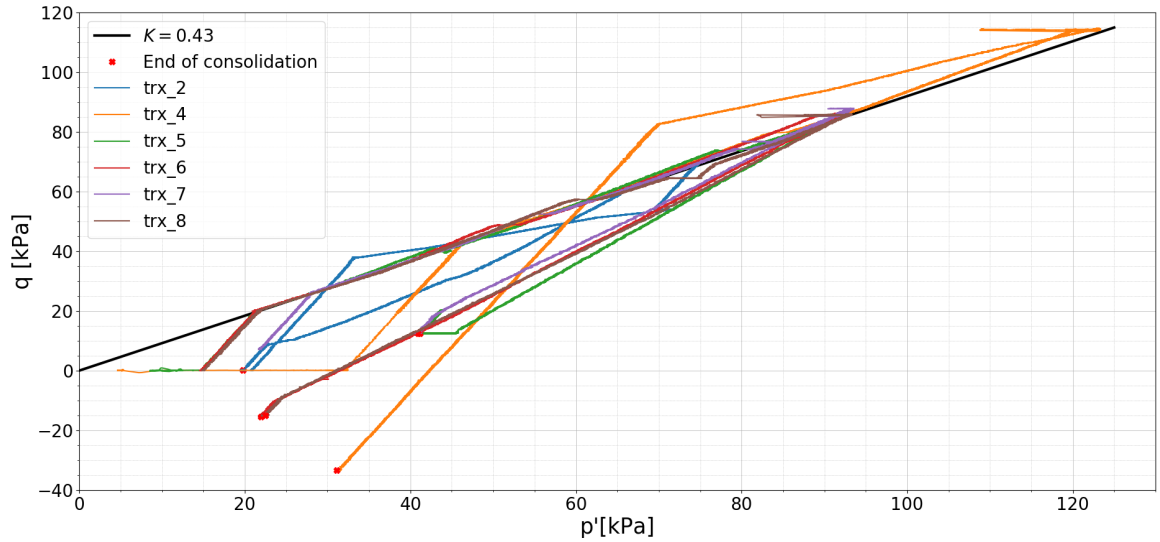

Figure 3.3: p'-q plot of consolidation phase over consolidated samples

ter extrusion. Another possibility could be a small leak in one of the tubes connecting the drains to the measuring device. The "jump" is shown in Figure 3.4. Besides the deviating consolidation behaviour was there an error in the computer programme controlling the triaxial machine during the consolidation of sample 7 as well. The sample had to be placed in another machine and reconsolidated. The error occurred at a σ'_v of approximately 90 kPa. The sample was eventually consolidated 150 kPa, well into the virgin compression zone of the sample. However, the void ratio was not determined when the sample was moved. Trx 7 is therefore not displayed in graphs containing void ratio.

In Figure 3.5 the axial strain versus the volumetric strain during is shown. When the right K_0 is chosen and thus one-dimensional compression is well simulated, the axial strain is equal to the volumetric strain. Most of the samples plot slightly above the $\epsilon_{axial} = \epsilon_{volumetric}$-line. This indicates that the K_0-value is too high. The deviation from the $\epsilon_{axial} = \epsilon_{volumetric}$-line is maximally 12% for the triaxial compression samples. The extension samples (trx 7 and 8) show rather large deviations. This is caused by the fact that the samples are taken from blocks of clay that are left over. The water content,

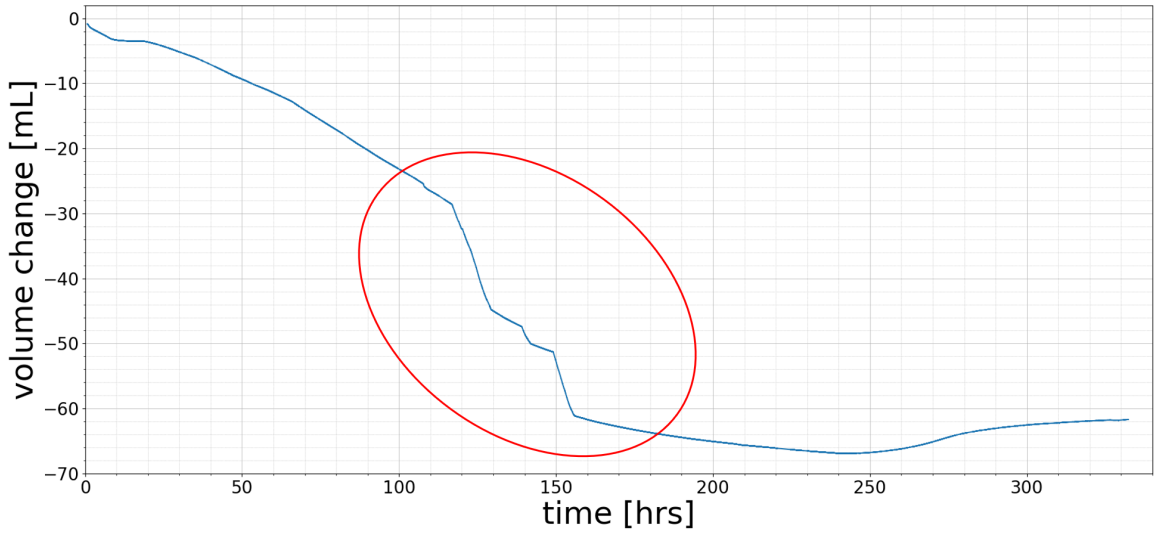

Figure 3.4: "Jump" in pore volume change during consolidation of sample 7

and thus void ratio, of the samples is therefore lower. In Figure 3.6 the void ratio during is plotted against vertical effective stress during consolidation. The void ratio is based on the water extrusion and does not completely match the measured void ratio at the end of the test. The difference in loading and unloading stiffness is clearly visible. Also the effect of the waiting period of 48 hrs that is assumed is clearly visible. A significant change in void ratio is obtained at the end of every loading step. This is the result of pore pressure dissipation and creep effects. The effect is smaller after unloading than after loading. The change in void ratio is significant compared to the total change in void ratio during unloading. In Figure 3.7 creep effects are also clearly visible. In the figure the stresses, vertical strain and strain rate of TRX 4 is shown. During the relaxation period the strain continues, the strain rate however slowly decreases with time. Also the difference in positive and negative strain rate is nicely illustrated. The different phases, i.e. (un)loading, relaxation and shearing, are separated by dashed lines. Similar plots for each sample are available in Appendix A.

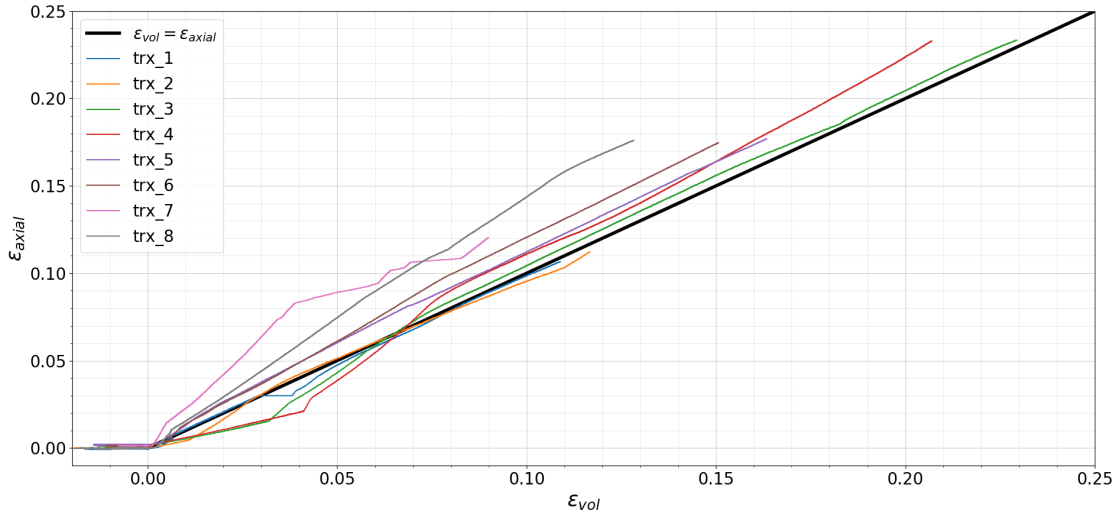

Figure 3.5: Axial strain versus volumetric strain during compression phase

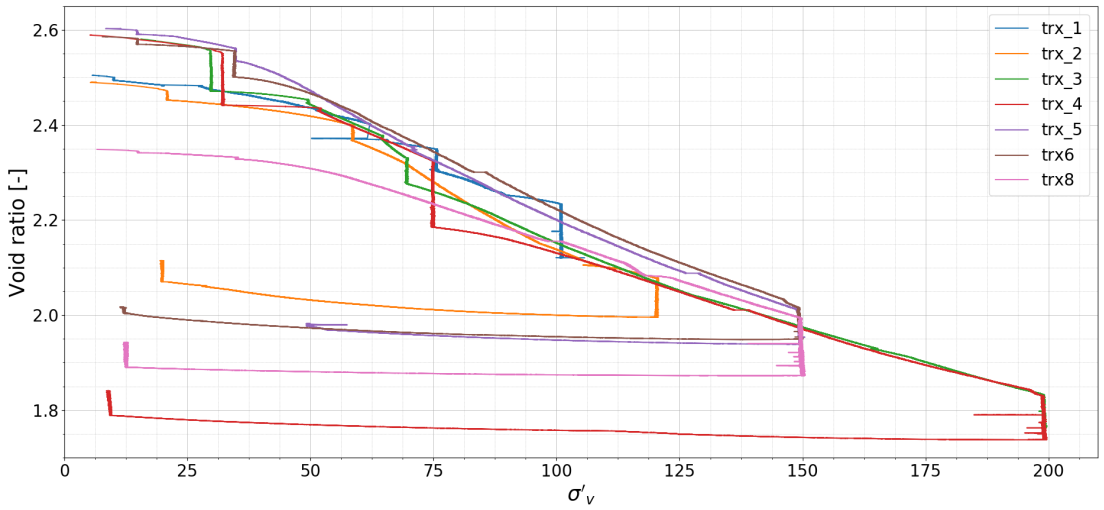

Figure 3.6: Void ratio of triaxial samples during consolidation

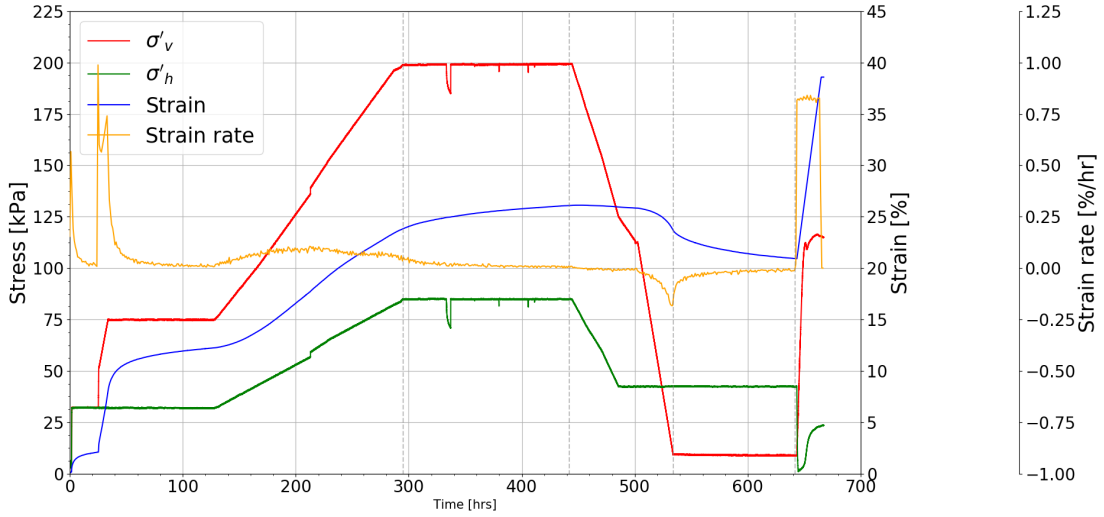

Figure 3.7: Stresses, vertical strain and strain rate of TRX 4

3.2.2. Shearing phase

In order to realise undrained shearing the drainage valves are closed before shearing started. A shearing rate of 1% strain/hr is chosen. The percentage is relative to the height of the sample at start of shearing. In Figure 3.9 the stress paths of the shearing phases are shown in p'-q space. The slopes of the M_c and M_e lines are determined in Sections 4.1.2 and 4.1.3. The stress paths nicely bend towards the M_c line. In Figure 3.10 the deviator stresses during shearing is plotted as a function of strain. TRX 4 and 6 have the most distinct peak which can be related to the failure mechanism, which in turn can be related to the stress state of the sample. OC samples show clear shear bands. TRX 4 and TRX 6 (OCR of 20 and 12 respectively) even show two shear bands cross wisely oriented with an angle of approximately 60° to the horizontal. TRX 2 and TRX 5 (OCR of 6 and 3 respectively) show only one shear band and the NC samples (TRX 1 and TRX 3) do not show shear bands. All the samples shown a barrel shape after failure. Pictures of the samples after shearing are displayed in Appendix A. The OC samples show more brittle behaviour compared to the NC samples. Also the is the response of the OC samples less stiff. This is nicely illustrated by Figures 3.10 and 3.8. Figure 3.8 shows normalised $p' - q$ space including strain contours. The contours of the OC samples are more closely spaced then the contours of the NC samples.

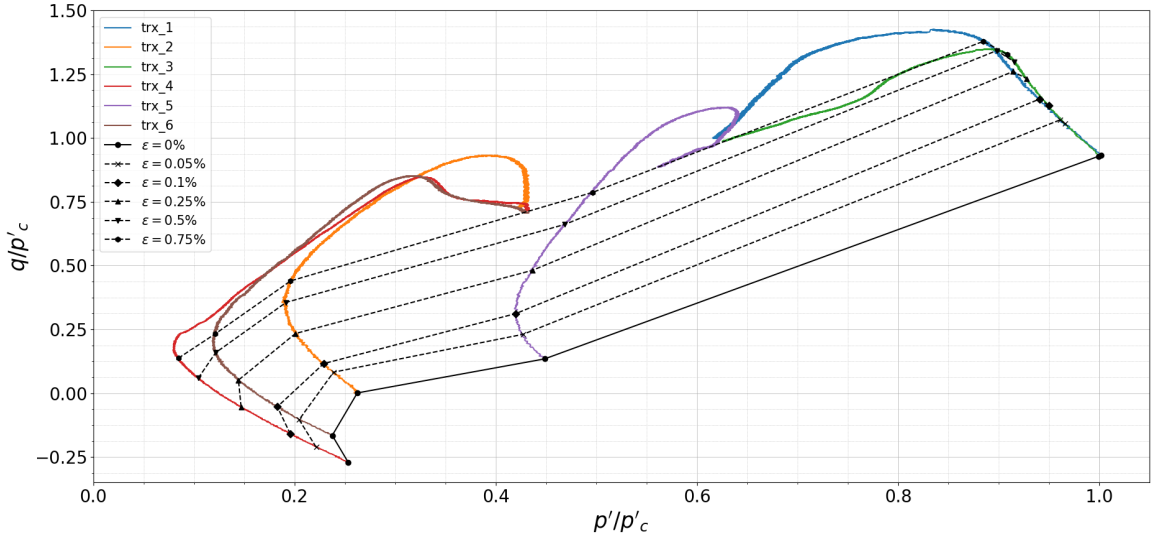

Figure 3.8: Strain contours in p'-q space normalised by the maximum p' reached during consolidation (p'_c)

In Figure 3.11 the pore pressures during shearing are shown. The OC samples show a peak in pore pressure roughly between 0 and 8 % strain. The NC samples do not show a peak, Δu in TRX 3 does even increase with strain and does not stabilise towards ultimate state. It is therefore questionable whether the NC samples really reached critical state or not.

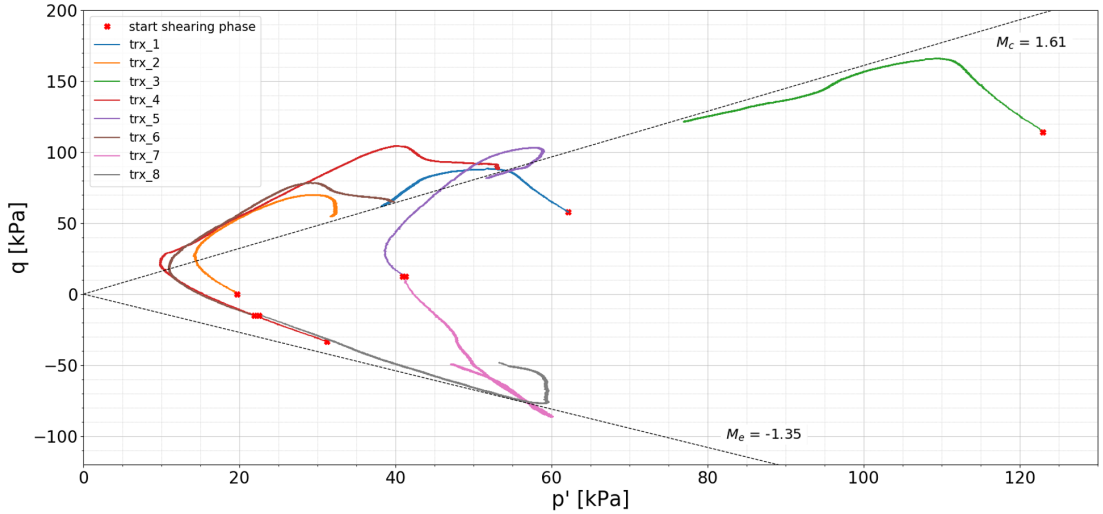

Figure 3.9: p'-q plot of shearing phase

The two extension tests that are executed also had a shearing rate of 1%/hr and are executed using smooth end platens. During standard triaxial tests a relatively large shear tension occurs between the sample and the porous end platens caused by friction. In order to limit the influence of the shear stress on the sample behaviour grease is used. Besides limiting the friction between samples and porous plates, a height/diameter ratio of 1.8 to 2.2 is assumed [23]. In extension tests necking is known to appear. The stresses are calculated by assuming a constant volume, the height of the sample is recorded and thus the average surface area can be calculated. Necking means that strains localise in the sample. As a result the surface area is much smaller than the rest of the sample and the stresses are not representative anymore. The moment of necking is tried to be recorded by a camera. Necking

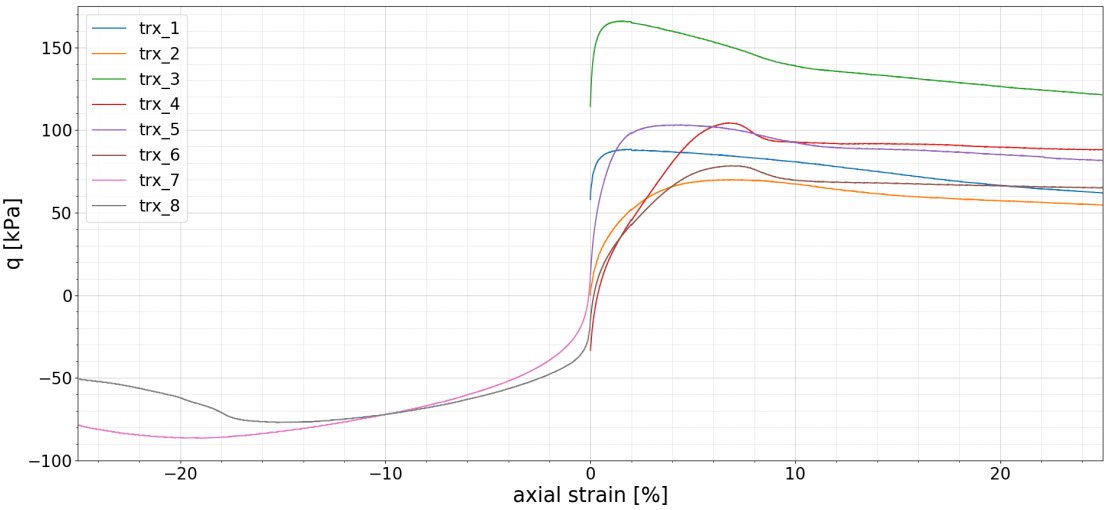

Figure 3.10: deviator stress during shearing

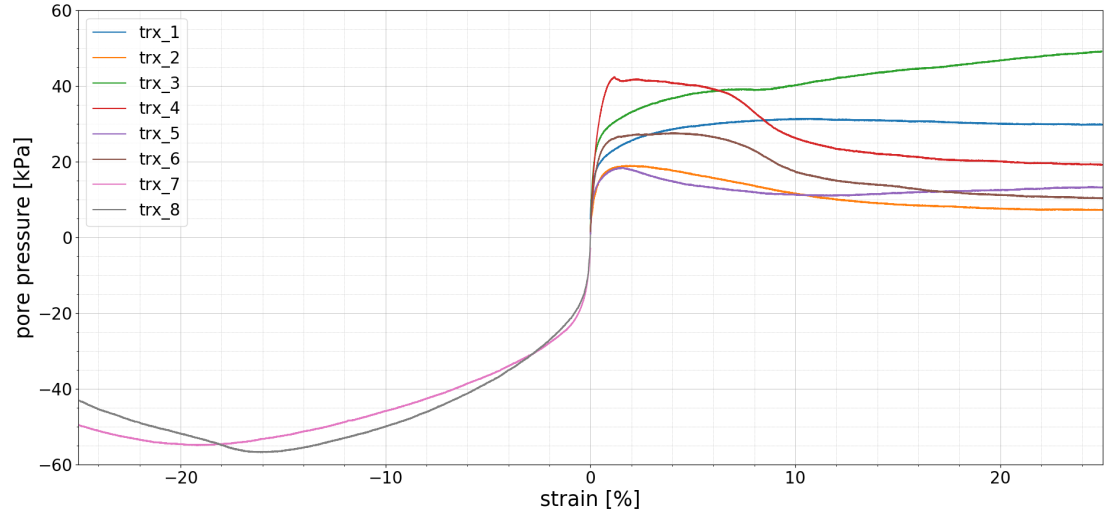

Figure 3.11: pore pressure development during shearing

generally starts far before ultimate state is reached, determination the stresses at ultimate state is therefore inaccurate. In order to correct for this effect the surface area has to be recalculated from the point that necking or shear banding occurs. This is however an approximation. The moment that necking or shear banding occurs is determined by taking pictures that were merged to a video, as shown in Appendix A. A $p' - q$ plot and a $q - \epsilon_1$ is plotted simultaneously with the video recordings. In this way the strain level at which the shear band started to form can be determined. From the data the surface area and thus the current diameter of the sample can be estimated. An interpolation of the surface area can be made between the start of shear banding and ultimate state. When shear banding occurs the surface area is best described by an oval shaped and calculated as follows:

$$A = \pi \cdot \frac{1}{2} diameter_1 \cdot \frac{1}{2} diameter_2 \tag{3.1}$$

However, if necking occurs the stress surface is still best described by a circle but not the radius has to be estimated from images instead of the radius recorded by the triaxial apparatus. Sample 7 however showed relatively little necking and shear banding, therefore no geometrical correction is applied. Sample 8, showed a very clear shear band. The stresses are corrected as described above.

3.2.3. Procedure and data correction

The data from the tests are analysed manually by using data processing software Spyder, which can be programmed with Python. Stress corrections for the effect of filter paper and membrane strength around the sample are applied according to [11]. Furthermore a correction was applied to the data of triaxial test 1. Due to a software update the computer regulating the triaxial apparatus switched off during the weekend. As a result the triaxial test was uncontrolled and no data was gathered for approximately 3 days. When the computer was restarted incorrect dimensions were entered resulting in wrongly recorded deviator pressures. The data is corrected based on the assumption that during the 3-day-gap 4 mL of water was expelled from the sample, probably because of creep. The amount of water expelled could be deduced from a comparison of the volume change measured during the test and the weight difference of the sample before and after the test. By correcting for the volume the sample dimensions and thus stress could be recalculated. As mentioned before was a geometrical correction applied to the triaxial extension results.

3.3. K_0-CRS tests

In addition to the triaxial tests two K_0-CRS tests are executed. The purpose is to obtain relevant soil properties such as compression and swelling index and K_0. Also the creep rate can be determined from the test results. Creep has an effect on the void ratio after consolidation, which makes it more difficult to reach the required void ratio. Due to limited material availability several triaxial samples are taken in horizontal direction. Since the material is remoulded, anisotropy in compression parameters is not expected. To confirm this, one of the K_0-CRS tests is executed on a horizontally taken sample.

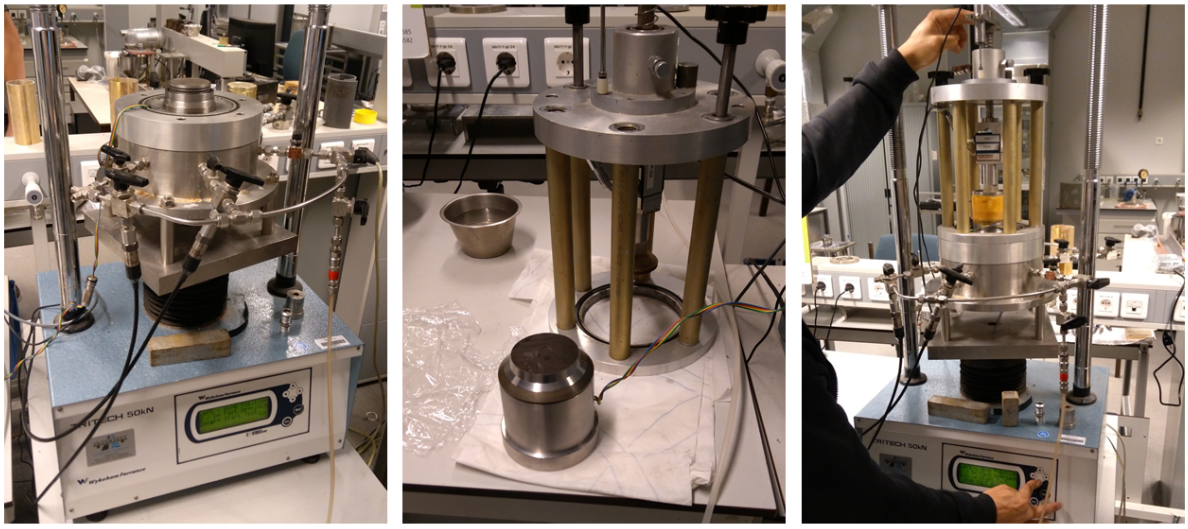

Figure 3.12: Left: Empty load cell. Middle: K_0-ring including sample next to the loading frame. Right: Complete K_0-CRS set-up

3.3.1. Procedure and data correction

Samples of 20 mm height and a radius of 63 mm are placed in the K_0-ring on top of a porous stone and then placed in the load cell. This is shown in Figure 3.12. Originally it was planned to use the same testing programme for both tests. However, because of a human error instead of a constant height relaxation time constant pressure is implemented. In Table 3.4 the testing conditions are shown. This represents the range of the stress paths followed during triaxial testing. Also relaxation time is included in the test to measure the creep effects. A loading rate of 0.036 mm/hr is chosen based on previous laboratory work on OVP clay. The data from the tests is analysed manually by using data processing software Spyder, on the basis of Deltares standards [6]. The vertical stress is averaged over the sample and corrected for wall friction in a simplified manner. Compression parameters CR and RR as well as the lateral stress ratio K_0 are determined graphically. The preconsolidation pressure is determined using the Casagrande method, which is also a graphical method.

Table 3.4: Test description K_0-CRS test (* = unplanned test programme)

Descriptions		rate		boundary condition	
0	start			0	kPa
1	loading phase	0.036	mm/hr	120	kPa
2	unloading phase	0.036	mm/hr	10	kPa
3	reloading phase	0.036	mm/hr	200	kPa
4	relaxation	48	hr	constant height	
4*	unloading phase	48	hr	200	kPa
5	unloading phase	0.036	mm/hr	10	kPa

3.3.2. Results

In Table 3.5 the results of the K_0-CRS tests are summarized. From the results can be concluded that the two tests executed for this thesis give very similar results. As expected the consolidation pressure is different, which is the obvious result of the sampling direction. However, the consolidation pressure of CRS 1 is not equal to K_0 multiplied by the consolidation pressure of CRS 2 but significantly higher. The results show a difference in RR and consequently κ values. CSSM parameters λ and κ are recalculated from CR and RR respectively by the following equation, where κ is calculated in the same way from RR:

$$\lambda = \frac{CR}{LN(10)} * (1 + e_0) \tag{3.2}$$

e_0 has a large influence on the result, the larger the e_0 the larger λ and also the relative influence of e_0 on the outcome of equation 3.2. The difference in unload-reload parameters between old and new data is caused by the stress range that is applied. The unload line is not linear with respect to the natural logarithm of vertical stress, which makes it stress dependent. The K_0 and K_{ur} are used in determination of the stress paths applied in the triaxial tests. In Figure 3.13 the determination of CR, RR and the consolidation stress of test 1 is shown. All data plots of the tests are shown in Appendix B.

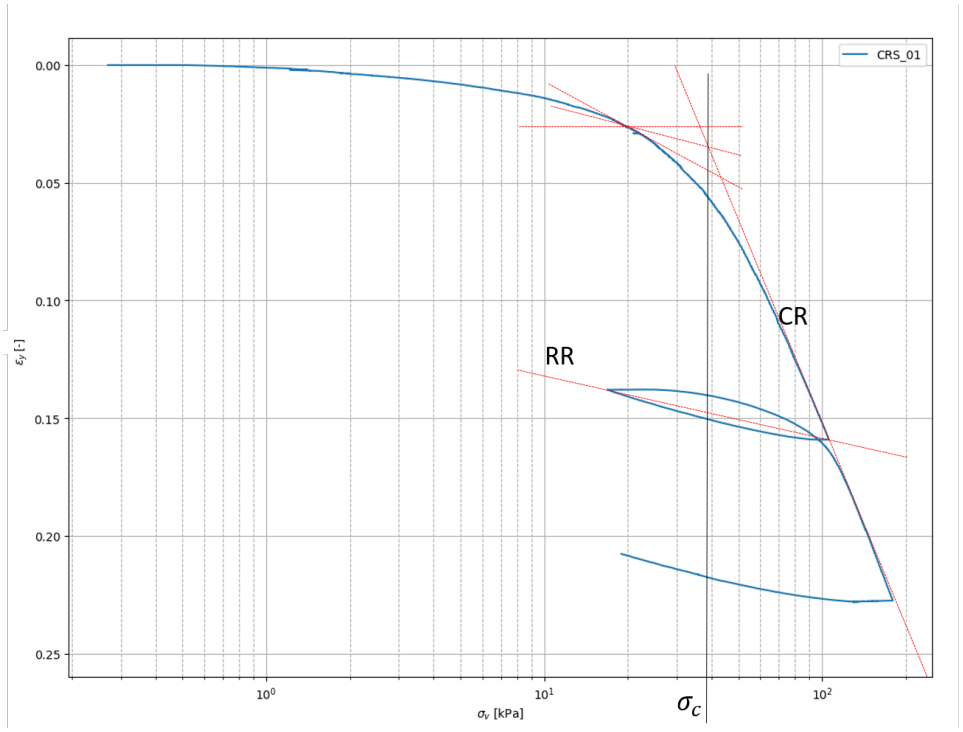

Figure 3.13: Vertical strain as a function of vertical stress of K_0-CRS test 1

From the K_0-CRS results can be concluded that the sampling direction has little to no effect on the

Table 3.5: Summary of the K_0-CRS test results

Test nr.	Cell nr.	Sample direction	CR	RR	λ	κ	σ_c [kPa]	K_0	K_{ur}	ν_{ur}	e_0
CRS 1	2	↔	0.29	0.038	0.43	0.06	39	0.43	0.27	0.21	2.51
CRS 2	2	↕	0.30	0.043	0.45	0.07	53	0.43	0.26	0.21	2.52
					Old data						
OVP_C1	1	↕	0.33	0.024	0.54	0.04	48.2	0.40	0.22	0.18	2.79
OVP_C2	2	↕	0.34	0.024	0.53	0.04	58.6	0.38	0.22	0.18	2.61

compression index CR and ratios K_0 and K_{ur}, as was expected. The triaxial data can therefore be compared on an equal basis. There is a rather large difference in unload/reload index RR, which can be explained by the difference in stress range in which RR is determined. Also the difference in CSSM parameter λ is remarkable. This is partly explained by the void ratio.

3.4. Isotropic compression test

The third type of tests that is executed is an isotropic consolidation test. The triaxial cell is used to apply isotropic stress. In order to determine effective stresses, the lower drain of the triaxial machine was closed during the consolidation. This allows for measuring the pore pressure development in the sample. In order to determine the average pore pressure throughout the sample an assumption in pore pressure profile in the sample is made. A Plaxis simulation to estimate the loading rate and compute the excess pore pressure distribution throughout the sample is made as well, this is shown in Chapter 3.5. A simplified assumption is made that the average pore pressure in the sample is approximately 30% of the measured excess pore pressure at the bottom of the sample. In Figure 3.14 the void ratio is plotted as a function of the natural logarithm of the effective mean stress. The figure does not show a perfect consolidation path as the K_0-CRS test does. The virgin compression line before and after the unload/reload cycle are not on one line but the slope of the line is equal. In the unloading line also shows a small disturbance. Like the triaxial tests and K_0-CRS tests a waiting period is applied after every loading step. The effects are clearly visible in the figure. Loading parameters λ and κ are derived and indicated in the figure.

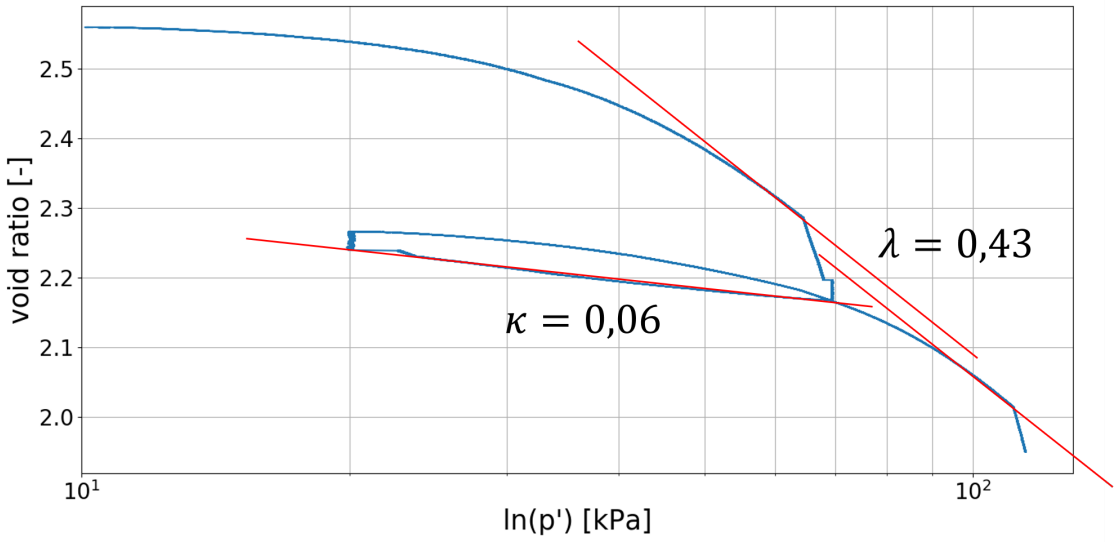

Figure 3.14: Void ratio as a function of ln(p')

3.5. Loading rate

During earlier triaxial testing on OVP clay a consolidation rate of 0.18 kPa/hr, in terms of cell pressure, is used for both loading and unloading. When applying this rate the complete series of test would reach outside the time frame of this thesis. 0.18 kPa/hr was chosen based on the condition that no excess pore pressure would occur in the sample during consolidation. For this thesis a different condition was used. Namely that the sample should not fail before reaching the specified pre-consolidation pressure. Excess pore pressure is however allowed. The new rate is based on numerical simulations in Plaxis and experience of the lab technician. There are three modes of consolidation: K_0-seeking, isotropic and deviatoric. The K_0-seeking consolidation is based on a constant nominal diameter of the sample. A certain increment of cell pressure is applied to the sample. This causes extrusion of a certain volume of water which is measured. A certain axial displacement is now applied such that the vertical displacement times the sample area is equal to the distorted volume of water. When keeping the cell pressure increments small a constant surface area is approximated. This is a simulation of natural soil conditions. When loading the sample too quickly excess pore pressure is generated which makes the extorted volume of water incorrect and thus the surface cannot be kept constant.
In Figure 3.15 a Finite Element model in Plaxis is shown. Half of the cross section of the triaxial sample is modeled, since axial symmetry is applicable. The left boundary is impermeable while the other three boundaries are permeable. The right and the top boundary can deform freely while the left boundary is horizontally fixed and the bottom boundary is vertically fixed. From the figure can be concluded that the pore pressure is highest in the middle of the sample because the drainage path is longest there. Therefore are the pore pressures calculated for a node in the middle of the sample in the following computations. For the isotropic test a similar simulation is done. The boundary conditions were, however, different. The deformation boundary conditions are the same, but the isotropic sample can not drain through the bottom drain to be able to measure the pore pressure generation during consolidation. The bottom boundary should therefore be modelled as a impermeable boundary. The resulting pore pressure distribution is shown in Figure 3.16.

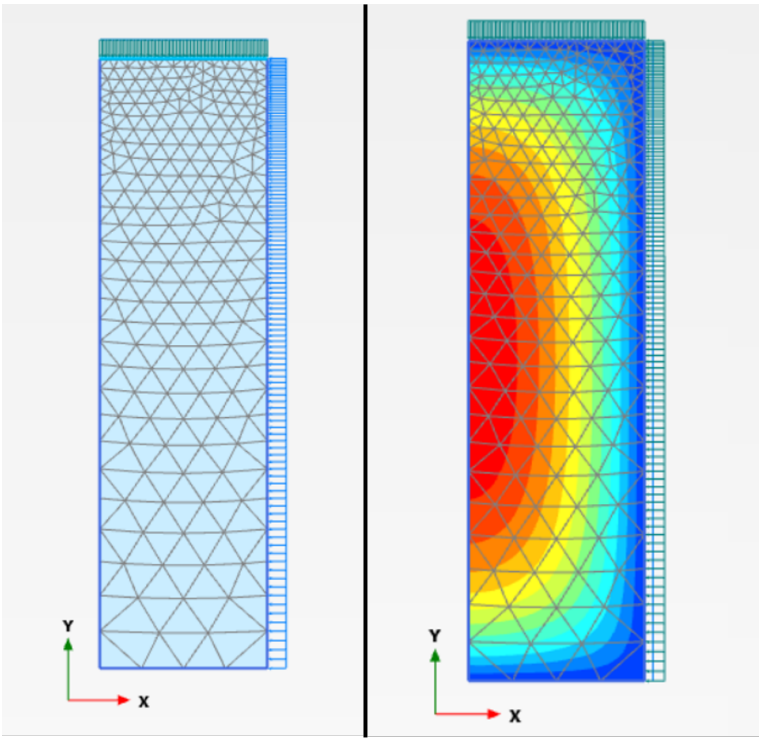

Figure 3.15: Left: The mesh of the Finite Element model. Right: Pore pressure in triaxial sample distribution during consolidation

Isotropic consolidation means application of stress increments from all directions uniformly. This is in practice done by increasing the cell pressure. This is often done rapidly, in the range of 3-5 kPa/hr, because the sample cannot fail as it is compressed from all sides. Deviatoric consolidation encompasses

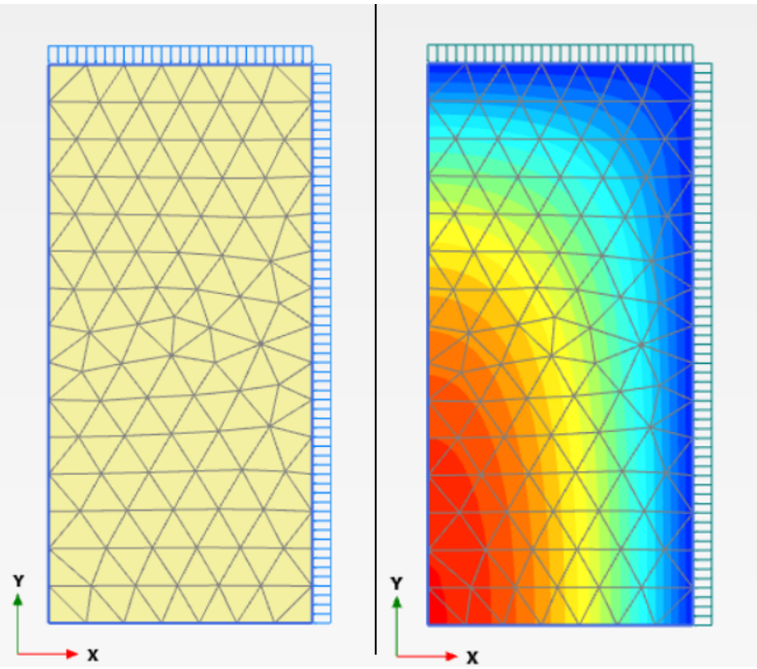

Figure 3.16: Left: The mesh of the Finite Element model. Right: Pore pressure distribution in isotropic sample during consolidation

application of deviator pressure only, a consolidation rate of approximately 3 kPa/hr in vertical direction is applied maximally according to the lab technician. Anisotropic consolidation is the application of unequal increments of vertical and horizontal stresses. This can be done K_0-seeking as explained above, or by applying a constant predefined K_0. In Figure 3.17 a comparison of pore pressure generation as a result from isotropic-, K_0- and deviatoric consolidation is shown. Equal vertical stress increments and stress application is used for the three loading modes, for both loading and unloading. It can be seen that isotropic consolidation (upper line) causes significantly larger pore pressure generation. As mentioned before is the isotropic loading rate however higher then the other loading modes. The difference between K_0 (middle line) and deviatoric (lower line) loading is much smaller. For unloading the excess pore pressure generation is much smaller. This is a result of stiffer behaviour for un/reloading of soils.

In Figure 3.18 the effects of consolidation rate are shown. The excess pore pressure for an anisotropic loading rate (in terms of cell pressure) of 1, 0.5 and 0.33 kPa/hr with predefined K_0. Obviously the highest loading rates results in the highest pore pressure. The sample does however not fail, even at loading rate of 1 kPa/hr.
In Figure 3.19 the excess pore pressure is shown as result of consolidation according to the stress path of triaxial test 2. This means isotropic compression until 20 kPa, deviatoric loading until K_0-line and finally K_0 consolidation until a pre-consolidation pressure of 120 kPa. A waiting time of at least 48 hours is obeyed. Then unloading to a stress of 32 kPa with a rate of 0.8 kPa/hr. Again a waiting time is applied before undrained shearing of the sample. Three constitutive models are used, namely: Creep S-Clay1S, the Deltares modification of Creep S-Clay1S and the Soft Soil Model. The results are nearly identical. For the computation a consolidation rate of 0.5 kPa/hr is used.
The sample does not fail under a consolidation rate of 1 kPa/hr (cell pressure increment) according to the Plaxis simulations. A significant amount of excess pore pressures is however generated. The lab technician also expected that a loading rate of 1 kPa/hr would be risky. Therefore it is decided to apply a loading rate of maximally 0.5 kPa/hr when applying K_0 loading. However K_0-seeking is not applied. Instead a K_0 value of 0.43 is applied in all tests.

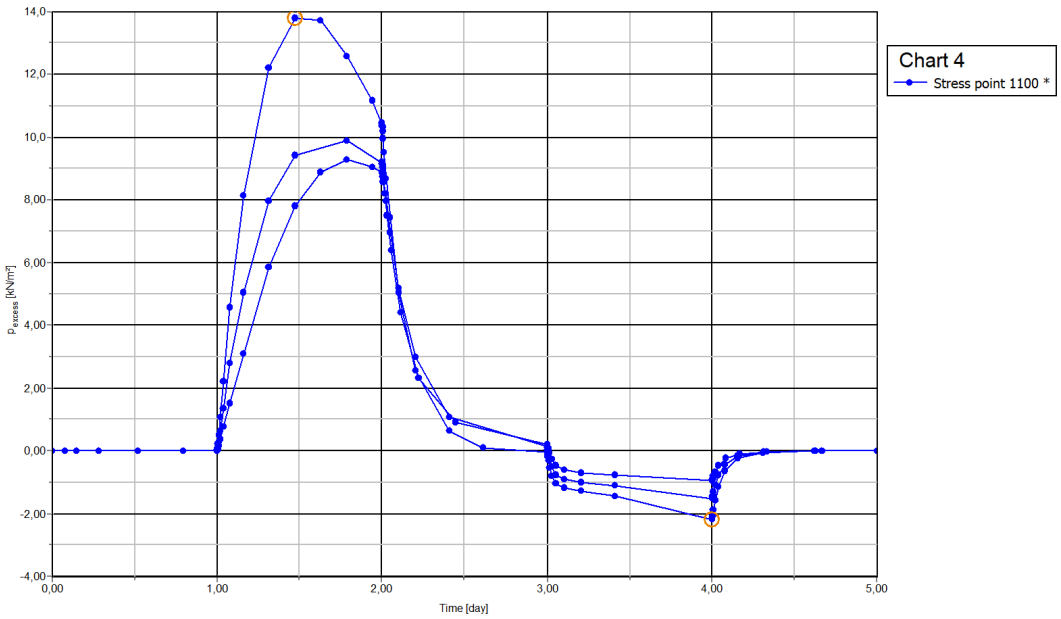

Figure 3.17: Comparison of excess pore pressure resulting from different consolidation modes

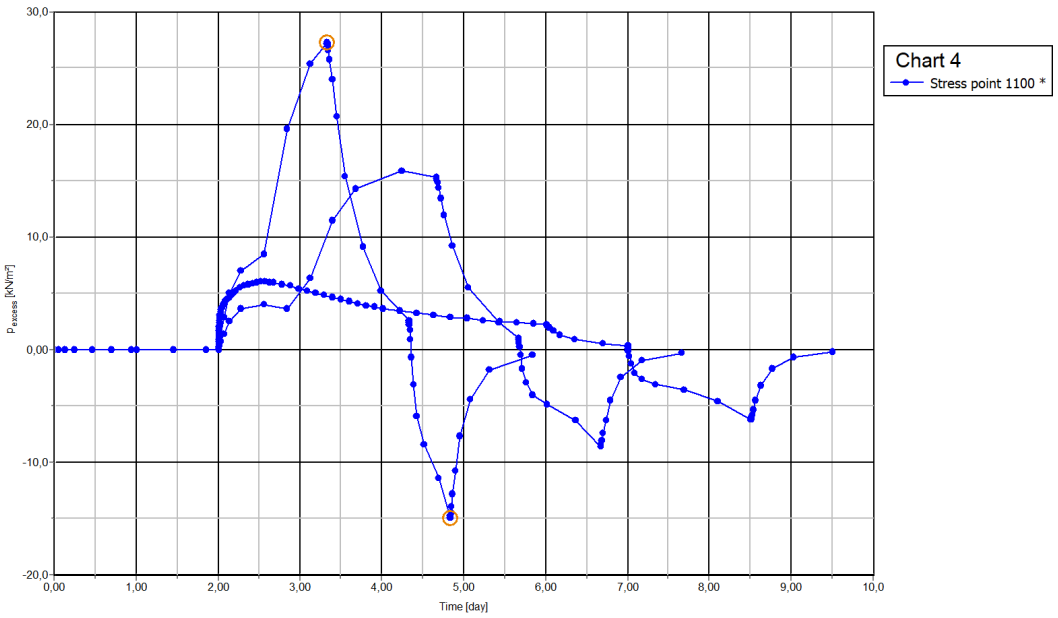

Figure 3.18: Comparison of excess pore pressure resulting from different consolidation rates

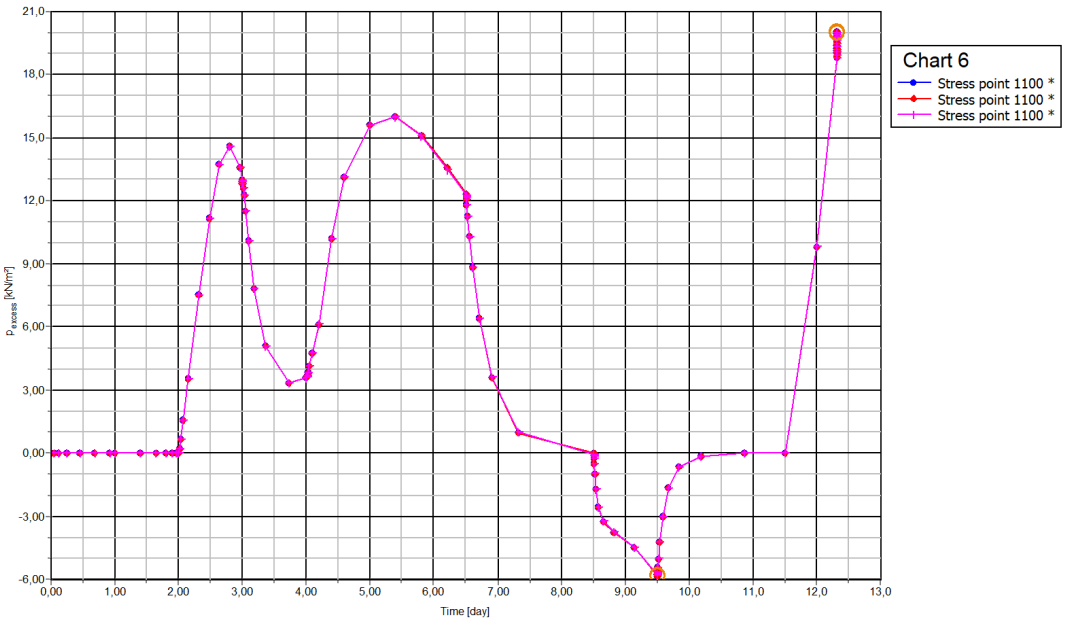

Figure 3.19: Excess pore pressure as a result of consolidation following stress paths of triaxial test 2

4

Results analysis

In this chapter the results of the laboratory tests are discussed. The results are placed in the CSSM framework and fitted to the SHANSEP equation. This is done by normalising the results as well as comparison to analytical equations. By doing so the results of both methods can be compared. Results from previous work on OVP clay is also used to compare the data too. However, the applied shear rate used during earlier research was 2%/hr while 1%/hr was used in the laboratory work of this thesis. Hence the triaxial data can not be compared on an equal basis, but forms a reference. Generally a faster shearing rate results in a higher undrained shear strength (e.g. [17]).

4.1. CSSM

CSSM does cover a very large ranges of soil behaviour. Many soil parameters are related to CSSM and linked to each other by equations from which numerous secondary relationships can be derived. But CSSM also provides of a precise description of soil behaviour under undrained conditions, as described in Section 2.5, to which the data is compared. The data is compared to CSSM by looking at the following features and relations:

1. Qualitative soil behaviour
2. $p' - q$ relationship i.e. M_c and M_e
3. $p' - e$ relationship i.e. NCL, CSL and K_0CL lines
4. MCC relationships.

4.1.1. Qualitative soil behaviour

In this section the soil behaviour observed in the triaxial tests is described. In order to compare the soil behaviour at different stress levels and OCRs the data is normalised. Normalising is a useful tool to obtain more insight in the relative soil behaviour. The data is normalised by p'_0 in line with CSSM, as well as by σ'_{v0} in accordance to the SHANSEP procedure. Which are the mean effective stress and vertical stress at the end of consolidation respectively.

The shape of the stress paths strongly depends on the amount of excess pore pressure that is generated. In Figure 3.11 the pore pressures during the shearing phase are displayed for each test. The NC samples remain constant after the maximum excess pore pressure is reached. Remarkable is a small increase in Δu of trx 3. The OC samples show a large decrease in pore pressure after the peak. This can be explained by dilation. The peak is more distinct for larger OCRs. In Figure 4.1 Δu is normalised by p'_0. In Figure 4.2 Δu is normalised by σ'_{v0} . When comparing the two figures it is evident that Figure 4.2 shows a clearer pattern. The position of the samples relative to each other in the graph perfectly ranked by OCR for the complete range of axial strain. The fact that trx 1 and 3 do not coincide is remarkable. Figure 4.1 gives an unclearer result. The lines of all samples cross each other at different strain levels. In Figure 4.3 is the Skempton A factor shown as function of strain.

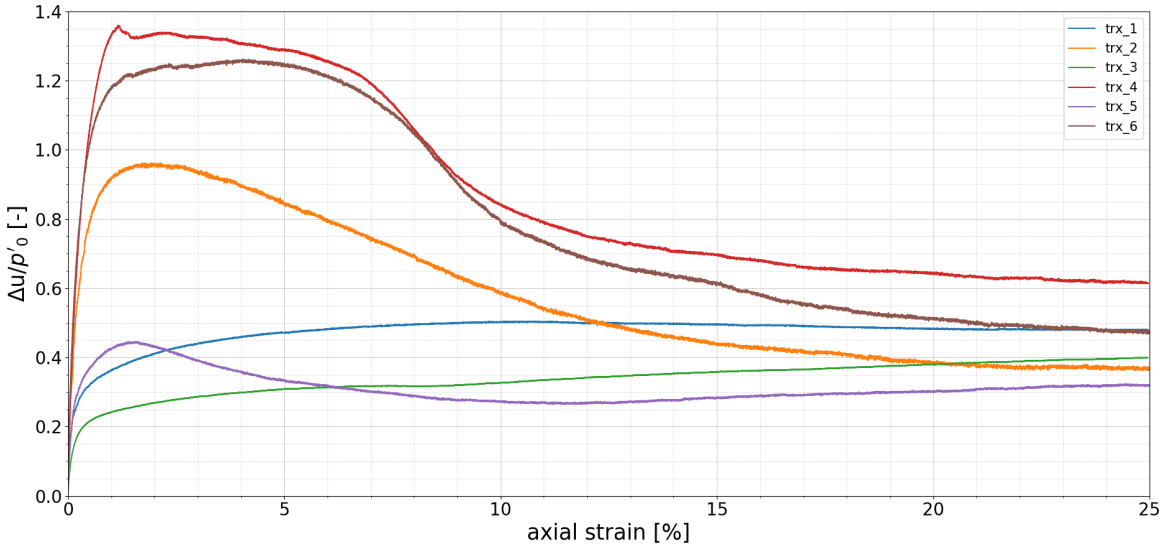

Figure 4.1: Excess pore pressure normalised by p'_0 as a function of strain

Table 4.1: Skempton parameters and back pressure of triaxial tests.

Sample	Initial B-factor [-]	Backpressure [kPa]	Final B-Factor [-]	A-factor [-]
trx 1	0,76	300	1,00	4,33
trx 2	0,75	300	0,97	0,13
trx 3	0,82	300	1,00	4,95
trx 4	0,84	300	0,98	0,16
trx 5	0,72	300	0,98	0,19
trx 6	0,84	300	0,98	0,13
trx 7	0,4	400	0,98	0,46
trx 8	0,83	400	0,97	0,10

Skempton's A-factor is the magnitude of pore pressure increment relative to the increment in deviator stress during shearing. The larger A the more plastic is the behaviour of the soil. Skempton's B-factor is a measure of saturation. Before starting a triaxial tests a B-factor of at least 0.97 has to be reached. As expected do the NC samples reach a larger A value than the OC samples. There is however no trend visible with OCR. In Table 4.1 the Skempton parameters at ultimate state for samples 1 to 6 and at peak strength for samples 7 and 8 are summarised.
In Figures 4.4 and 4.5 similar trends in deviator stress are visible. Normalisation by p'_0 gives an unclearer image then normalisation by σ'_{v0}. Trx 1 and 3 plot nearly on the same line in Figure 4.5, which was not the case for Δu.

In Figure 3.9 the effective stress paths of all compression triaxial tests are shown. The NC samples show behaviour comparable to the behaviour that is theoretically expected and shown Figure 2.8. Trx 1, however, crossed the failure line before reaching ultimate state already while trx 3 approached the failure line, then bends and follows the failure line until ultimate state. The shape of the stress paths of the OC samples, however, is not as expected. At small strains the stress path run rather diagonal. Theoretically the stress paths are expected to run much more vertical upwards, as shown for example in Figure 2.9. A trend is visible in the length of the stress path that is traveled before the stress path bends towards the failure line. This is illustrated in Figure 4.6. Where the stress path are shown in normalised $p' - q$ space. There is however normalised by p'_c, the maximum p' reached during consolidation, instead of p'_0. The x-axis then represents the inverse of R_0. The figure shows clearly that the larger the OCR the longer the stress path traveled before the first buckling point. At larger strains trx 4 and 6 and trx 2 and 5 show similar behaviour. Trx 4 and 6 show an extra bend in the

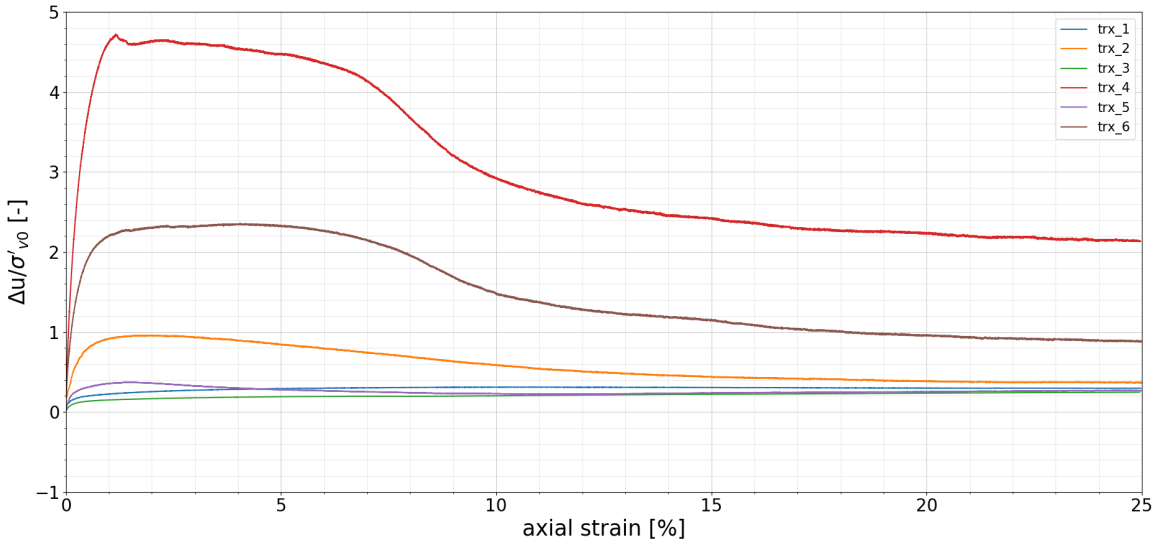

Figure 4.2: Excess pore pressure normalised by σ'_{v0} as a function of strain

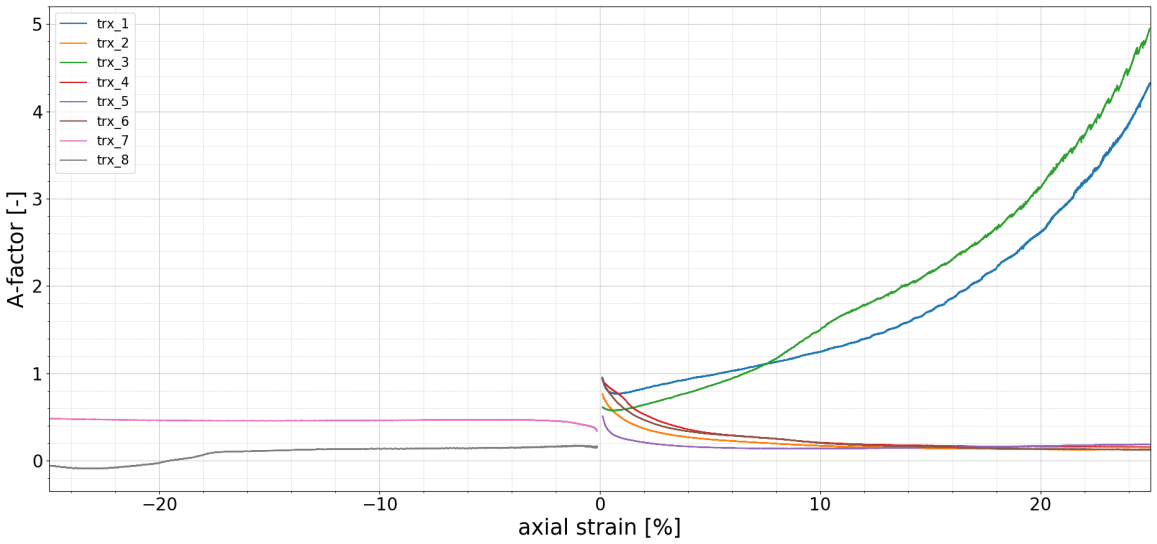

Figure 4.3: Skempton A parameter as a function of axial strain

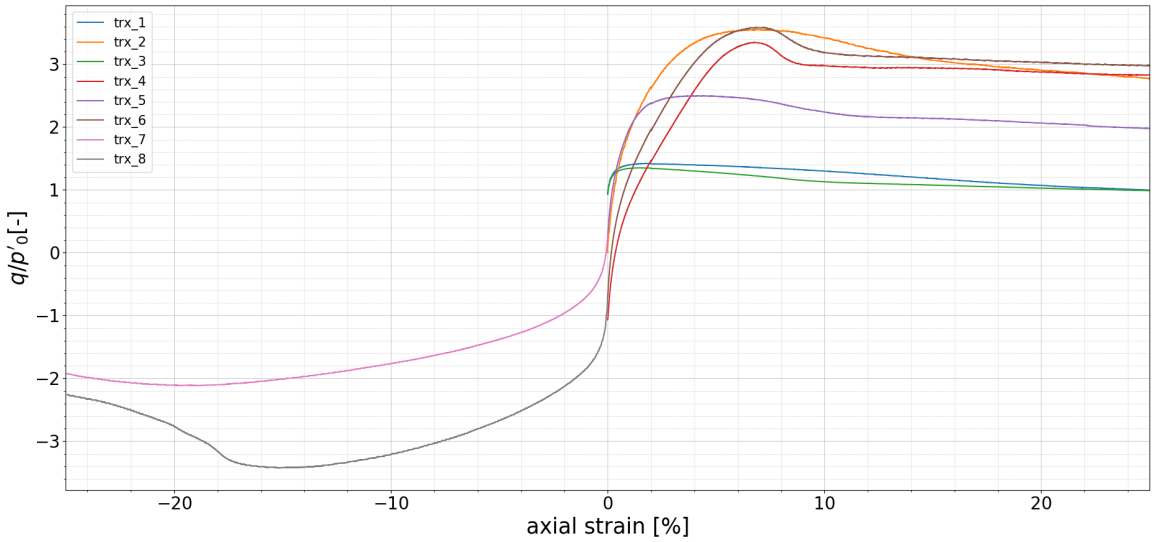

Figure 4.4: Deviator stress normalised by p'_0 as a function of strain

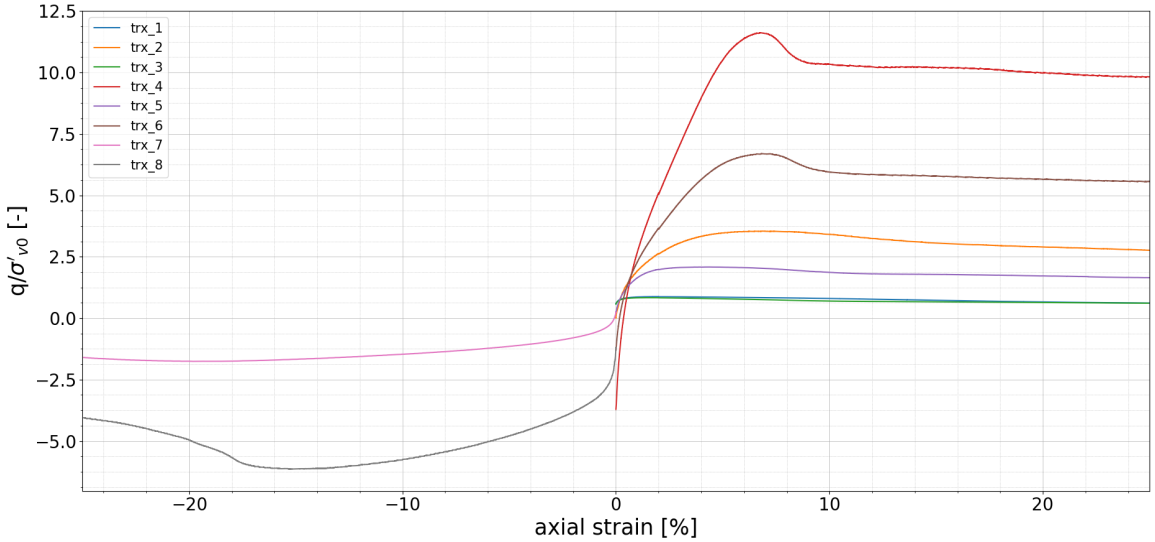

Figure 4.5: Deviator stress normalised by σ'_{v0} as a function of strain

stress path that is followed. While trx 2 and 5 directly bend towards the failure line. One of the reasons can be the failure mechanism; trx 2 and 5 developed one shear band while trx 4 and 6 developed two shear bands during shearing. The shape of the stress paths is probably strongly influenced by the laboratory tests and does not represent intrinsic soil behaviour. The starting points of the stress paths lie not completely on a straight line. This is caused by a disturbance in the unload phase of trx 2 and 4 as described in Chapter 3.2.1.

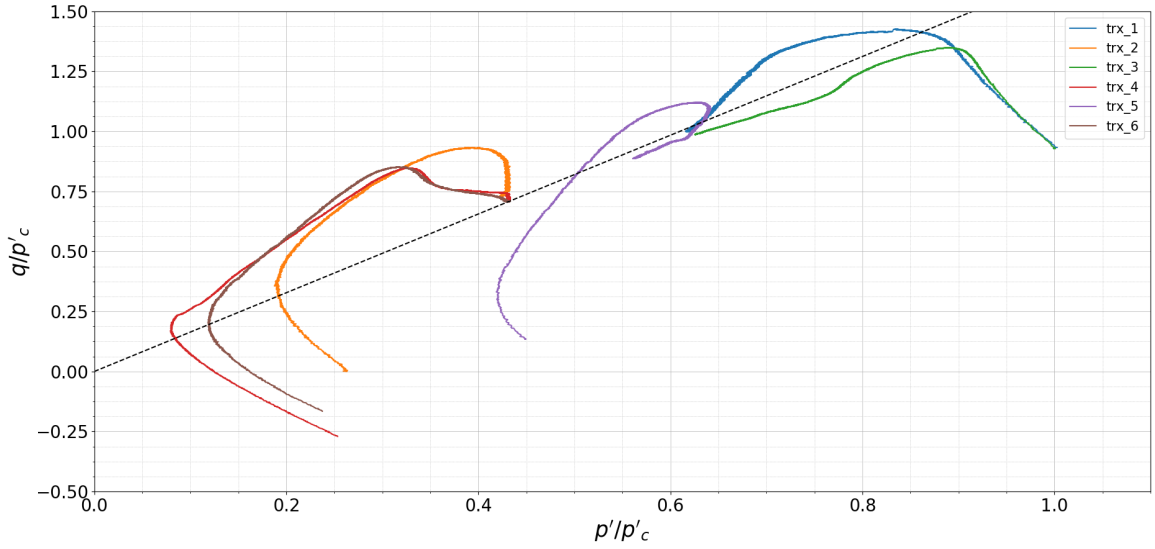

Figure 4.6: Stress paths of triaxial compression tests in $p' - q$-space normalised by p'_c

When comparing the normalised results it can be concluded that normalising by σ'_{v0} gives more satisfying results. The normalised results perfectly show the effect of OCR at ultimate state as well as during the complete shearing phase. The results normalised by p'_0 are unclearer. p' is a more complex parameter which entails more information on the stress conditions than σ_v. p' entails both σ'_v and σ'_h and thus also depends on K_{ur} which is directly dependent on the Poisson's ratio ν_{ur}. Under K_0-consolidated conditions, especially when analysing over-consolidated samples, normalisation by σ'_{v0} is more convenient than normalisation by p'.
In Figures 4.7, 4.8 and 4.9 the $p' - q$ plots of the triaxial samples including the MCC yield surface and stress paths are shown. The MCC model predicts a completely different stress path for the NC samples. Much less increase in deviator stress is predicted. p' at failure is however predicted to be larger and thus the reached S_u too. In Figure 4.8 is clearly indicated that the MCC stress path do not show strain softening and therefore overestimates S_u. The yield surface of triaxial sample 2 is nearly reached by the actual stress path. The yield surface of sample 4 is, however, not nearly reached. Samples 5 to 8 are all consolidated to the same pre-consolidation stress of 150 kPa. But since M_c and M_e are different is the yield surface also different, as shown in Figure 4.9. In compression the yield surface describes the limits of the stress paths rather well. Again S_u is not well predicted because softening is not modelled. In extension the yield surface is very inaccurate, the peak strength is however well predicted by the critical state from the MCC computation.

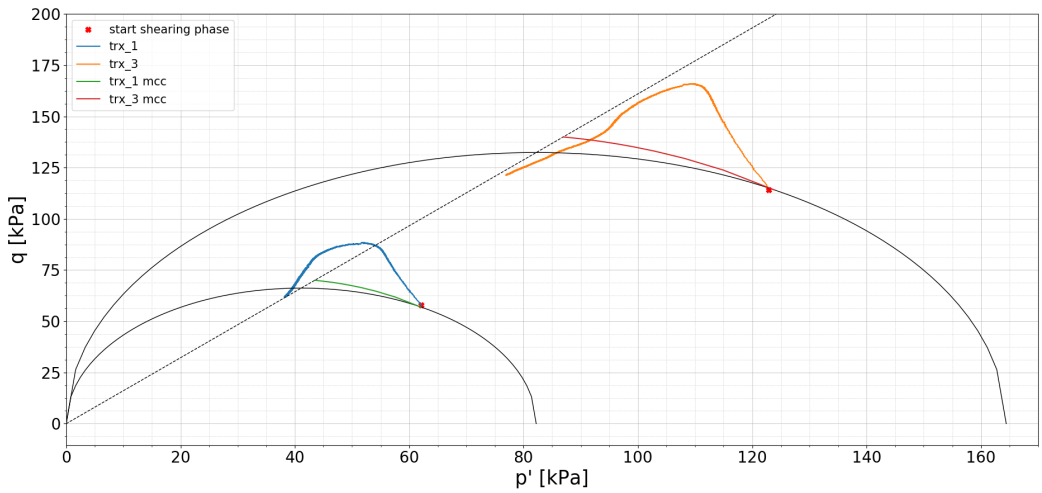

Figure 4.7: $p' - q$-plot of the NC triaxial samples including MCC yield surface and stress path

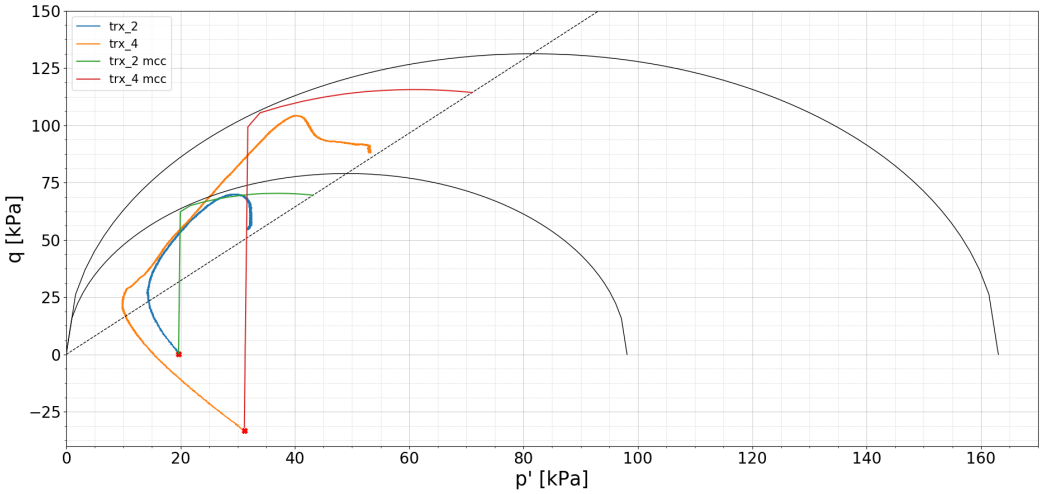

Figure 4.8: $p' - q$-plot of triaxial samples 2 and 4 including MCC yield surface and stress path

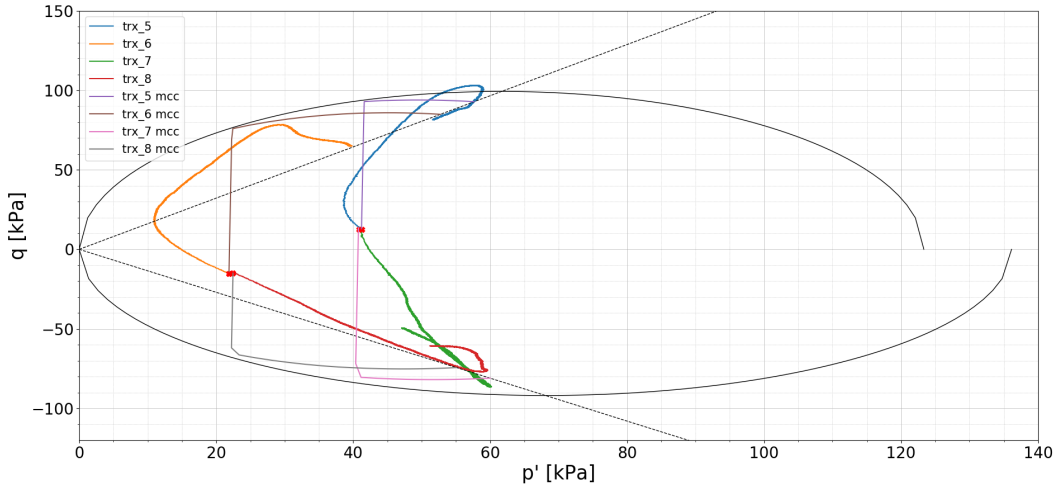

Figure 4.9: $p' - q$-plot of triaxial samples 5 to 8 including MCC yield surface and stress path

4.1.2. M_c

As explained in Section 2.3, there are several definitions of failure and thus of undrained shear strength. Three definitions are looked at during the analysis of the results, these definitions are listed in Section 2.3. At these three definitions of failure an M_c value is determined, this is shown in Figure 4.10. Linear fits through the origin are computed. M_c is represented by the coefficient shown in the separate graphs. The figure clearly shows that only at ultimate state the results are consistent. At peak strength and maximum p'/q ratio the data points are far off the fitted line. Also is the R^2-value small. The average value of M_c at ultimate state for the six triaxial compression tests is determined to be 1.61. Which is slightly lower than 1.66, which was determined from earlier research on OVP clay.

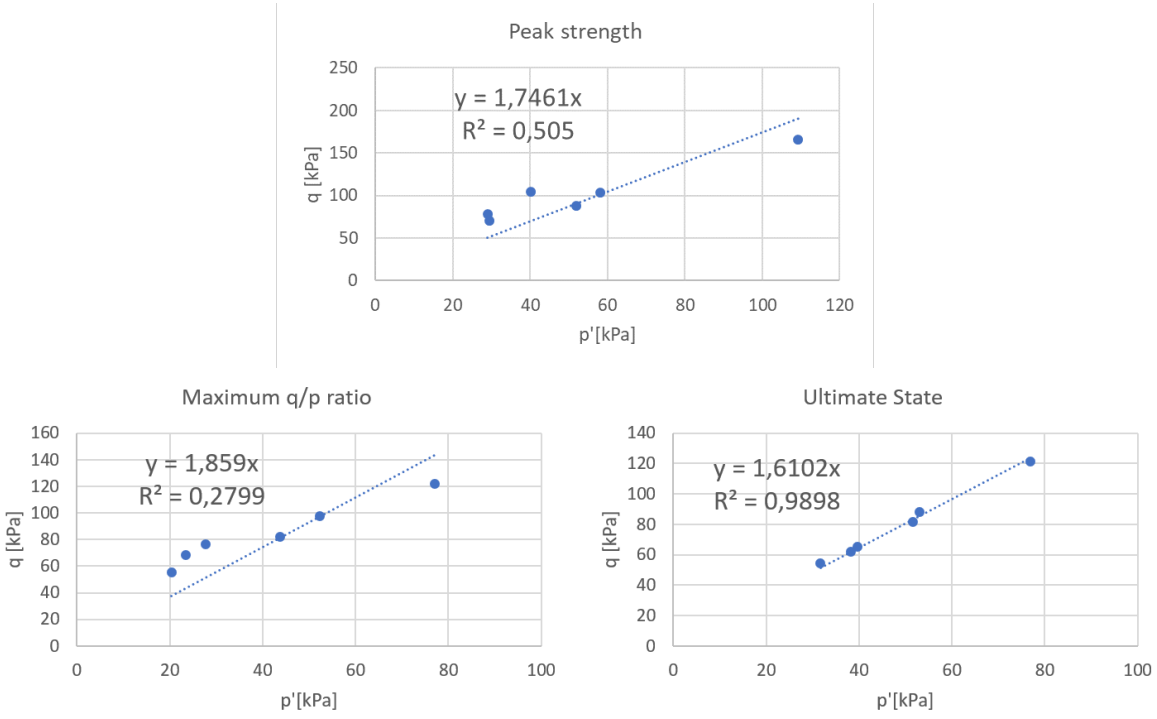

Figure 4.10: M_c fitted through three definitions of failure

The critical state friction angle ϕ_{cs} can be related to M_c as shown below in Equation 4.1 ([28]) and is 40.1°.

$$M_c = \frac{6 \cdot sin(\phi)}{3 - sin(\phi)} \tag{4.1}$$

4.1.3. M_e

Besides the triaxial compression tests, extension tests are executed and analysed as well. Again the different definitions of failure are analysed and shown in Figure 4.11. Since the number of extension tests that are executed is limited to two tests, data from previous research is also included in the graph. As mentioned earlier are those tests executed using a shear rate of 2%/hr instead of 1%/hr. The comparison is therefore not completely equal but gives a good indication.
The figure illustrates that, in contrast to the compression test, the maximum q/p' ratio results in the best fit. Maximum q/p' ratio nearly coincides with peak strength. Peak strength is a more common and intuitive definition of failure and M_e at peak strength is thus displayed in $p' - q$-plots. In all previously executed extension tests necking was observed. In trx 7 a shear band was observed, however to a relatively small extent. The stresses are therefore not corrected. Trx 8 mainly showed a shear plane and not so much necking. In Figure 4.12 the stress paths during shearing of all extension tests are shown. The ultimate states are therefore not representative. At ultimate state q, p and Δu far from stable. The corresponding graphs and pictures are shown in Appendix A. The results of the previously executed work can be found in [31]. The peak strength and maximum q/p' ratio failure point do show

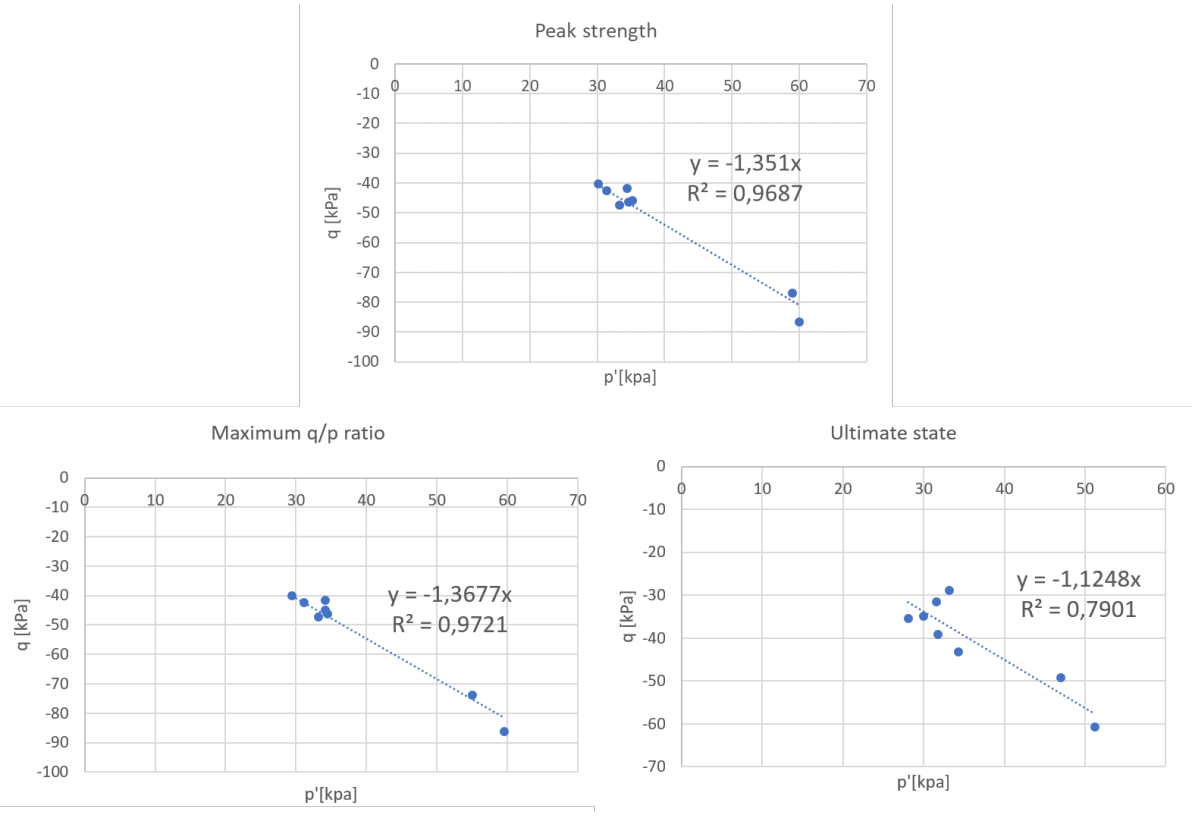

Figure 4.11: M_e fitted through three definitions of failure

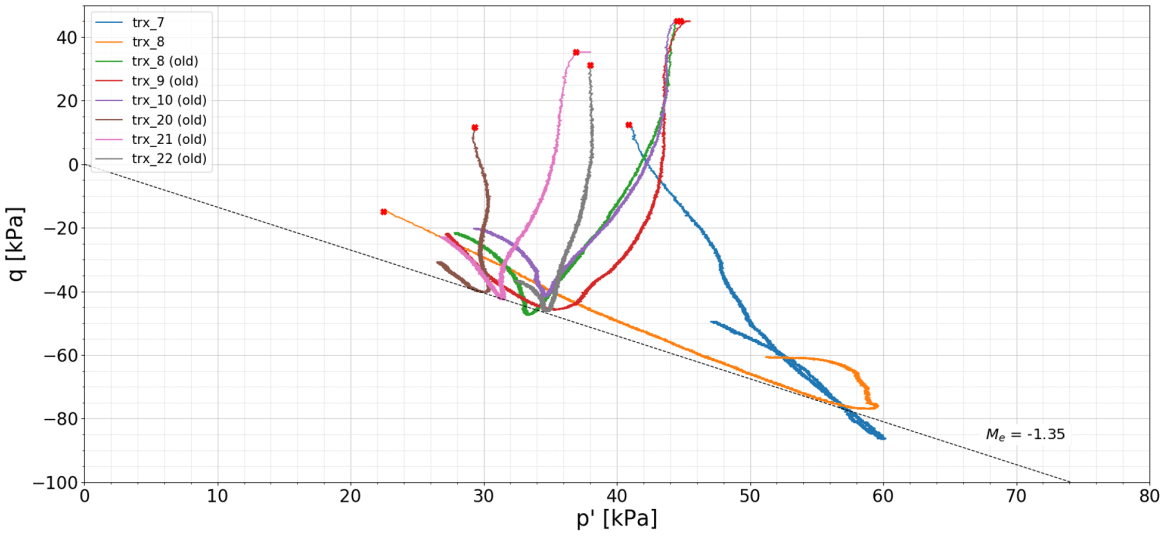

Figure 4.12: Stress paths of all available extension tests plotted in $p' - q$-space

a rather good fit. Maximum q/p' ratio has even a slightly better R^2 value than the peak strength. Trx 7 is furthest off the fitted lines, also in $p' - q$-space sample 7 is furthest of the M_e-line, as shown in Figure 4.12. Despite the not having the best fit, M_e at peak strength is used to determine the friction angle. M_e is determined to be 1.35, corresponding to $\phi = 33.5°$. The ratio $M_e/M_c = 1.35/1.61 = 0.84$ is larger than the ratio found previously (0.79) [31]. Following the Mohr-Coulomb criterion M_c/M_e is

([28]):

$$M_e/M_c = \frac{3 - sin(\phi)}{3 + sin(\phi)} \tag{4.2}$$

This results in a ratio of 0.65 for ϕ found in compression or a ratio of 0.69 for ϕ found in extension. However, M_c was determined at ultimate state while M_e was determined at peak strength. When only using the data that was gathered for this thesis and ignoring the other available data very similar values and a similar trend is found.

4.1.4. Compression and recompression indices

A fundamental assumption of CSSM is a logarithmic decline of void ratio with isotropic compression. The parameters for describing the CSL, ICL and K_0CL can be derived in different ways. As described in Section 2.4, the lines are parallel and thus is the slope of all three lines described by λ. To describe the three lines completely also the intercept of the line with p' = 1 kPa needs to be determined. This intercept of the CSL, ICL and K_0CL is represented by Γ, N and N_0 respectively. Γ can only be derived from the triaxial test data, N from isotropic compression test data and N_0 from both K_0-CRS and triaxial test data. However, by assuming the yield surface of the Modified Cam clay model, N_0 can be calculated from N and vice versa, the parameters calculated assuming the Modified Cam clay model are indicated by *. This is done following the method described in [7].
The CSSM parameters λ and κ are derived from different tests to be able to compare the results and fit the data eventually to shear strength calculations. λ is determined in three ways, namely from:

- one-dimensional compression in K_0-CRS test
- one-dimensional compression in triaxial test
- isotropic compression in triaxial apparatus

The determination of CSSM compression parameters from the K_0-CRS test results is explained and shown in Chapter 3.3.2.

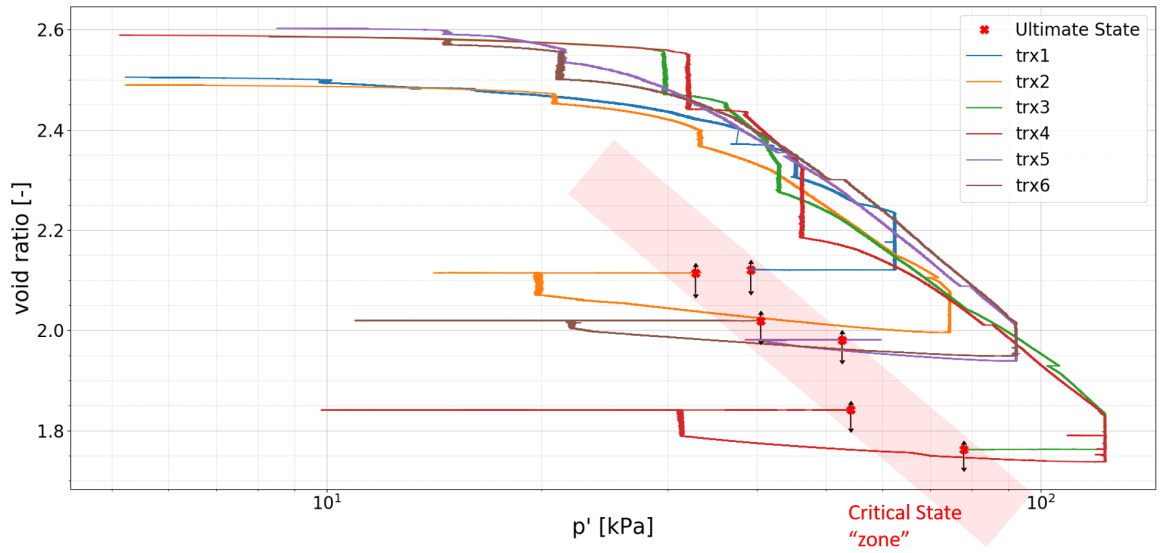

Figure 4.13: Void ratio as a function of p'

The failure points do not fit on a exact CSL line. A critical state "zone" is fitted to the data that includes error bars. The width of this critical state zone is approximately 20 kPa isotropic stress. This critical state 'band' is parallel to the compression line.
The determination of above mentioned parameters from the triaxial tests is done based on the results presented in Figure 4.13. The void ratio is determined based on the water extortion recorded during the triaxial test and not based on the water content measurement done after the test, which is the

usual practice. This is done to have a consistent recording of the void ratio during consolidation. The consolidation of the samples show a similar trend as the K_0-CRS tests. The consolidation lines are however disturbed by the fact that the consolidation was not constant. As described in Chapter 3 the consolidation started isotropically after which K_0 consolidation started. Also the consolidation of some of the samples was interrupted. At large stresses all stress paths converge towards a constant value of approximately $\lambda = 0.51$. λ and κ are also determined from the isotropic test. The average liquid limit of OVP clay that was determined during previous research results in a void ratio of 3.82. This is rather near the values of Γ that were found. One would however expect that it would be an approximation of N instead of Γ. The results are summarised in Table 4.2. It should be noted that void ratio e is used instead of specific volume v. From the table can be concluded that the the K_0-CRS tests and the isotropic consolidation test give nearly identical results for the compression parameters, Γ, N_0 and N differ quite much. The triaxial tests result in slightly higher values of λ, Γ, N_0 and N. The K_0-CRS test is a better representation of the actual soil behaviour. During the triaxial tests K_0 and K_{ur} are namely imposed on the samples. The boundary conditions imposed by the test type differ for the three tests that are compared. In Chapter 4.1.6 a correction factor for conversion between isotropic and 1D unload/reload parameters is explained. Applying this factor to the K_0-CRS results in $\kappa = 0.07$. Remarkably does not applying the correction factor result in a better agreement between the isotropic test and K_0-CRS test. The differences are however small.

Table 4.2: Overview of CSSM parameters determined in different ways

test	λ	κ	Γ	N_0	N	Λ
K_0-CRS	0.44	0.06	3.87*	3.96	4.14*	0.86
Triaxial test	0.51	0.05	3.93	4.22	4.35*	0.92
Isotropic compression test	0.43	0.06	3.78*	3.92*	4.04	0.86

Several factors contribute to the uncertainty of the $p' - e$ relation. The uncertainty of $p' - e$ is relatively much larger than the uncertainty of the $p' - q$ relationship. The contributing factors are discussed below. Pore pressure is not measured during the consolidation phase which makes it impossible to determine the effective stresses. As a result actually not effective means stress p' is shown in Figure 4.13 but total means stress p. The consolidation rate is chosen such that the development of excess pore pressure is limited. Still does this cause a small inaccuracy in the determination of the K_0-consolidation line. Another phenomenon that effects the $p' - e$ relation is creep. Creep causes a continuous small decrease in void ratio. Due to creep the stress paths move away from the K_0CL line during relaxation. This is clearly visible in the figure. As mentioned in Chapter 3 the void ratio determination is prone to errors. An error calculation is performed to estimate the uncertainty of the relations that are established based on the void ratio. The void ratio at the end of the triaxial tests is calculated based on the void ratio at the start of the tests and the water extrusion that is measured by the triaxial apparatus during the test, the steps are indicated in Table 4.3. At the start of the tests the void ratio is measured conform ISO standards. The void ratio can be calculated from the water content by assuming a particle density. From earlier research the absolute uncertainty of $\pm$ 0.135 kN/m^3 is calculated. From the dimensions of the triaxial sample the volume of solid particles and the volume of water can be determined. The volume of solid particles remains constant but the volume of water can be determined from the initial volume of water and the water extrusion. After shearing a significant amount of water is trapped between the sample and the membrane and is contained in the drainage strips and porous end platens of the triaxial apparatus. This water is extruded but not captured in the void ratio determination. Together this "uncaptured" water is estimated to add up to 4 mL of water. Void ratio determination based on the water content after the test would entail a similar error. The total amount of "uncaptured" water probably increases during the test the uncerainty therefore increases during the test as well. Possibly is most of the "uncaptured" water extruded during shearing, but not drained from the sample since the drains are closed during shearing. There cannot be a negative amount of "uncaptured" water, the maximum relative error is therefore +2.0% in void ratio but ranges from -0.6 to +2.0 %, which resembles -0.01 to 0.04 unit less value of void ratio. Which is approximately 10% of the change in void ratio during a triaxial tests. The relative errors are based on triaxial sample 1 and differ from test to test but are expected to be very near the values indicated in the table. From Table 4.3 it can be concluded that the inaccuracy in the void ratio is mostly caused by the inaccuracy

of the determination of expelled water after the test. The complete width of the critical state band, as shown in Figure 4.13, is however larger. Not finding a unique p'-e relation can thus not be completely explained by the inaccuracy of the void ratio determination.

Table 4.3: Error propagation of void ratio determination

Step	Absolute error	Relative error	Cumulative relative error
Water content determination	$\pm$ 0.015 gr	$\pm$ 0.07%	$\pm$ 0.1%
Void ratio calculation from water content	$\pm$ 0.135 kN/m^3	$\pm$ 0.58%	$\pm$ 0.6%
Sample volume determination	$\pm$ 0.15 mm	$\pm$ 0.25%	$\pm$ 0.6%
Void ratio calculation at the end of triaxial test including water extrusion	+4.3 mL	+ 1.88%	+ 2.0%

4.1.5. 3D p'-q-e relation

A fundamental relationship that can be derived from CSSM is the unique $p' - q - e$-relationship. As explained in Chapter 2.4 p' is linked to void ratio. p' is in turn related to q. The figure shows the stress paths of the compression tests in 3D. The critical state line is also plotted in the figure. The CSL fits rather well through the ultimate state points of the stress paths. The line does not fit perfectly but the shape clearly resembles Figure 2.6. A html file containing a interactive 3D plot is attached. The file contains a $p' - q - e$-plot including MCC yield surfaces and MCC stress paths.

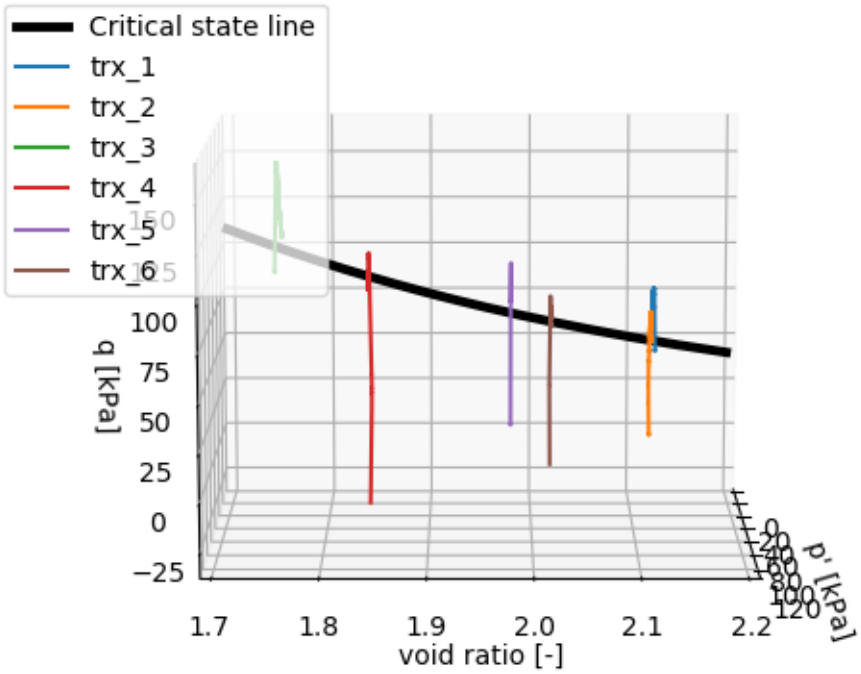

Figure 4.14: interactive figure of 3D p'-q-e plot (click on figure for movement)

4.1.6. MCC relations

From the fundamental relations of CSSM numerous useful equations can be derived, these equations are explained in Chapter 2.7. Firstly the normally consolidated samples are compared to Equations 2.9 and 2.18. Equation 2.9 can be directly derived from the fundamentals of CSSM while Equation 2.18 is derived from the MCC model. The MCC model in Plaxis does not distinguish between M at compression and extension. The results are computed using the same equation and numerical computations but entering an M value of 1.35 instead. The normalised undrained shear strength of the NC samples that is computed is compared to the laboratory data and shown in Table 4.4 below. Γ is chosen to be equal to the void ratio at the liquid limit. Γ determined from the different laboratory tests gave inconsistent results. Also is the liquid limit is a commonly determined parameter for clays.
From Table 4.4 it can be concluded that Equation 2.9 overestimates S_u/σ'_{v0} in compression while S_u/σ'_{v0} is underestimated in extension. Also Equation 2.18 overestimates S_u/σ'_{v0} in compression. In extension, however, a S_u/σ'_{v0} is well predicted. The laboratory results show a rather large deviation.
Besides the normally consolidated samples also over consolidated samples are compared to the MCC equations. The results of Equation 2.20 are plotted in Figure 4.18 and 4.19. The results for the normally consolidated samples are equal to the results obtained through Equation 2.18 that are shown

Table 4.4: Comparison of MCC equations for normally consolidated samples

		TRX 1	TRX 3	TRX 8 (old)	TRX 9 (old)	TRX 10 (old)
Laboratory results		0,31	0,30	0,32	0,31	0,28
$\frac{s_u}{\sigma'_{v0}} = \frac{M}{2*\sigma'_{v0}} * exp(\frac{\Gamma - e_0}{\lambda})$	(Eq. 2.9)	0,37	0,35	0,27	0,28	0,27
$\frac{s_u}{\sigma'_{v0}} = \frac{M}{2} * (\frac{\eta_0^2 + M^2}{2M^2})^{\Lambda} * \frac{1+2K_0}{3}$	(Eq. 2.18)	0,35	0,35	0,32	0,32	0,32

in Table4.4. Besides computation of S_u through application of the MCC equations, also Plaxis is used. The consolidation path of the triaxial tests are simulated in the Soil Test module. Parameters are used as determined from the K_0-CRS tests as reported in Table4.2. The K_0-CRS test parameters are used because these are actual independent 1D consolidation parameters, while during the consolidation process of the triaxial samples a certain stress path was imposed. These stress paths are chosen such that they simulate 1D consolidation but are not independent like the K_0-CRS test parameters. The model input parameters are summarized in Figure 4.15. A small difference can be observed between the PLAXIS computed results and the implementation of Equation 2.18 at larger normalised strength values. The largest difference is 1.44% and is probably this difference is caused by rounding errors.

Material set	
Identification	MCC
Material model	Modified Cam-Cl
Stiffness	
λ (lambda)	0,4400
κ (kappa)	0,06000
ν'_{ur}	0,2100
e_{init}	2,510
Strength	
M	1,610

Figure 4.15: Soil parameters implemented in the PLAXIS MCC element test

One of the reasons the results are overestimated is the value of κ. It is determined from 1D unload/reload parameter RR as described by Equation 2.13. Even though this is common practice, e.g. shown in [15] [29], this method is not correct. RR is based on $log(\sigma'_v)$ while κ is based on $ln(p')$. Which means that there is a factor $ln(10)$ difference. This is however only true when the ratio of σ'_v and σ'_h, K, is constant, as is the case during virgin compression and the sample is thus normally consolidated. As soon as unloading starts, the ratio K starts to change. This is clearly indicated by Figure 4.17. As a result an additional correction factor should be included to the equation that contains OCR and R_0 to determine κ correctly. The above becomes clear when plotting the results of the K_0-CRS tests on a p' and σ'_v scale simultaneously, as is shown in Figure 4.16. The figure shows clearly that in the NC window the lines run parallel but in the OC window the slopes not only curve upward with decreasing pressure, which means that the unload parameters are stress dependent, but also the two lines run no longer parallel.

As presented by [27], recalculation of κ from RR, including an additional correction factor that corrects for the above described phenomenon can be done as follows:

$$\kappa = \frac{RR * (1 + e_0)}{ln(10)} * \frac{ln(OCR)}{ln(R_0)} = \frac{RR * (1 + e_0)}{ln(10)} * \frac{ln(OCR)}{ln(\frac{(2*K_0^{NC}+1}{(2*K_0^{NC}+1) - (1 - \frac{1}{OCR}) * (2 * \frac{\nu_{ur}}{1-\nu_{ur}+1}}))} \tag{4.3}$$

Including the correction factor shown above increase the value of κ which in turn lowers the value of

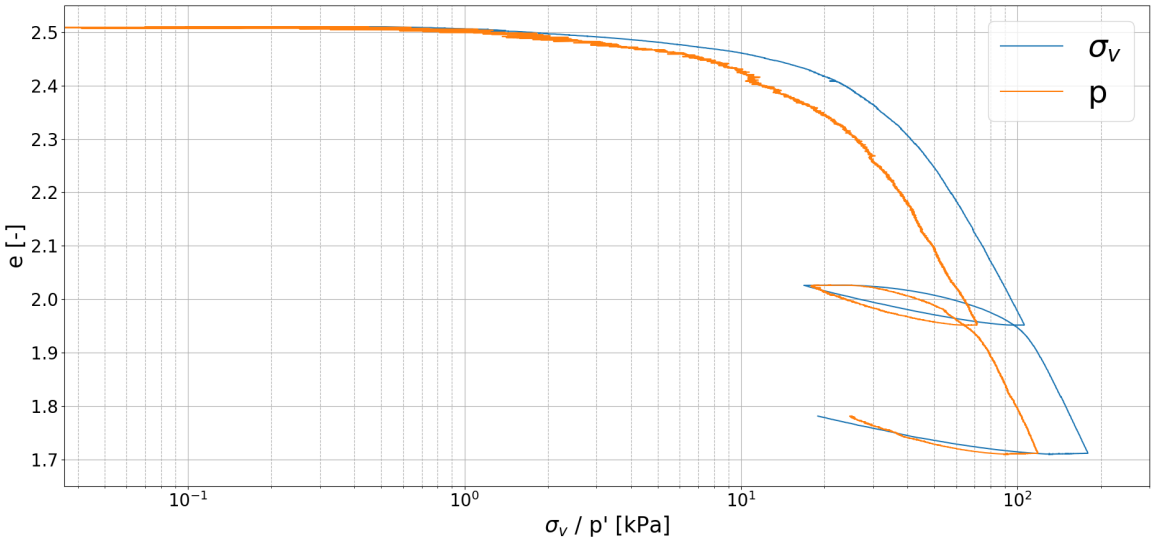

Figure 4.16: Void ratio versus p' and σ'_v simultaneously

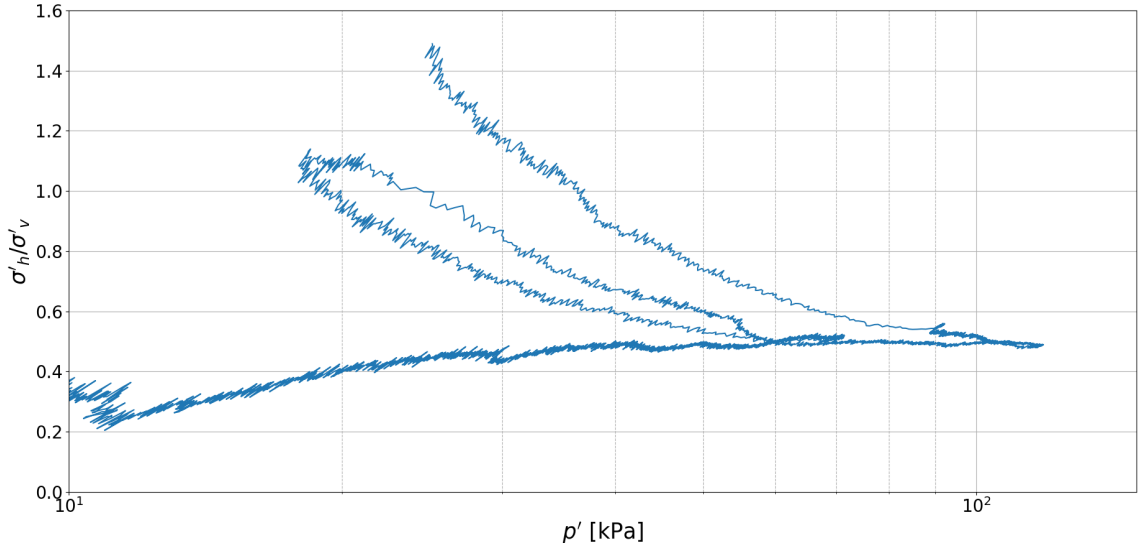

Figure 4.17: Ratio $K = \sigma'_h/\sigma'_v$ as a function of isotropic mean stress

Λ in Equation 2.18. Resulting in lower values of normalised shear strength. Equation 4.3 does relate κ and C_s ,determined from Figure 4.16, with a deviation of only 1%, which is probably the result of rounding errors. Thus Equation 4.3 seems to be valid. However, when applying the correction factor to the results presented in Table 4.2 the difference in results fall within the inaccuracy range.
The figure shows that in compression the MCC model overestimates the normalised shear strength of all the samples, also when the correction factor is included in the calculation. The degree of overestimation increases with increasing value of normalised shear strength. For extension, however, the uncorrected results predict S_u/σ'_{v0} well. Correcting κ results in an underestimation of S_u/σ'_{v0}.

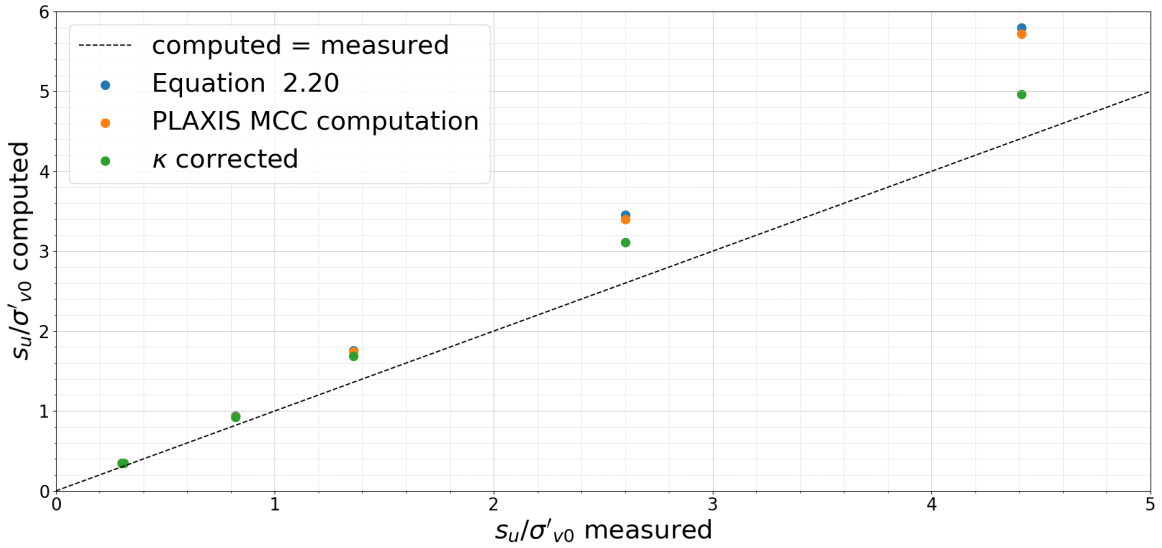

Figure 4.18: Measured S-ratio vs. computed S-ratio of triaxial compression by Equation 2.20

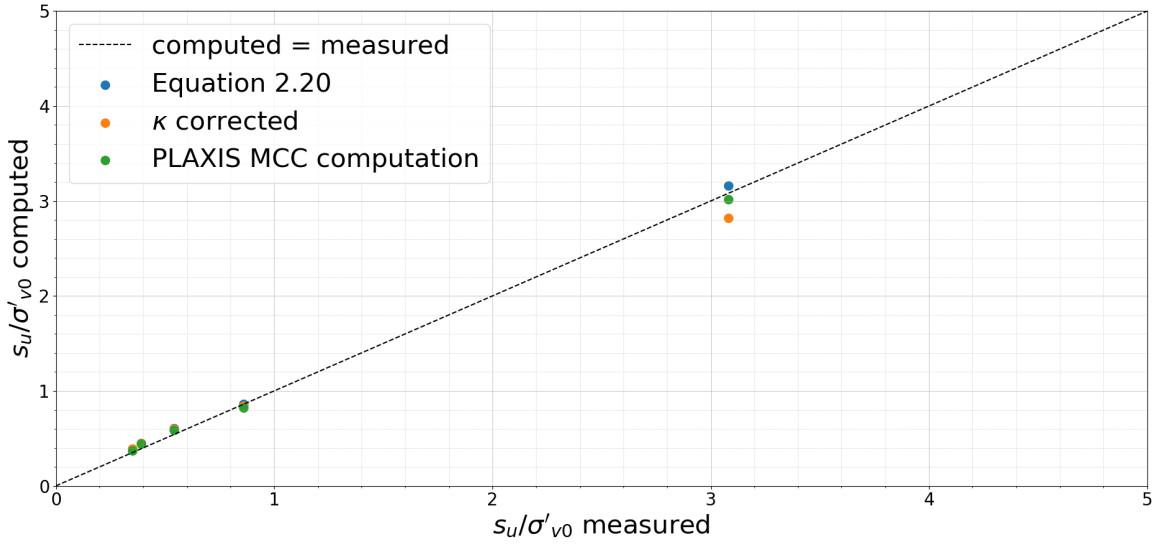

Figure 4.19: Measured S-ratio vs. computed S-ratio of triaxial extension tests by Equation 2.20

4.2. SHANSEP

The most relevant feature of the SHANSEP method, concerning macrostability, is the relation between OCR and normalised undrained shear strength. A power function is fitted through the data using Excel. Again the three definitions of shear strength are analysed. In Figure 4.20 the results are shown. For all three definitions of shear strength and for both compression as well as extension a similar trend is visible and a rather good fit is obtained. The point at an OCR of 20 seems to be furthest off the trend line for all the graphs. At such a high OCR the the trend line underestimates the S ratio and thus the shear strength. Which suggests that the m-coefficient should increase at large OCR. However, When looking at the unload-reload graph determined from the K_0-CRS tests (Figure 4.16), RR and κ to a greater extent even, increase slightly at large OCR. As a result the plastic volumetric strain ratio decreases, instead of increases. WBI prescribes ultimate state for the determination of S and m. This results in an S ratio of 0.30 and and an m coefficient of 0.87 in compression. As explained earlier the m coefficient can be estimated by the plastic volumetric strain ratio Λ. Λ varies between 0.86 and 0.92 for different tests. The extension tests generally plot under the compression results. The ultimate state results however cross each other, but as mentioned before the ultimate state results for extension are not representative.

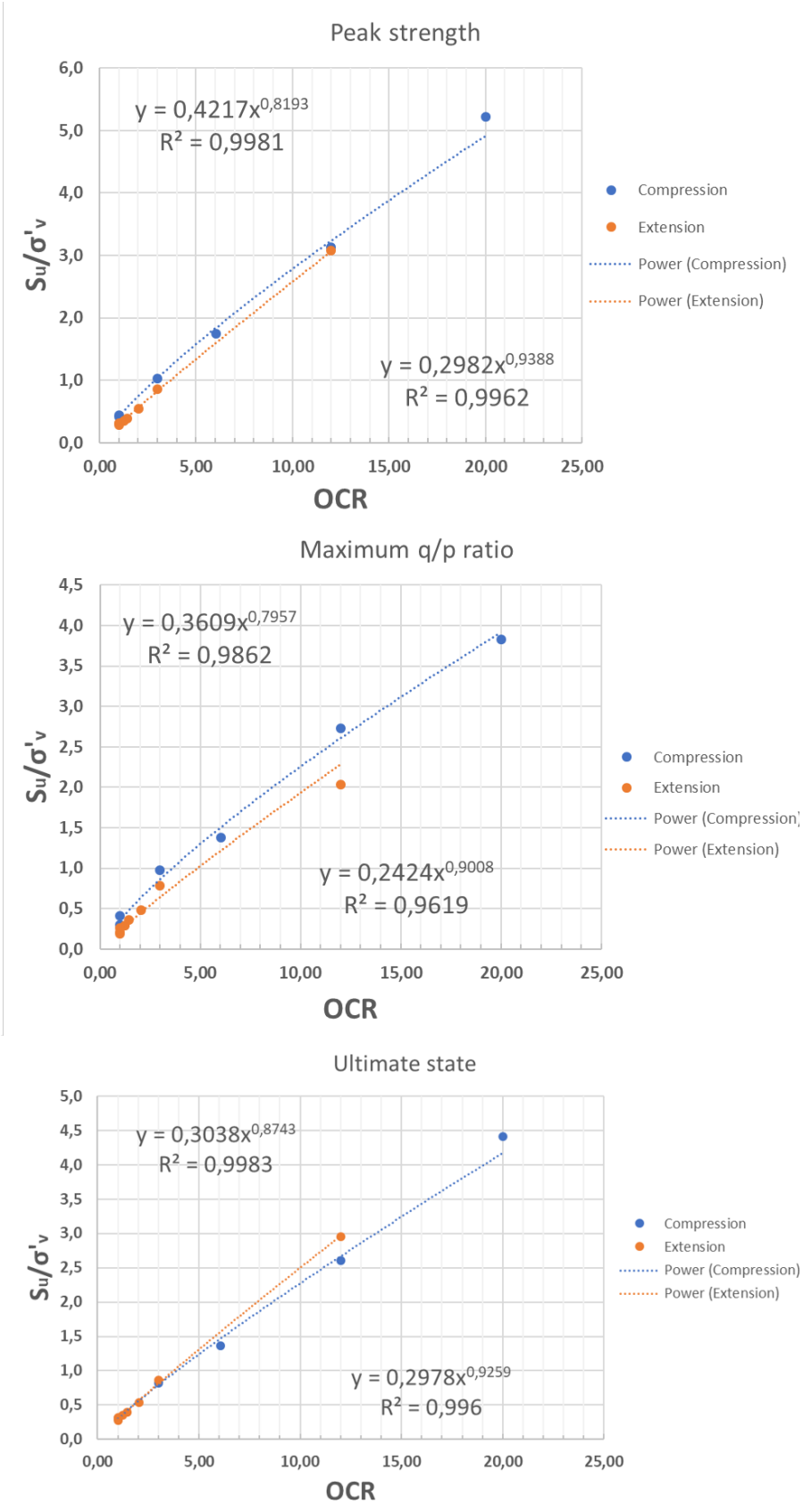

Figure 4.20: Results of triaxial tests in SHANSEP framework

5

Discussion

In this chapter a discussion of the results is outlined. Most of uncertainties are already mentioned in combination with the laboratory test descriptions and results analysis. Laboratory work brings certain boundary conditions with it that are linked to the type of test that is executed. These imposed boundary conditions are, however, not actually present in the field. The goal of this thesis is to analyse of the actual intrinsic soil behaviour. The boundary effects, that have an effect on the observed behaviour are therefore discussed in this chapter. In order to place the analysis of the MCC relations in the right perspective, the accuracy of certain soil parameters is discussed as well.

5.1. Laboratory work

In Chapter 3 the boundary effects that are imposed by the types of testing are mentioned. Corrections for strength of the membrane and drainage strips are applied. Also is the observed behaviour analysed on laboratory effects. Certain features observed in the stress paths in $p' - q$ space can be explained by the failure type that occurred during the test. The normally consolidated samples only showed a barrel shape after shearing. The over consolidated samples also showed a shear band and the heavily over consolidated samples even showed two shear bands. Furthermore during the extension tests a number of difficulties occurred. During consolidation deviating behaviour was observed which could not clearly be explained. Also the occurrence of necking and the formation of severe shear bands caused difficulties in the analysis of the results. The results are therefore to be interpreted with larger uncertainty than the compression results. Another uncertainty that is analysed is the void ratio determination. More specifically the void ratio determination after shearing. A relative error of approximately 2% is found. 2% seems a small deviation but relative to the change in void ratio this error is approximately 10 %. The most important factor contributing to the uncertainty is the measurement of water extrusion, that not captures all the water that is actually extruded. A more correct way could be achieved by measuring the water content of the complete sample including drainage strips after shearing. Usually only part of the sample is tested. To correct for the actual weight of the dry strips the weight of the drainage strips should be recorded before the test. Then there is probably still a difference between void ratio determined through water extrusion and determined from the water content.

5.2. Organic clay

A often observed phenomenon in organic clays, such as OVP clay, is creep. Creep, or secondary consolidation, is continues deformation of soil under constant load. This mechanical process results in an apparent OCR. In fact the stresses σ'_{vc} and σ'_{v0} do not change. The structure of the soil, however, does change to a configuration resembling a larger stress level. Keeping apparent OCR in mind, one could question whether the OCR behaviour of the soil samples actually resembles the OCR that is measured. Figure 3.6 clearly shows a decrease in void ratio at constant pre-consolidation pressure. This is partly caused by a dissipation of excess pore pressure resulting from the consolidation. A part is however also caused by creep. In Figure 3.7 one can see that when the stresses are kept constant, strain still continues for several hours. The void ratio is thus effected by creep, which makes $p' - e$ relations less accurate. The change in void ratio occurring during the waiting period is relatively

large compared to the total change in void ratio during consolidation, especially large compared to the change in void ratio that occurs during an unloading step. In Appendix A the creep rate after the final consolidation step is recorded. Creep also continues during shearing, which makes that stabilisation of $\Delta u, p'$ and q take longer. As mentioned before were the stresses at ultimate state of the NC samples not completely stabilised yet. The NC samples also showed the largest amount of creep rate after consolidation. Another feature of the material that is used and that could affect the observed soil behaviour is the silt fraction that is present in OVP clay. Soils can show transitional behaviour and do not show a unique critical state line nor consolidation line [5]. OVP clay is a lightly organic, strongly silty clay. The silt fraction is 71%. The silt fraction can contribute to the fact that a unique $p' - e$ relation is not found.

5.3. Modified Cam Clay model

The Modified Cam Clay has been used to predict the behaviour of OVP clay. A single parameter set giving reliable results for all tests was not found. In compression the MCC model over estimated S_u, which is in line with literature [19]. One of the limitations of the MCC models is the shape of the yield surface that is used. The MCC model adapts an ellipse shaped yield surface that is symmetric around the p'-axis. In natural clays often strength anisotropy is observed. In order to take into account soil anisotropy, an inclined elliptical yield surface can be adopted. Since anisotropic consolidation is used in the triaxial tests that were executed, stress induced anisotropy is expected to occur in the samples. This behaviour can be covered by changes in the inclination of the yield surface[22] and is thus not captured by the MCC model. The inaccuracy of the yield surface is clearly shown in Chapter 4.1.1. The MCC model also assumes a fixed spacing ratio $r = 2$. The spacing ratio represents the ratio of p'_c and p' at the intersection of an unloading line and the CSL. By fixing r a certain rigidity is imposed to the model. The laboratory results show that r fluctuates between approximately 1.4 and 2.4. This range is rather large since the critical state band, as found in Chapter 4.1.4, is rather wide as well. Furthermore the MCC model may allow for extremely large shear stresses. This is particularly the case for stress paths that cross the critical state line [15]. Another feature that is not captured in the MCC model is strain-rate dependency of the yield point of natural clays, this is however influencing peak strength and not ultimate state [10].

6

Conclusions and recommendations

The purpose of this thesis is to investigate undrained material behaviour of Dutch organic clay in triaxial tests following the SHANSEP procedure as prescribed in the WBI and compare to the CSSM framework. This goal is achieved by answering several research questions.

6.1. Conclusions

The conclusions are formulated by answering the research questions, as formulated in Chapter 1, one-by-one.

1. How well does CSSM describe the undrained soil behaviour in anisotropically consolidated triaxial tests?
The results show that in qualitative terms CSSM describes the undrained soil behaviour of OVP clay in triaxial compression tests well. The $p' - q$-relation described in CSSM can be very well established from the six triaxial compression tests that are executed. At ultimate state undrained shear strength shows consistent results and fit to an M_c-line of value 1.61 with an R^2-value of 0.99. The $p' - e$-relation, on the other hand, is less consistent and a accurate fit could not be found. A critical state line could not be fitted in $p' - e$-space accurately. A critical state "zone" with a range of approximately 20 kPa can be recognized. As a result the 3D $p' - q - e$-relation shows the same deviation. The shape of the "text book" 3D images can, however, clearly be recognized. Triaxial extension tests are much harder to interpret. The results are also less consistent. S_u at peak strength does result in an M_e of value 1.35 resulting in an R_2-value of 0.97. The quantitative description of S_u, determined through the MCC model does overestimate the compression results. A better estimation of S_u was obtained when correcting κ. Since M_c could be determined accurately and q_f is calculated from p'_f through M_c, it can be concluded that p'_f is incorrectly estimated by the MCC model. In extension S_u/σ_{v0} at peak strength is very well estimated by the MCC model. Correction of κ resulted in a worse estimation of S_u.

2. How well does the triaxial test data fit in the SHANSEP equation?
The SHANSEP equation, as defined by [14], is a very adequate manner of normalising the undrained shear strength of OVP clay for a large range of OCR's. For all three definitions of failure that are examined in this thesis a good fit is obtained. At ultimate state in compression, as prescribed by the WBI, an S-ratio of 0.30 and m-coefficient of 0.87 is determined. At an OCR of 20 S_u/σ_{v0} is slightly underestimated. In extension the best fit is obtained at peak strength, resulting in an S-ratio of 0.30 and an m-coefficient of 0.94.

3. Can isotropic and anisotropic unload/reload soil parameters be recalculated from each other correctly?
The determination of λ from the triaxial tests, K_0-CRS tests and isotropic compression test results in slightly different values. The K_0-CRS and isotropic compression test, however, gave very similar results and are assumed to be more reliable. Also determination of κ from the K_0-CRS test and the isotropic test result in the same value. Besides the usual conversion between σ'_v-based and p'-based

parameters determined from K_0-CRS tests, an additional equation (Equation 4.3) can be used to obtain accurate conversion of unload parameter κ from e.g. RR. This is caused by the change is horizontal to vertical stress ratio during unloading. This resulted in a better result in the MCC computations, however, an equal vale of κ was found from K_0-CRS test and the isotropic test, without applying the correction factor. The extent of the correction often falls within the inaccuracy range of the κ determination. The larger the unloading the larger correction factor and thus the larger the significance. At small OCR's, thus small unloading steps, the significance of the correction factor is questionable.

4. What is the definition of undrained shear strength according to different theories and how do these definitions fit in the CSSM framework?
In this thesis three definitions of failure and accessory S_u have been analysed. Namely failure at: ultimate state, peak strength and maximum q/p' ratio. Undrained shear strength is defined as one-half of the deviator stress at the point of failure. In compression ultimate state shows very consistent results. p', q and Δu of the NC samples at ultimate state were not completely stable yet at ultimate state but were clearly moving towards a stable situation. A possible explanation is the effect of creep. Extrapolation of p', q and Δu suggests that a stable situation could be reached within 5% additional strain beyond ultimate state. The OC samples, on the other hand, showed stable, p', q and Δu values at ultimate state. Ultimate state is therefore the most consistent way of defining critical state in triaxial compression tests. For extension tests S_u at ultimate state was not reliably determinable. Because of severe deformation, necking or occurrence of a shear band, the stresses at ultimate state are not representative at ultimate state. At maximum q/p' ratio the results are rather consistent. Peak strength and maximum $p' - q$ ratio do often nearly coincide.

5. What is the difference in undrained shear strength S_u between isotropically and K_0-consolidated triaxial tests in numerical simulations of the Modified Cam Clay model?
As explained in Chapter 2 does a normally consolidated sample that is isotropically consolidated result in a larger S_u/σ'_{v0} ratio than an anisotropically consolidated sample, for both compression and extension. The failure point in the MCC model is determined by p'_0 which means that the difference in S_u/σ'_{v0} of isotropic and anisotropic consolidation depends on K_0. Over consolidated samples are slightly more complex. It can be concluded that in general for lightly over consolidated samples S_u/σ'_{v0} in isotropic consolidation is larger than in anisotropic consolidation. At some point with increasing unloading, S_u/σ'_{v0} of anisotropically consolidated samples becomes larger, the tipping point depends on K_0 and K_{ur}. Thus for heavily over consolidated samples, anisotropic consolidation generally results in a larger S_u/σ'_{v0}. There should be noted that the soil test module in Plaxis does not allow for an exact definition of anisotropic loading and unloading stress path.

In summary it can concluded that CSSM is a suitable theoretical framework to describe the qualitative undrained behaviour of K_0-consolidated triaxial tests. At ultimate state the triaxial compression results are very consistent. An M_c-line can be determined with large precision. The extension results are less consistent, at maximum p'/q ratio the M_e- line can be obtained resulting in the best fit. Failure at maximum p'/q ratio is nearly identical to failure at peak strength. The unique relation between $p' - e$, as described in the CSSM could not be obtained accurately. This relation is thus not suitable for S_u determination in practical applications. This is partly caused by the determination method that is prone to errors. The data of both the triaxial compression and extension tests give a very good fit with the SHANSEP equation. Only at very large OCR, S_u/σ'_{v0} is underestimated at ultimate state in compression. In extension S_u at peak strength results in the best fit. The SHANSEP equation is therefore a good method to normalise the results and schematise S_u.

6.2. Recommendations

In the following section recommendations based on the insight gathered during the execution of this thesis is outlined. A differentiation between practical laboratory related recommendations and recommendations concerning undrained shear strength determination is made.

- In triaxial compression tests on remoulded organic clay ultimate state should be used as representation of critical state.
- In triaxial extension on remoulded organic clay tests peak strength or maximum p'/q ration should be used as representation of critical state.
- The use of the SHANSEP method to normalise undrained shear strength of remoulded organic clay S_u/σ_{v0} is recommended in accordance with [16], regardless of the definition of failure.
- In triaxial extension tests ultimate state should not be used as a definition of failure.
- The MCC model should not be used to determine undrained shear strength of remoulded organic clay. Which probably means that the MCC model is not suitable for undrained shear strength determination for dike stability assessment.

During the execution of the laboratory work several inconveniences came up, resulting in the following recommendations:

- In order to obtain a continuous recording of the void ratio during triaxial testing it is recommended to calculate void ratio from water extrusion. A rather large error compared to the void ratio range should be kept in mind.
- A consolidation rate of 0.5 kPa/hr, in terms of cell pressure, during anisotropic consolidation did not result in problems. When K_0-seeking consolidation is applied a lower consolidation rate is recommended.
- It could be interesting to record the shearing phase of triaxial compression tests as well, like was done for the triaxial extension tests. The assumption that was done in Chapter 4.1.1 that the bends in the stress paths in $p' - q$-space are caused by the formation of shear bands can be verified by plotting the stress paths in $p' - q$-space simultaneously with the recordings.

Bibliography

[1] Bjerrum, L. Problems of soil mechanics and construction on soft clays and structurally unstable soils-collapsible expansive and others. International Journal of Rock Mechanics and Mining Science Geomechanics Abstracts, 3:111–159, 1973.

[2] Brinkgreve, R. Cam-clay and Critical state theory - lecture notes course "Behaviour of Soils and Rocks". Delft University of Technology, 2017.

[3] Budhu, M. Soil Mechanics and Foundations. John Wiley & Sons, 3rd edition, 2011.

[4] Chang, M., Teh, C. I., and Cao, L. Critical state strength parameters of saturated clays from the modified cam clay model. Canadian Geotechnical Journal, 36:876–890, 1999.

[5] Coop, M. Limitations of a critical state framework applied to the behaviour of natural and transitional soils. Advances in Soil Mechanics and Geotechnical Engineering, 6:115–155, 2015.

[6] den Haan, E. and van den Berg, P. Interpretatie meetdata k0-crs apparaat. Report CO-710203/22 versie 1, 2001.

[7] Dev, K. L., Pillai, R. J., and Robinson, R. G. Estimation of critical state parameters from one-dimensional consolidation and triaxial compression tests. Indian Geotechnical Journal, 43:229–237, 2013.

[8] Hall, C. Laws and Models. CRC Press, 1999.

[9] Jaky, J. The coefficient of earth pressure at rest. Journal of the Society of Hungarian Architects and Engineers, pages 355–358, 1944.

[10] Karstunen, M., Yin, Z., Koskinen, M., Leoni, M., and Vermeer, P. Some recent developments in constitutive modelling of soft clays. In The 12th international conference of international association of computer methods and advances in geomechanics (IACMAG), 2008.

[11] Konstantinou, M. and Zwanenburg, C. A critical review of membrane and filter paper correction formulas for the triaxial testing of soft soils. Geotechnical Testing Journal, 43, 2019.

[12] Ladd, C. Stability evaluation during staged construction. Journal of Geotechnical Engineering, 117:540–615, 1991.

[13] Ladd, C. and DeGroot, D. Recommended practice for soft ground site characterization. In Arthur Casagrande Lecture, 2003.

[14] Ladd, C. and Foott, R. New design procedure for stability of soft clays. International Journal of Rock Mechanics and Mining Sciences & Geomechanics Abstracts, 1974.

[15] Laera, A., A Saratchchandran and Brinkgreve, R. PLAXIS The Creep-SCLAY1S model, 2018.

[16] Ministerie van Infrastructuur en Milieu. Schematiseringshandleiding macrostabiliteit, WBI. 2017.

[17] Mun, W., Teixeira, T., Balci, M., Svoboda, J., and McCartney, J. Rate effects on the undrained shear strength of compacted clay. Soils and Foundations, 56:719–731, 2016.

[18] NEN. NEN 9997-1/C2 (nl) Geotechnisch ontwerp van constructies - Deel 1: Algemene regels. 2017.

[19] Potts, D. and L, Z. Some piftalls when using modified cam clay. Imperial College, London, 1999.

[20] Roscoe, K. H. and Burland, J. B. On the generalized stress-strain behaviour of wet clay. In Engineering plasticity, pages 534–608, 1968.

[21] Roscoe, K. H., Schofield, A. N., and Wroth, C. P. On the yielding of soils. Geotechnique, 8:22–53, 1958.

[22] S.J. Wheeler, M. K., A. Näätänen and Lojander, M. An anisotropic elastoplastic model for soft clays. Canadian Geotechnical Journal, 40:403–418, 2003.

[23] Tigchelaar, J. Eindrapportage experimenteel onderzoek van het gedrag van organische klei. Number CO 710203/26. Delft Cluster, 2001.

[24] Tigchelaar, J., de Feijter, J., and den Haan, E. Shear tests on reconstituted oostvaardersplassen clay. In Soft Ground Technology. American Society of Civil Engineers, 2001.

[25] van den Berg, F., Van, M., de Hoef, J. V., Jelier, W., Roks, E., Schie, D. V., and Termaat, R. Project Overstijgende Verkenning Macrostabiliteit, Plan van Aanpak. Project Overstijgende Verkenning Macrostabiliteit, 2015.

[26] van Duinen, A. Grensverleggend onderzoek macrostabiliteit bij opdrijven fase 2.c. report 419230-0040. Versie 2., 2008.

[27] Visschedijk, M. Basisrapport eindige-elementenmethode (onderdeel 6.2.6a) project overstijgende verkenning macrostabiliteit. Report 11201406-002-GEO-0003, 2018.

[28] Wood, D. Soil Behaviour and Critical State Mechanics. Cambridge University Press, 1990.

[29] Wroth, C. The interpretation of in situ soil tests. Geotechnique, 34:449–489, 1984.

[30] Zwanenburg, C. The influence of anisotropy on the consolidation behaviour of peat. PhD thesis, Technische Universiteit Delft, 2005.

[31] Zwanenburg, C., Lange, D. D., and Konstantinou, M. Povm validatie, uitgangspunten en lange termijnontwikkeling. Report 11200999-004-GEO-0002, 2018.

Appendices

A

Triaxial tests

Sample name	**TRX1**
Type	Compression
Soil type	OVP clay
Soil classification	Silty clay
Before test	
Mass [g]	633.41
Height [mm]	129.2
Diameter [mm]	67.1
Void ratio [-]	2.51
Water content [%]	108.3
Particle density [kg/m^3]	2310
Bulk density [kg/m^3]	1386
B-factor	1.00
Backpressure [kPa]	300
Consolidation stage	
Vertical consolidation pressure [kPa]	100
Horizontal consolidation pressure [kPa]	43
Vertical pre-consolidation pressure [kPa]	100
Horizontal pre-consolidation pressure [kPa]	43
Creep rate [%/hr]	0.03
Shearing stage	
Shearing rate [%/hr]	1
Peak strength	
Vertical effective stress [kPa]	111.0
Horizontal effective stress [kPa]	22.4
Undrained shear strength [kPa]	44.2
M_c[-]	1.70
Ultimate State	
Vertical effective stress [kPa]	79.6
Horizontal effective stress [kPa]	17.7
Undrained shear strength [kPa]	31.0
M_c [-]	1.62
Max p'/q ratio	
Vertical effective stress [kPa]	98.3
Horizontal effective stress [kPa]	16.4
Undrained shear strength [kPa]	40.9
M_c [-]	1.88
After test	
Mass [g]	589.63
Void ratio [-]	2.12
Water content [%]	91.6

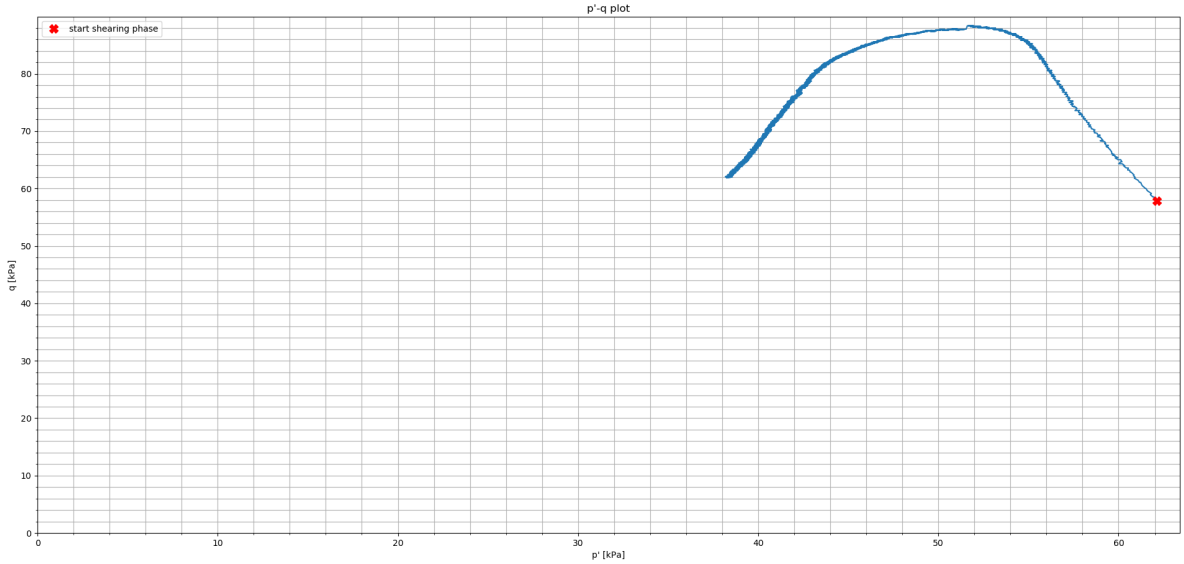
p'-q plot
start shearing phase
q [kPa]
p' [kPa]

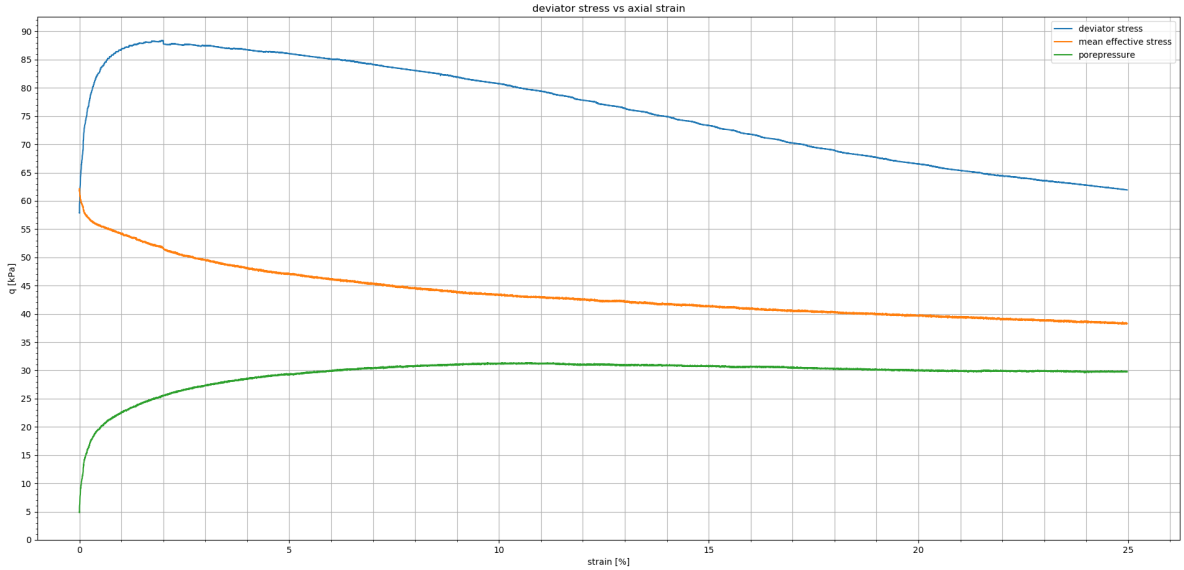
deviator stress vs axial strain
deviator stress
mean effective stress
porepressure
q [kPa]
strain [%]

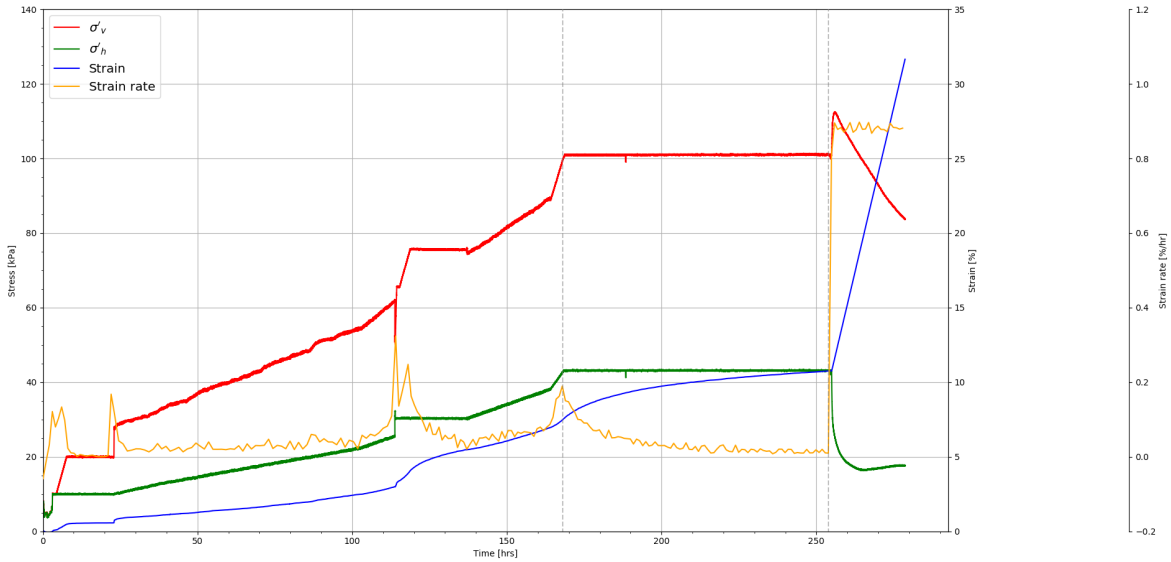
σ'_v
σ'_h
Strain
Strain rate
Stress [kPa]
Strain [%]
Strain rate [%/hr]
Time [hrs]

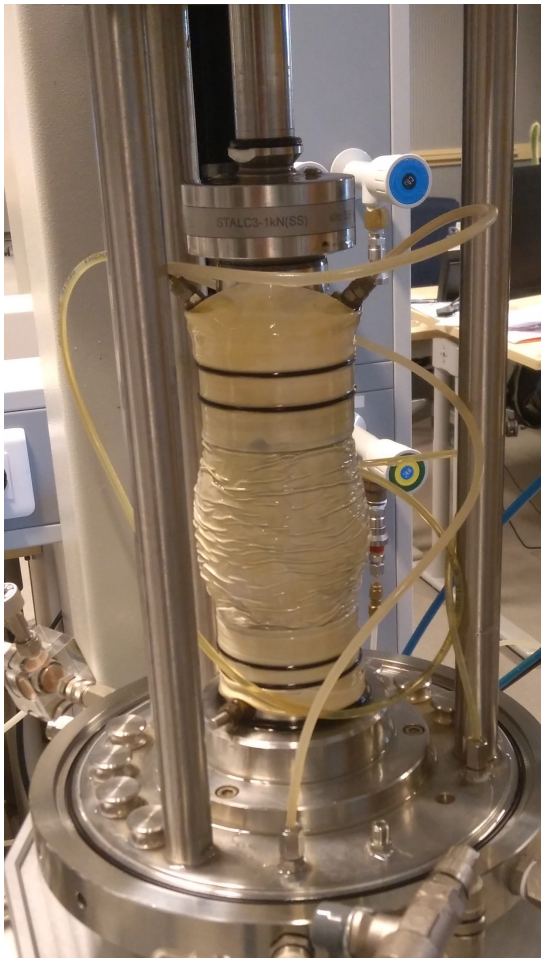
STALC3-1kN(SS)

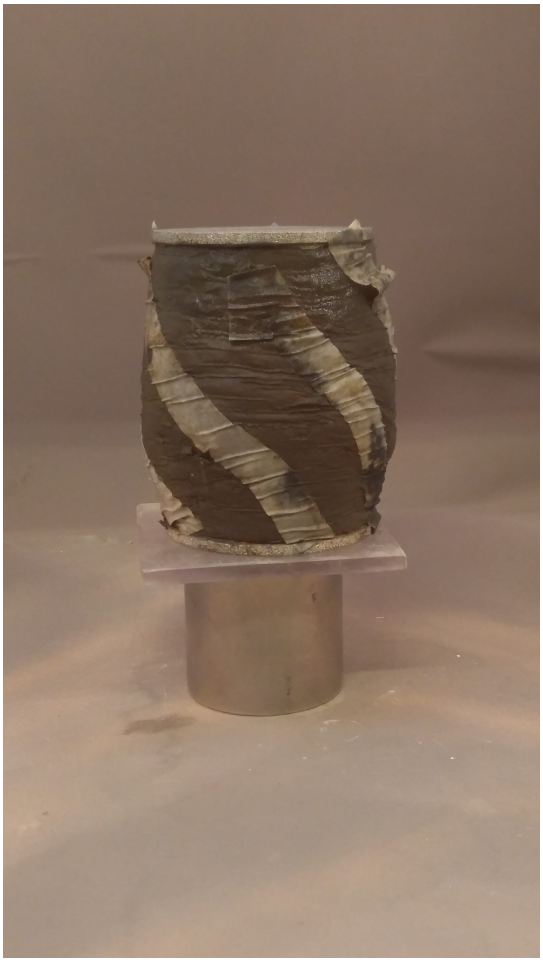

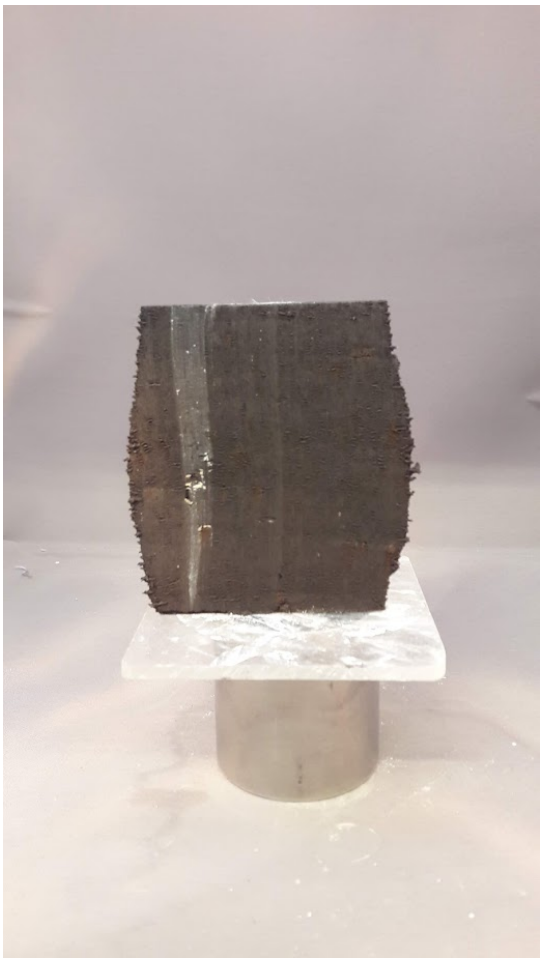

Sample name	**TRX2**
Type	Compression
Soil type	OVP clay
Soil classification	Silty clay
Before test	
Mass [g]	598.20
Height [mm]	123.3
Diameter [mm]	66.9
Void ratio [-]	2.49
Water content [%]	107.6
Particle density [kg/m^3]	2310
Bulk density [kg/m^3]	1380
B-factor	1.00
Backpressure [kPa]	300
Consolidation stage	
Vertical consolidation pressure [kPa]	20
Horizontal consolidation pressure [kPa]	19.5
Vertical pre-consolidation pressure [kPa]	121
Horizontal pre-consolidation pressure [kPa]	52
Creep rate [%/hr]	-0.02
Shearing stage	
Shearing rate [%/hr]	1
Peak strength	
Vertical effective stress [kPa]	76.1
Horizontal effective stress [kPa]	6.1
Undrained shear strength [kPa]	35.0
M_c[-]	2.37
Ultimate State	
Vertical effective stress [kPa]	68.1
Horizontal effective stress [kPa]	13.6
Undrained shear strength [kPa]	27.3
M_c [-]	1.72
Max p'/q ratio	
Vertical effective stress [kPa]	57.0
Horizontal effective stress [kPa]	2.0
Undrained shear strength [kPa]	27.5
M_c [-]	2.7
After test	
Mass [g]	559.80
Void ratio [-]	2.12
Water content [%]	91.4

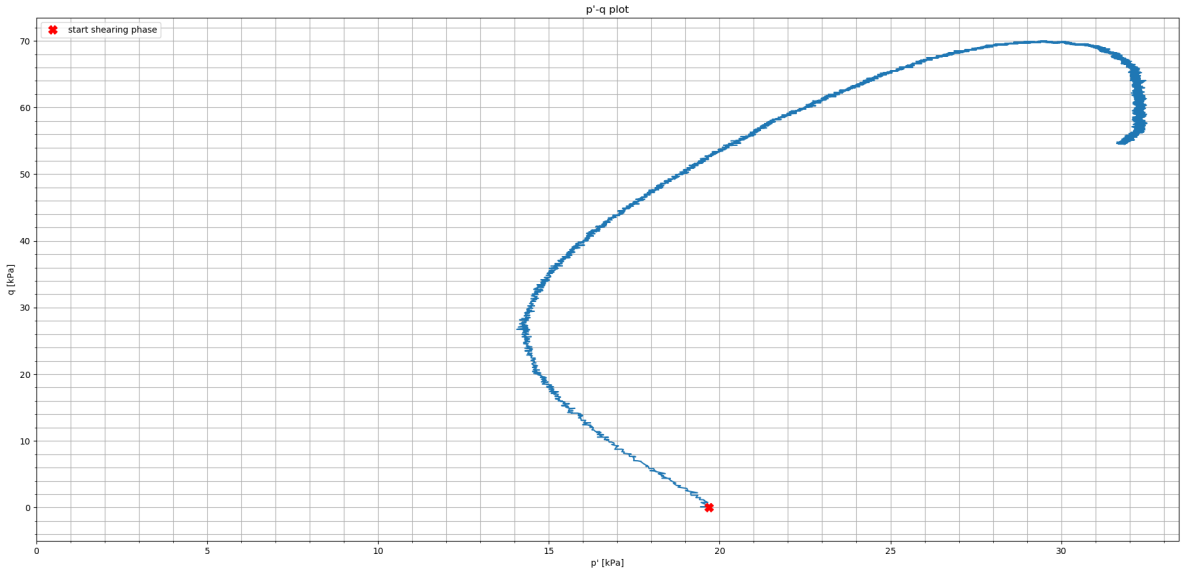
p'-q plot
start shearing phase
q [kPa]
p' [kPa]

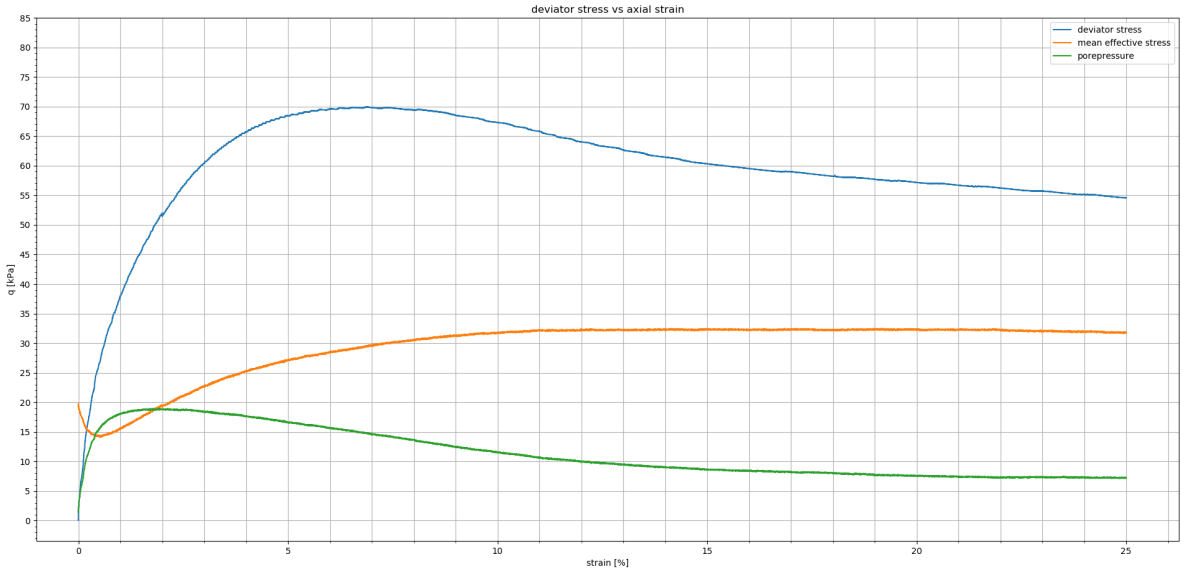
deviator stress vs axial strain
deviator stress
mean effective stress
porepressure
q [kPa]
strain [%]

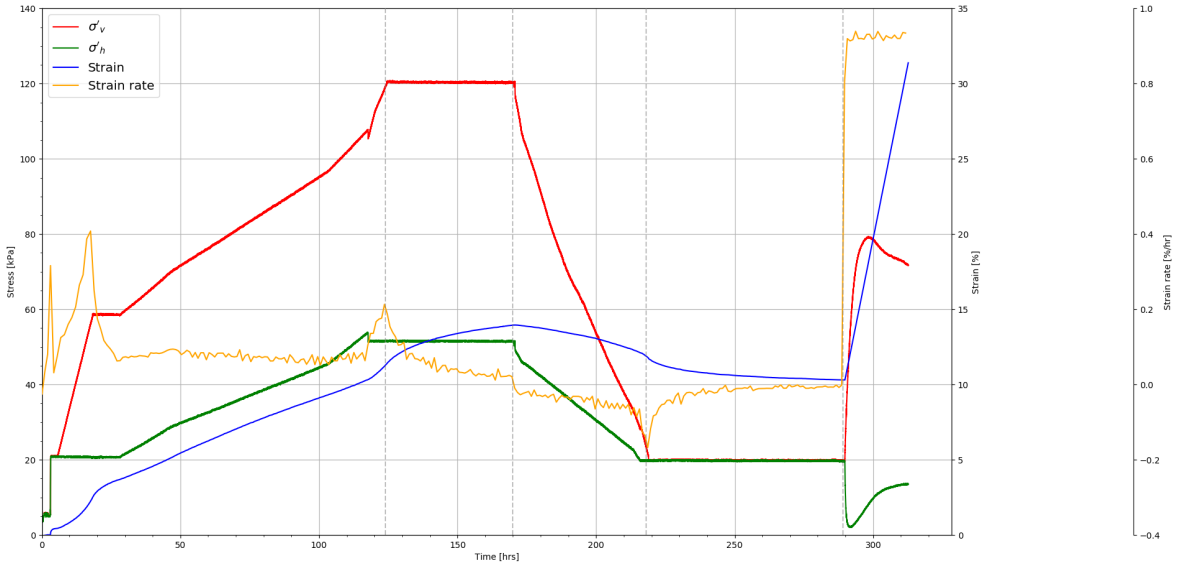
σ'_v
σ'_h
Strain
Strain rate
Stress [kPa]
Strain [%]
Strain rate [%/hr]
Time [hrs]

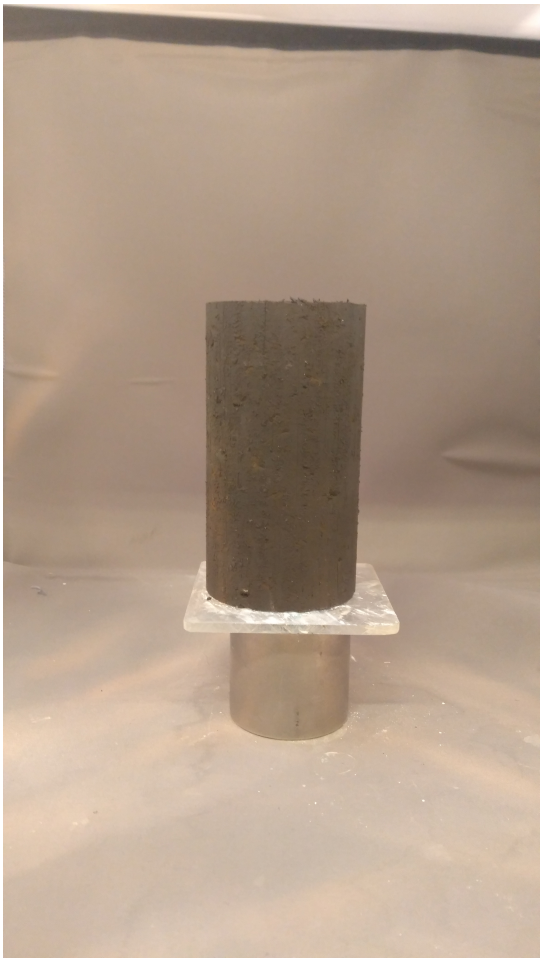

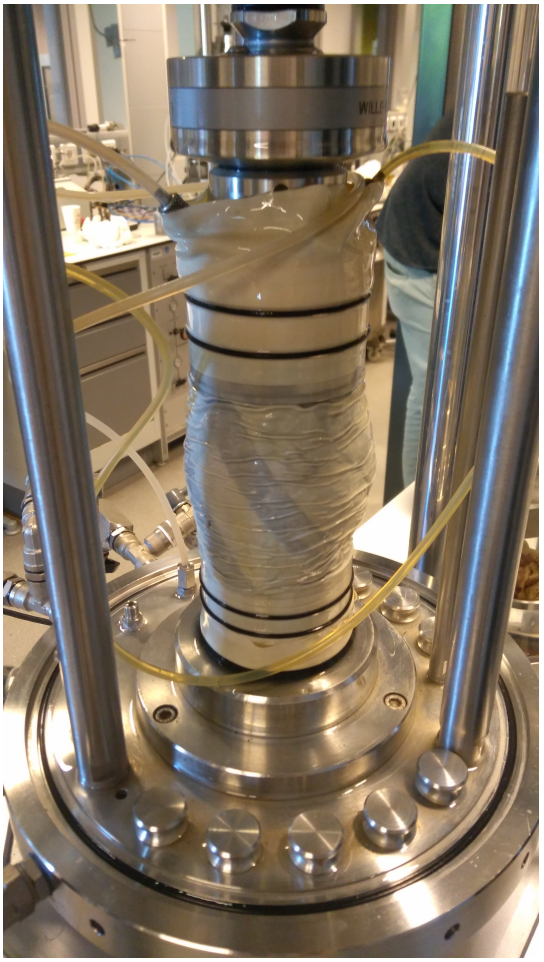

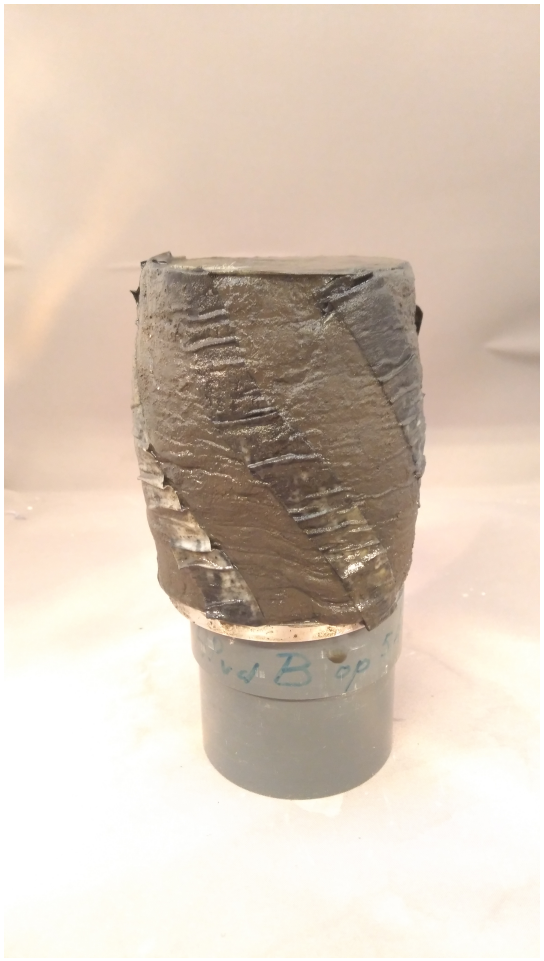

Sample name	**TRX3**
Type	Compression
Soil type	OVP clay
Soil classification	Silty clay
Before test	
Mass [g]	663.00
Height [mm]	116.2
Diameter [mm]	67.1
Void ratio [-]	2.58
Water content [%]	111.6
Particle density [kg/m^3]	2310
Bulk density [kg/m^3]	1370
B-factor	1.00
Backpressure [kPa]	300
Consolidation stage	
Vertical consolidation pressure [kPa]	200
Horizontal consolidation pressure [kPa]	86
Vertical pre-consolidation pressure [kPa]	200
Horizontal pre-consolidation pressure [kPa]	86
Creep rate [%/hr]	0.02
Shearing stage	
Shearing rate [%/hr]	1
Peak strength	
Vertical effective stress [kPa]	219.9
Horizontal effective stress [kPa]	53.9
Undrained shear strength [kPa]	83.0
M_c[-]	1.52
Ultimate State	
Vertical effective stress [kPa]	157.7
Horizontal effective stress [kPa]	36.6
Undrained shear strength [kPa]	60.6
M_c [-]	1.57
Max p'/q ratio	
Vertical effective stress [kPa]	158.3
Horizontal effective stress [kPa]	36.5
Undrained shear strength [kPa]	60.9
M_c [-]	1.58
After test	
Mass [g]	476.54
Void ratio [-]	1.76
Water content [%]	76.1

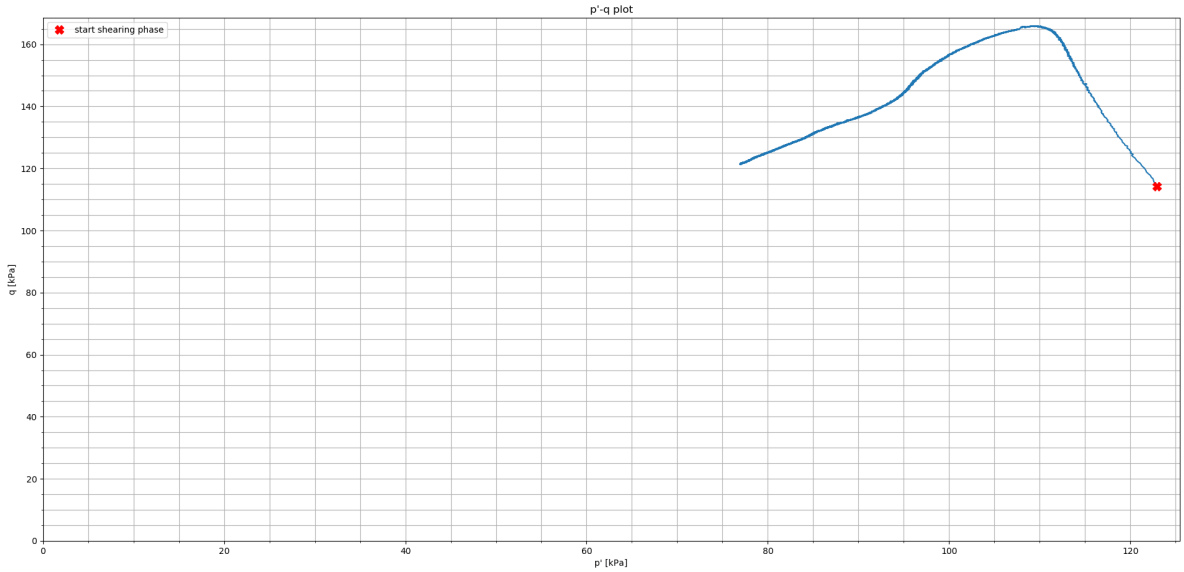
p'-q plot
start shearing phase
q [kPa]
p' [kPa]

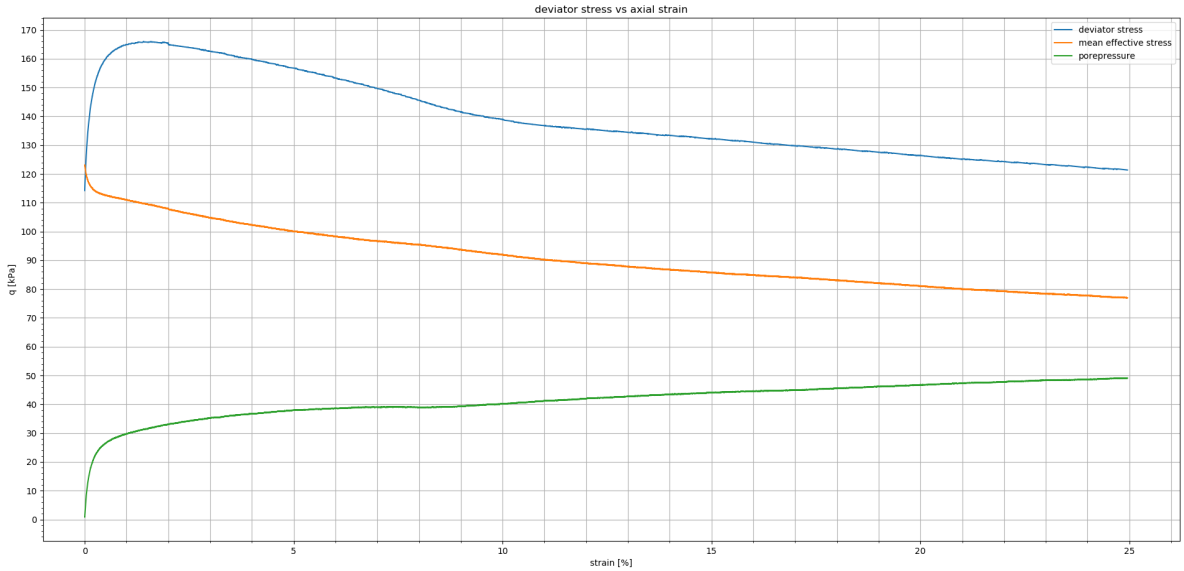
deviator stress vs axial strain
deviator stress
mean effective stress
porepressure
q [kPa]
strain [%]

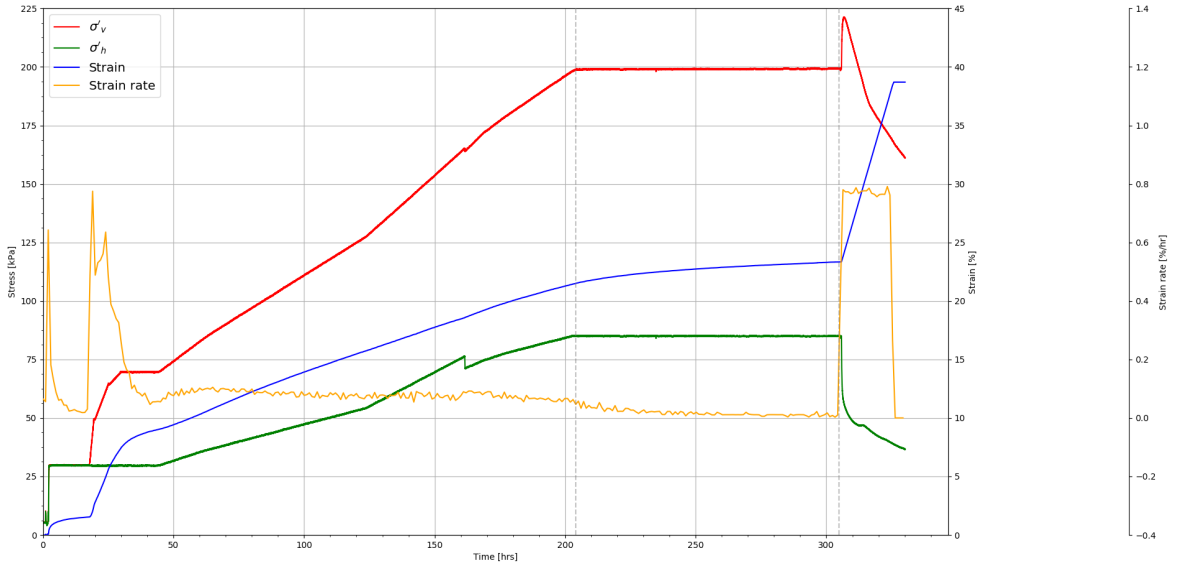
σ'_v
σ'_h
Strain
Strain rate
Stress [kPa]
Strain [%]
Strain rate [%/hr]
Time [hrs]

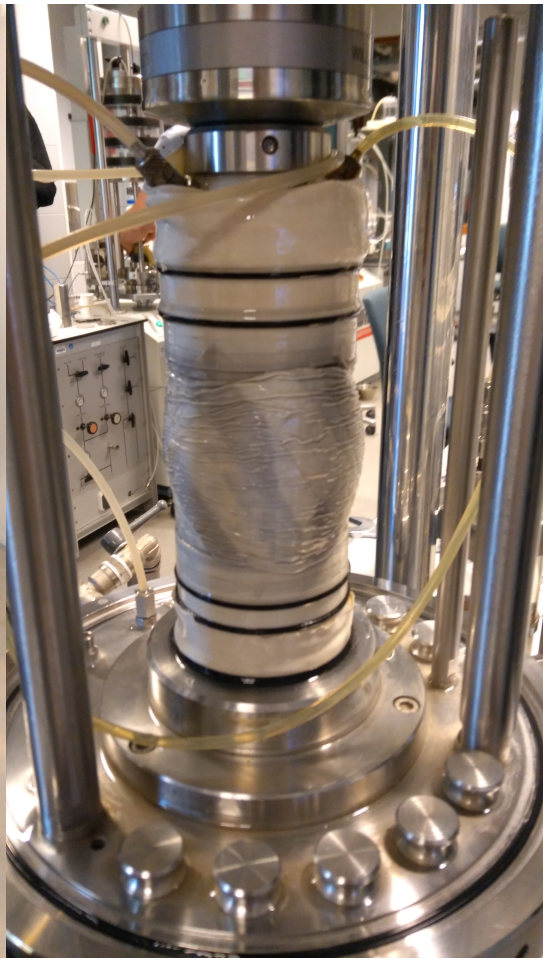

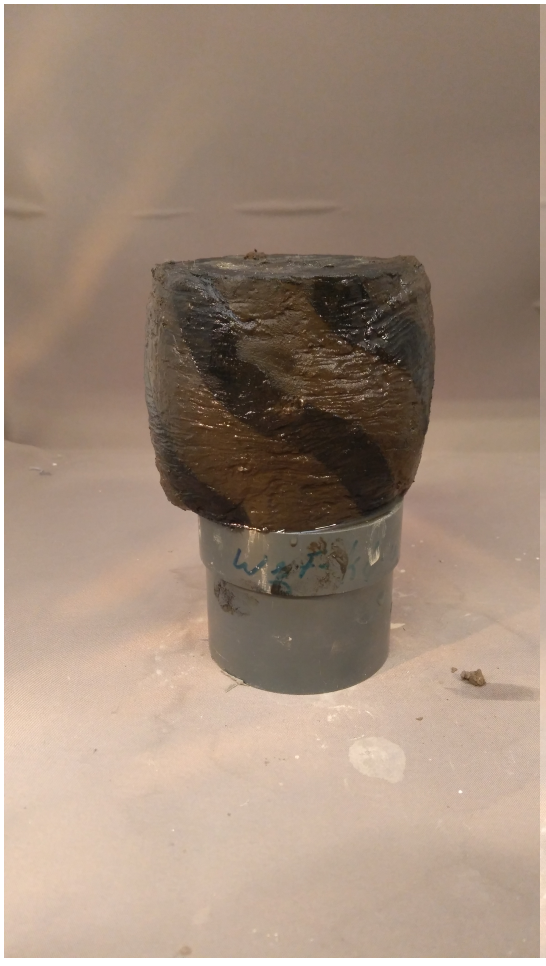

Sample name	**TRX4**
Type	Compression
Soil type	OVP clay
Soil classification	Silty clay
Before test	
Mass [g]	641.97
Height [mm]	132.1
Diameter [mm]	67.1
Void ratio [-]	2.59
Water content [%]	111.9
Particle density [kg/m^3]	2310
Bulk density [kg/m^3]	1374
B-factor	0.98
Backpressure [kPa]	300
Consolidation stage	
Vertical consolidation pressure [kPa]	10
Horizontal consolidation pressure [kPa]	42
Vertical pre-consolidation pressure [kPa]	200
Horizontal pre-consolidation pressure [kPa]	86
Creep rate [%/hr]	-0.02
Shearing stage	
Shearing rate [%/hr]	1
Peak strength	
Vertical effective stress [kPa]	109.7
Horizontal effective stress [kPa]	5.4
Undrained shear strength [kPa]	52.1
M_c[-]	2.60
Ultimate State	
Vertical effective stress [kPa]	111.9
Horizontal effective stress [kPa]	23.8
Undrained shear strength [kPa]	44.1
M_c [-]	1.66
Max p'/q ratio	
Vertical effective stress [kPa]	78.8
Horizontal effective stress [kPa]	2.15
Undrained shear strength [kPa]	38.3
M_c [-]	2.77
After test	
Mass [g]	554.97
Void ratio [-]	1.84
Water content [%]	79.5

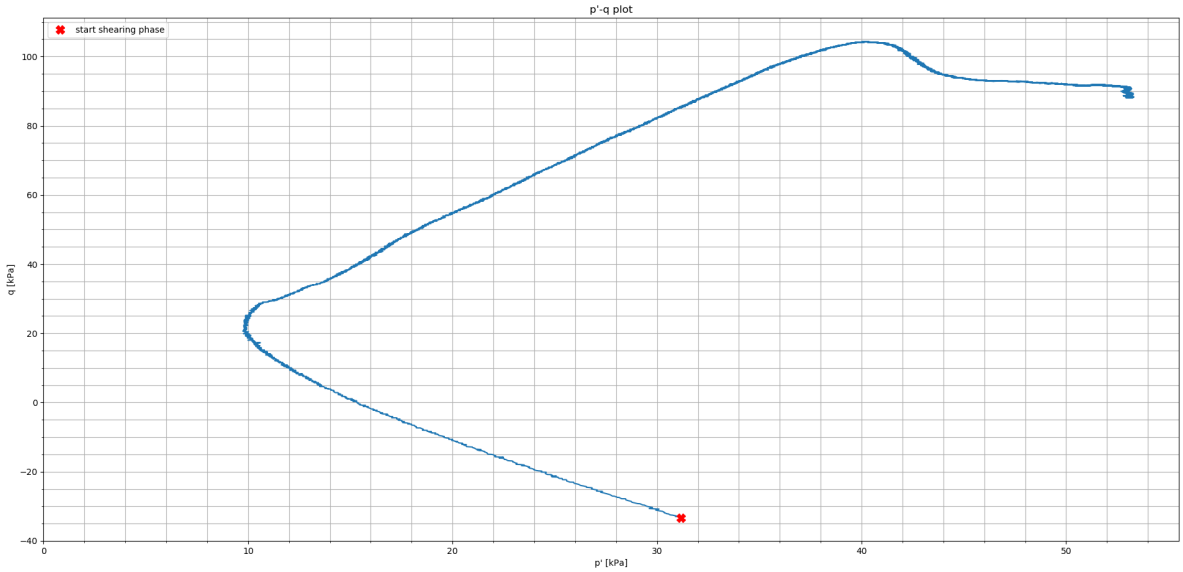
p'-q plot
start shearing phase
q [kPa]
p' [kPa]

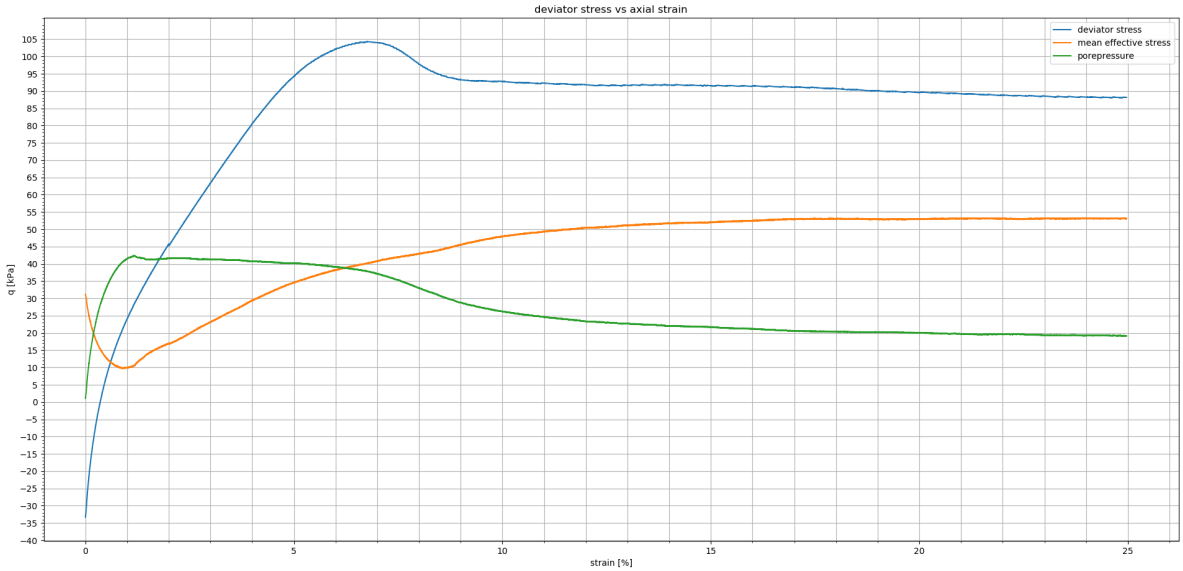
deviator stress vs axial strain
deviator stress
mean effective stress
porepressure
q [kPa]
strain [%]

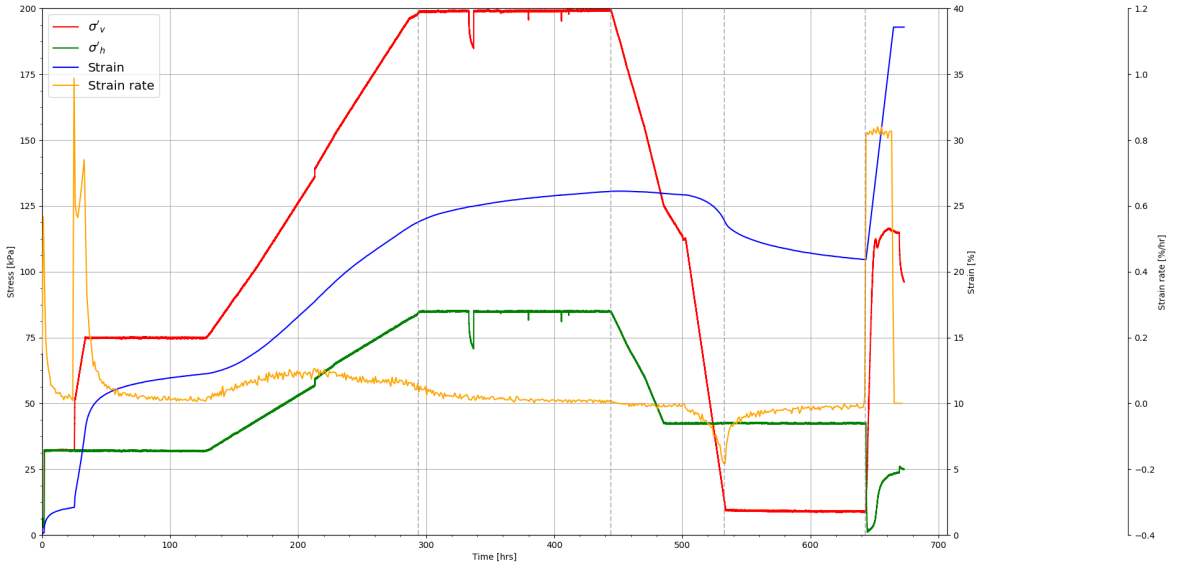
σ'_v
σ'_h
Strain
Strain rate
Stress [kPa]
Strain [%]
Strain rate [%/hr]
Time [hrs]

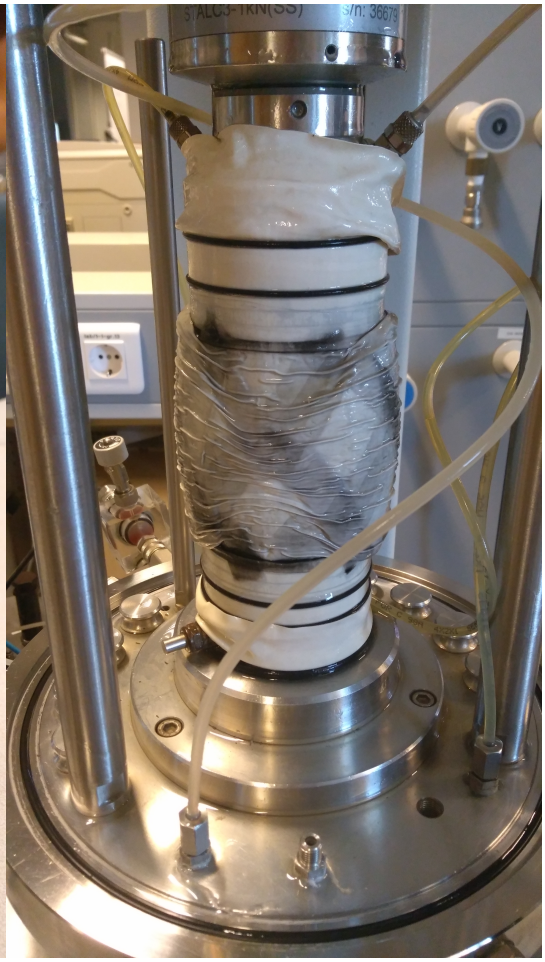

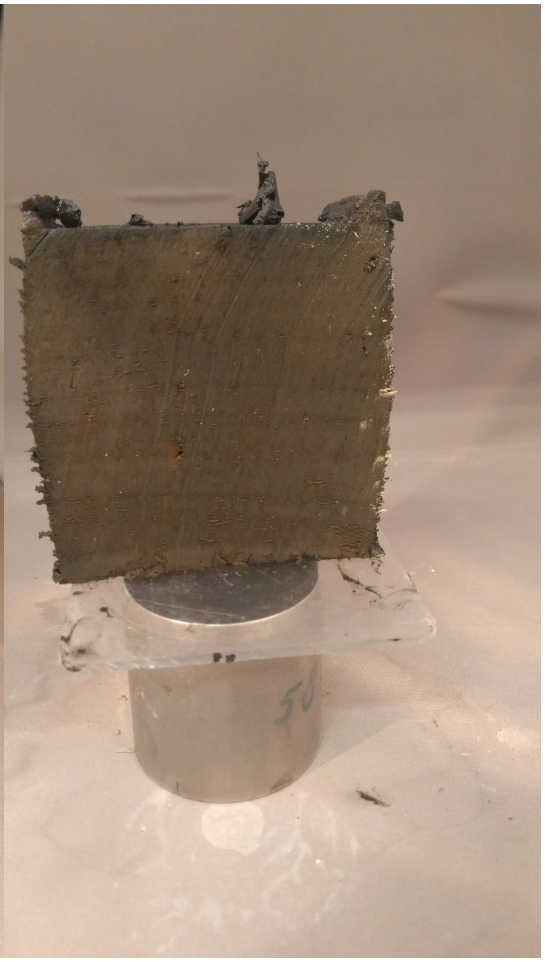

Sample name	**TRX5**
Type	Compression
Soil type	OVP clay
Soil classification	Silty clay
Before test	
Mass [g]	610.35
Height [mm]	126.4
Diameter [mm]	66.9
Void ratio [-]	2.60
Water content [%]	112.5
Particle density [kg/m^3]	2310
Bulk density [kg/m^3]	1374
B-factor	0.98
Backpressure [kPa]	300
Consolidation stage	
Vertical consolidation pressure [kPa]	50
Horizontal consolidation pressure [kPa]	37
Vertical pre-consolidation pressure [kPa]	150
Horizontal pre-consolidation pressure [kPa]	64.5
Creep rate [%/hr]	-0.01
Shearing stage	
Shearing rate [%/hr]	1
Peak strength	
Vertical effective stress [kPa]	126.8
Horizontal effective stress [kPa]	23.7
Undrained shear strength [kPa]	51.6
M_c[-]	1.78
Ultimate State	
Vertical effective stress [kPa]	106.0
Horizontal effective stress [kPa]	24.4
Undrained shear strength [kPa]	40.8
M_c [-]	1.58
Max p'/q ratio	
Vertical effective stress [kPa]	117.2
Horizontal effective stress [kPa]	19.9
Undrained shear strength [kPa]	48.7
M_c [-]	1.86
After test	
Mass [g]	541.51
Void ratio [-]	1.98
Water content [%]	85.5

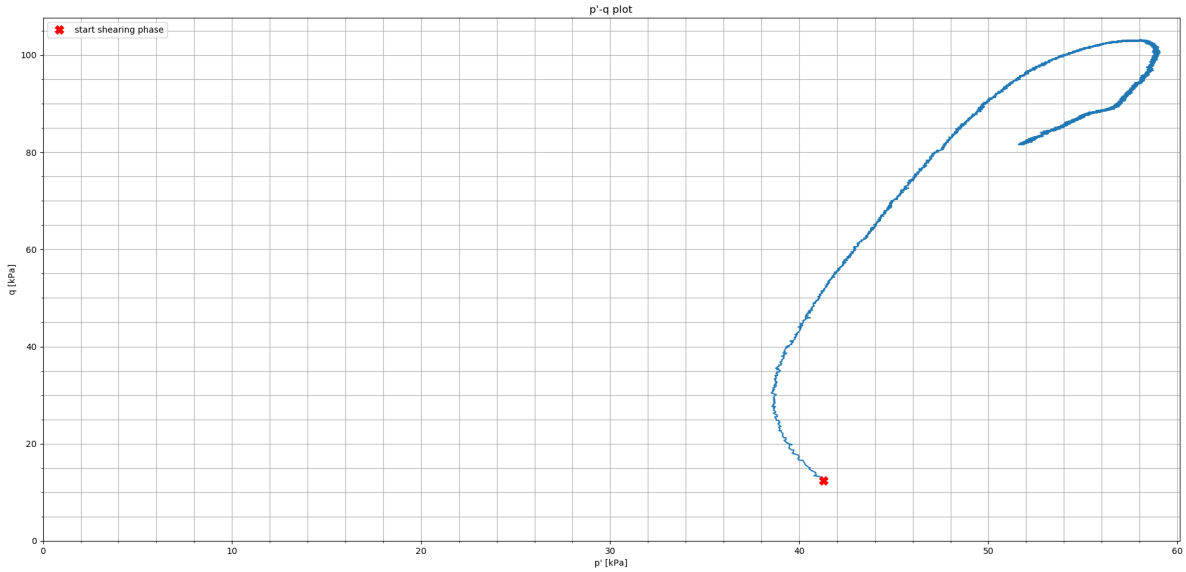
p'-q plot
start shearing phase
q [kPa]
p' [kPa]

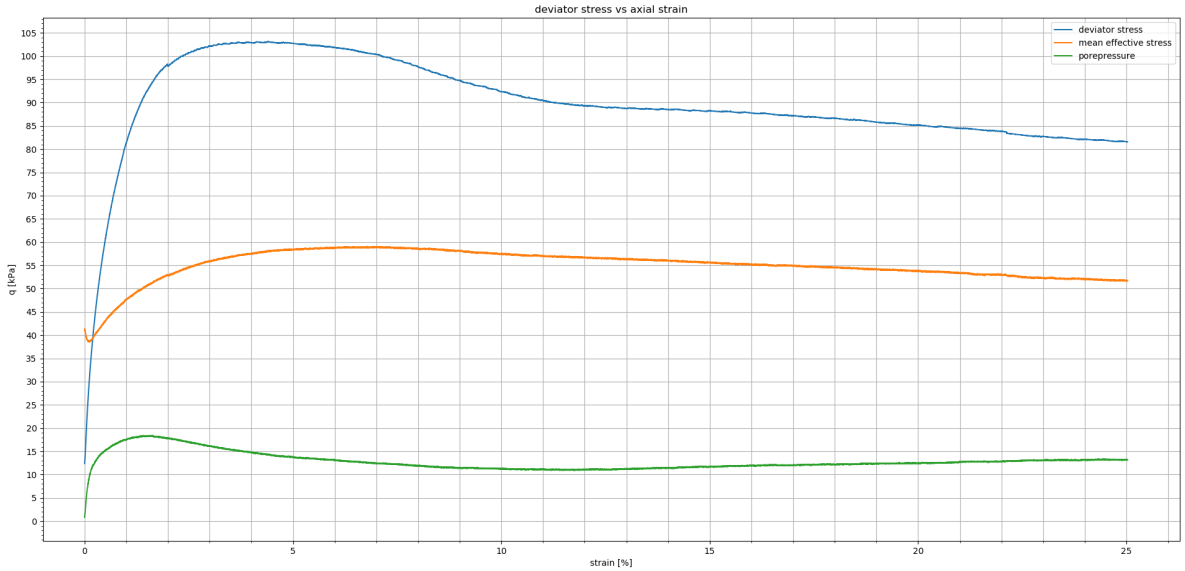
deviator stress vs axial strain
deviator stress
mean effective stress
porepressure
q [kPa]
strain [%]

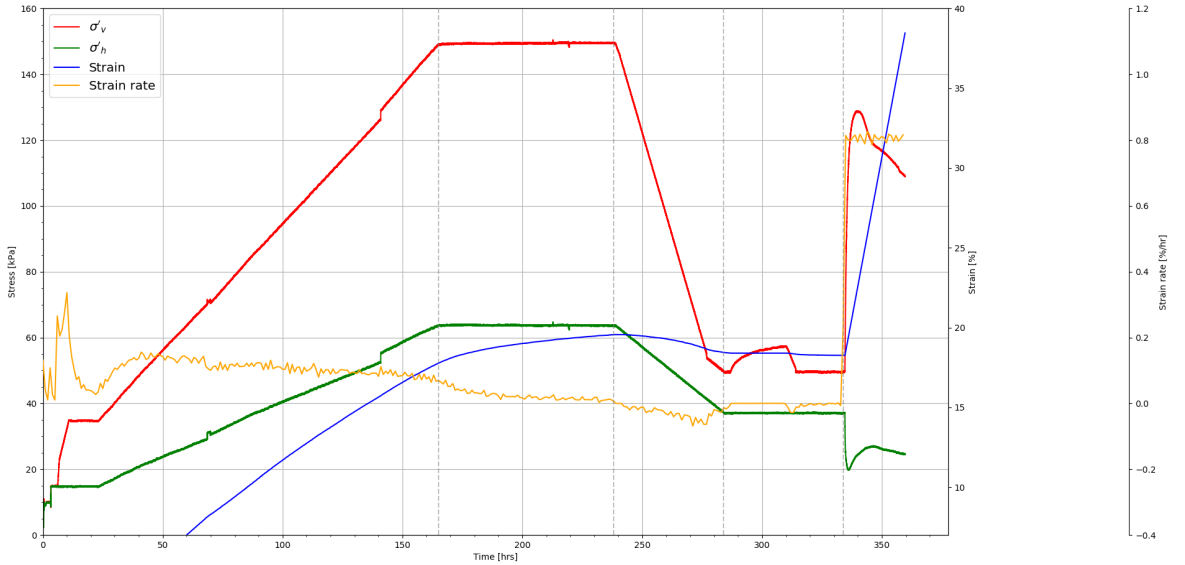
σ'_v
σ'_h
Strain
Strain rate
Stress [kPa]
Strain [%]
Strain rate [%/hr]
Time [hrs]

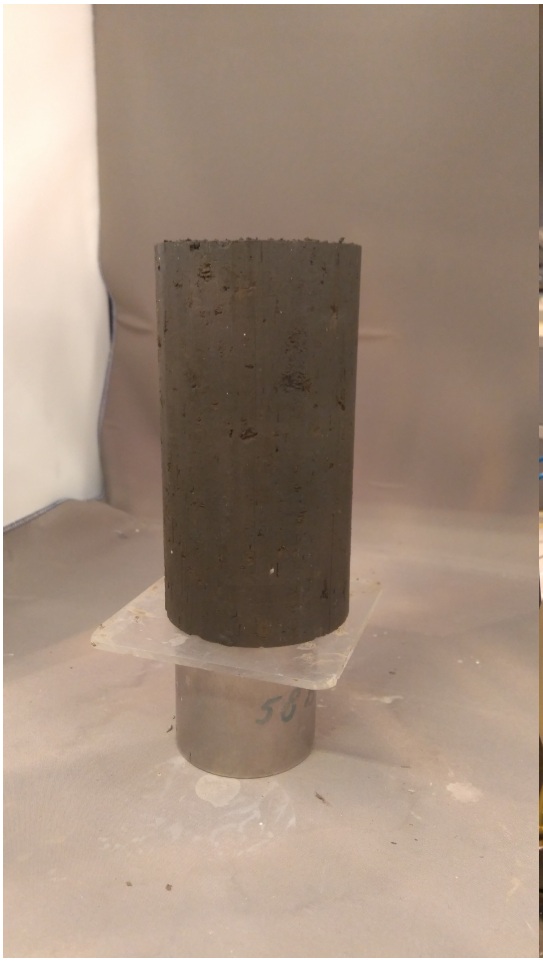

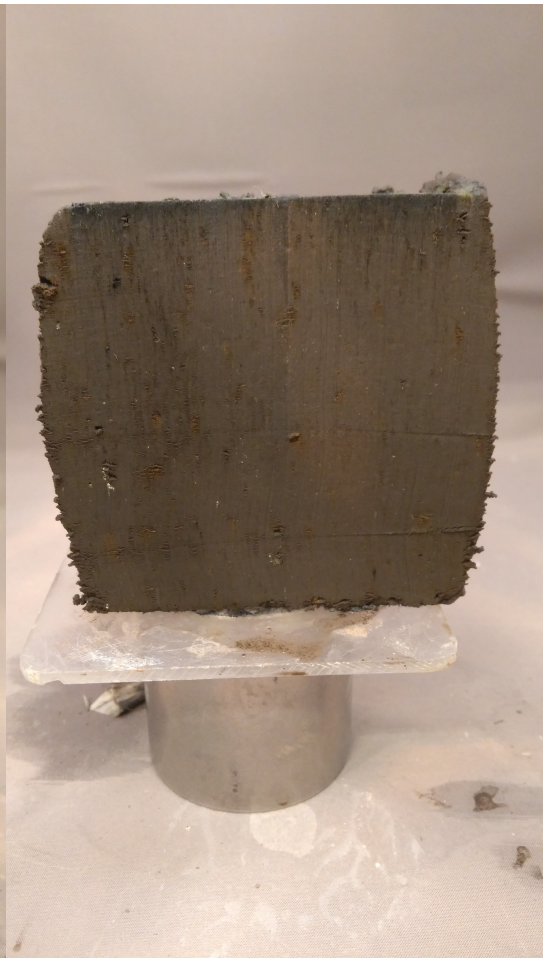

Sample name	**TRX6**
Type	Compression
Soil type	OVP clay
Soil classification	Silty clay
Before test	
Mass [g]	632.3
Height [mm]	130.3
Diameter [mm]	66.9
Void ratio [-]	2.59
Water content [%]	111.7
Particle density [kg/m^3]	2310
Bulk density [kg/m^3]	1381
B-factor	0.98
Backpressure [kPa]	300
Consolidation stage	
Vertical consolidation pressure [kPa]	12.5
Horizontal consolidation pressure [kPa]	26.5
Vertical pre-consolidation pressure [kPa]	150
Horizontal pre-consolidation pressure [kPa]	64.5
Creep rate [%/hr]	-0.02
Shearing stage	
Shearing rate [%/hr]	1
Peak strength	
Vertical effective stress [kPa]	81.3
Horizontal effective stress [kPa]	2.91
Undrained shear strength [kPa]	39.2
M_c[-]	2.70
Ultimate State	
Vertical effective stress [kPa]	83.0
Horizontal effective stress [kPa]	18.0
Undrained shear strength [kPa]	32.5
M_c [-]	1.64
Max p'/q ratio	
Vertical effective stress [kPa]	68.9
Horizontal effective stress [kPa]	0.8
Undrained shear strength [kPa]	34.1
M_c [-]	2.9
After test	
Mass [g]	572.81
Void ratio [-]	2.02
Water content [%]	87.1

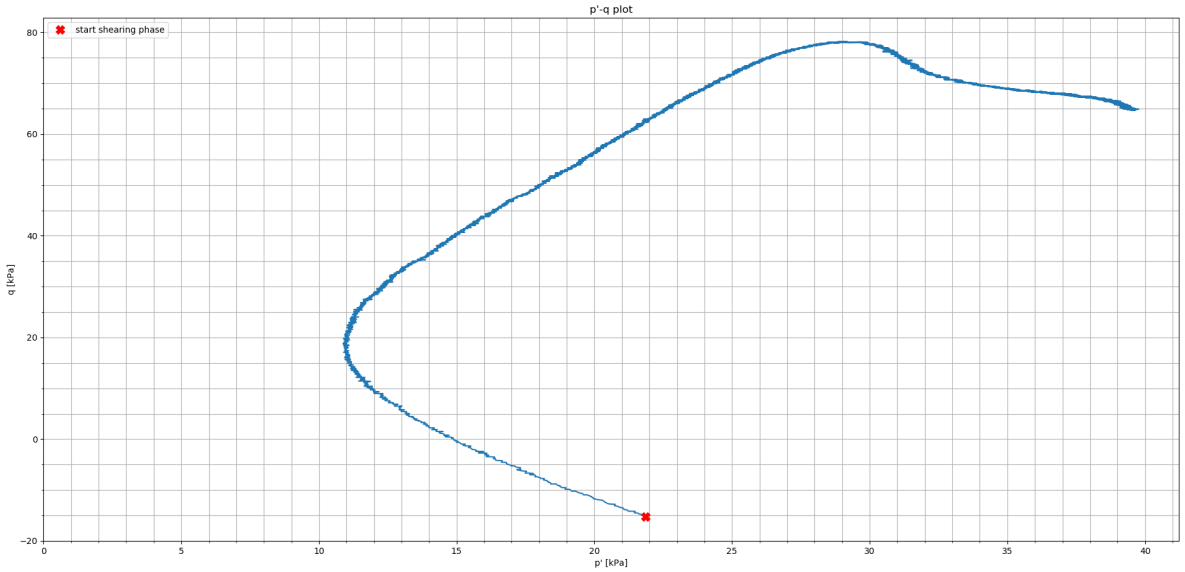
p'-q plot
start shearing phase
q [kPa]
p' [kPa]

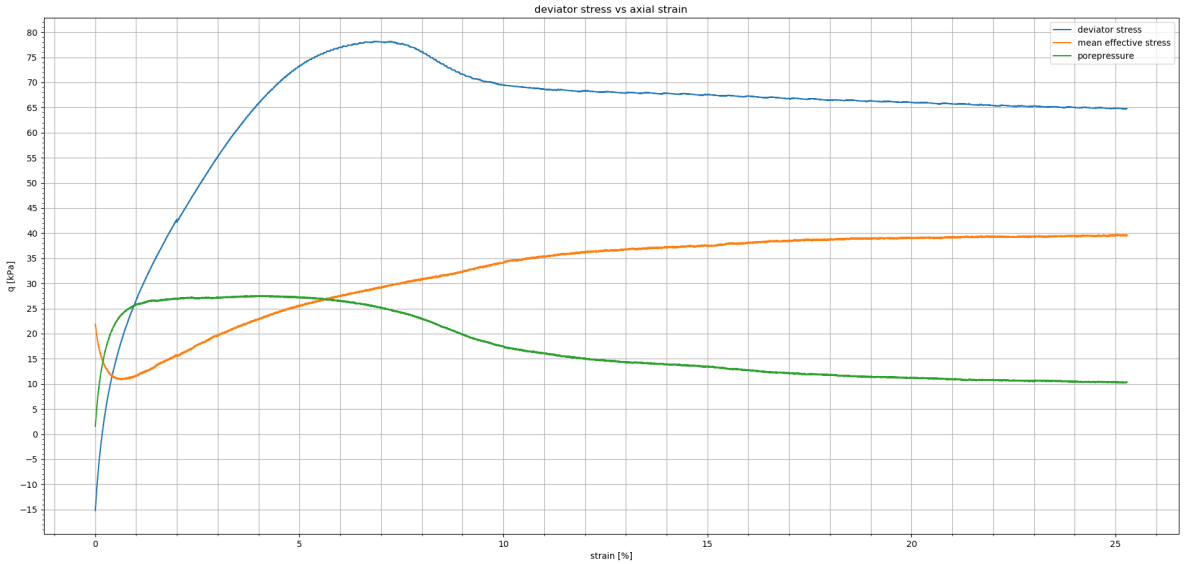
deviator stress vs axial strain
deviator stress
mean effective stress
porepressure
q [kPa]
strain [%]

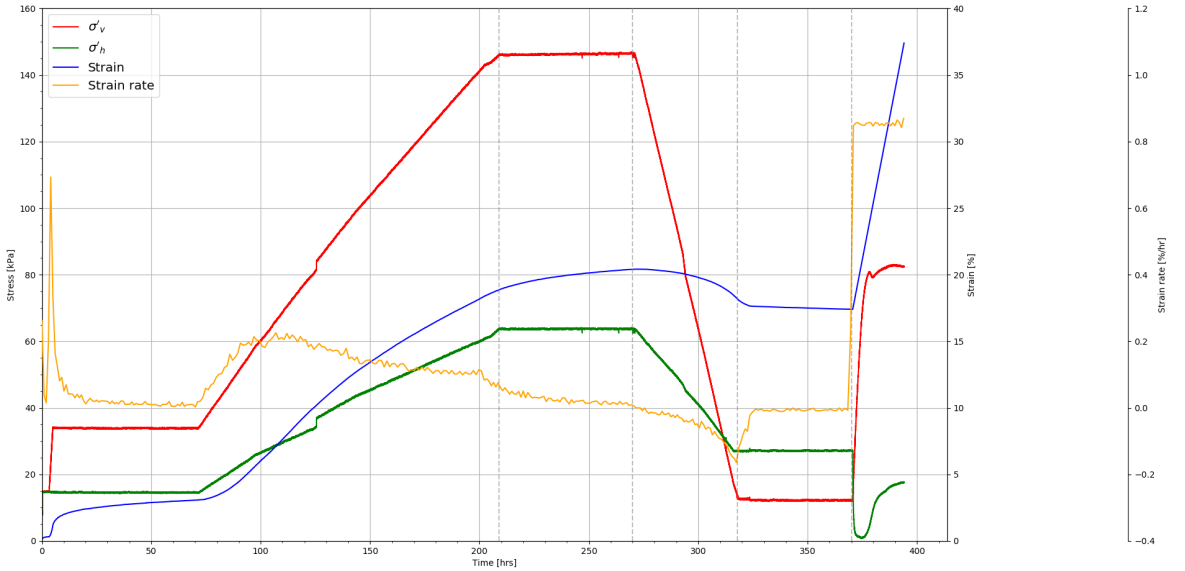
σ'v
σ'h
Strain
Strain rate
Stress [kPa]
Strain [%]
Strain rate [%/hr]
Time [hrs]

Sample name	**TRX7**
Type	Extension
Soil type	OVP clay
Soil classification	Silty clay
Before test	
Mass [g]	639.26
Height [mm]	129.4
Diameter [mm]	67.3
Void ratio [-]	2.35
Water content [%]	101.5
Particle density [kg/m^3]	2310
Bulk density [kg/m^3]	1389
B-factor	0.95
Backpressure [kPa]	300
Consolidation stage	
Vertical consolidation pressure [kPa]	50
Horizontal consolidation pressure [kPa]	36.5
Vertical pre-consolidation pressure [kPa]	150
Horizontal pre-consolidation pressure [kPa]	64.5
Creep rate [%/hr]	-0.01
Shearing stage	
Shearing rate [%/hr]	1
Peak strength	
Vertical effective stress [kPa]	117.6
Horizontal effective stress [kPa]	31.1
Undrained shear strength [kPa]	43.2
M_c[-]	-1.44
Max p'/q ratio	
Vertical effective stress [kPa]	117.1
Horizontal effective stress [kPa]	30.8
Undrained shear strength [kPa]	43.1
M_c [-]	-1.45
After test	
Mass [g]	551.4
Void ratio [-]	2.04
Water content [%]	87.5

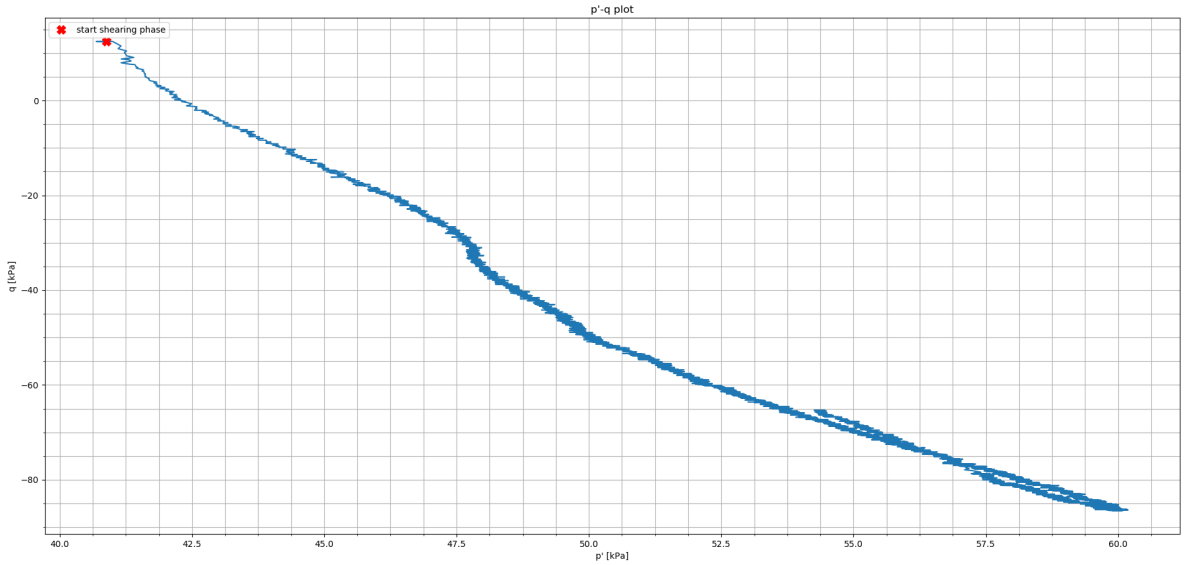
p'-q plot
start shearing phase
q [kPa]
p' [kPa]

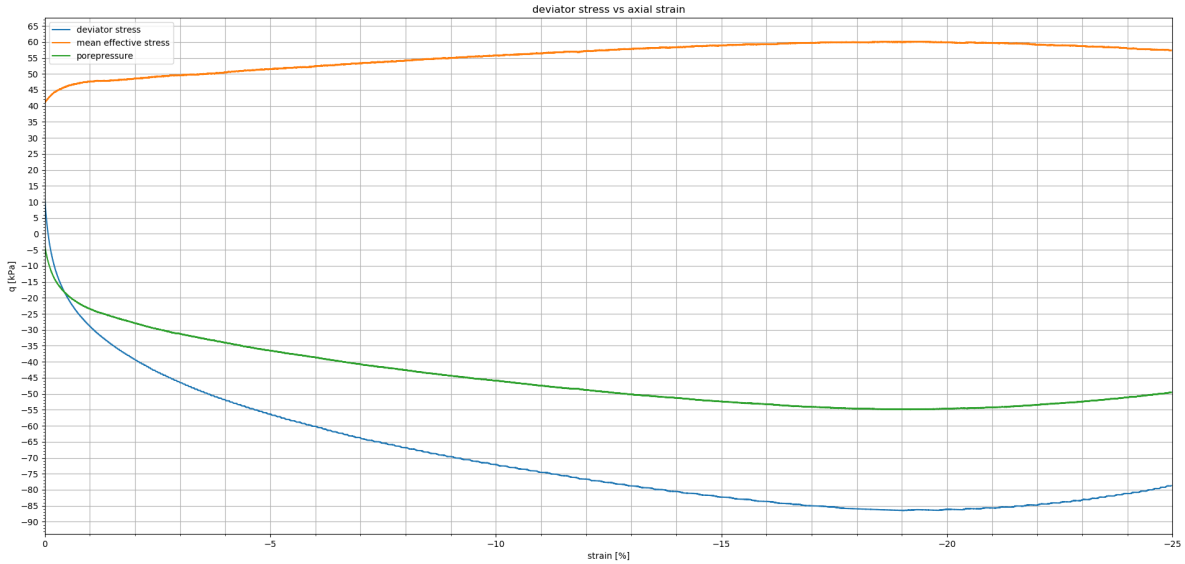
deviator stress vs axial strain
deviator stress
mean effective stress
porepressure
q [kPa]
strain [%]

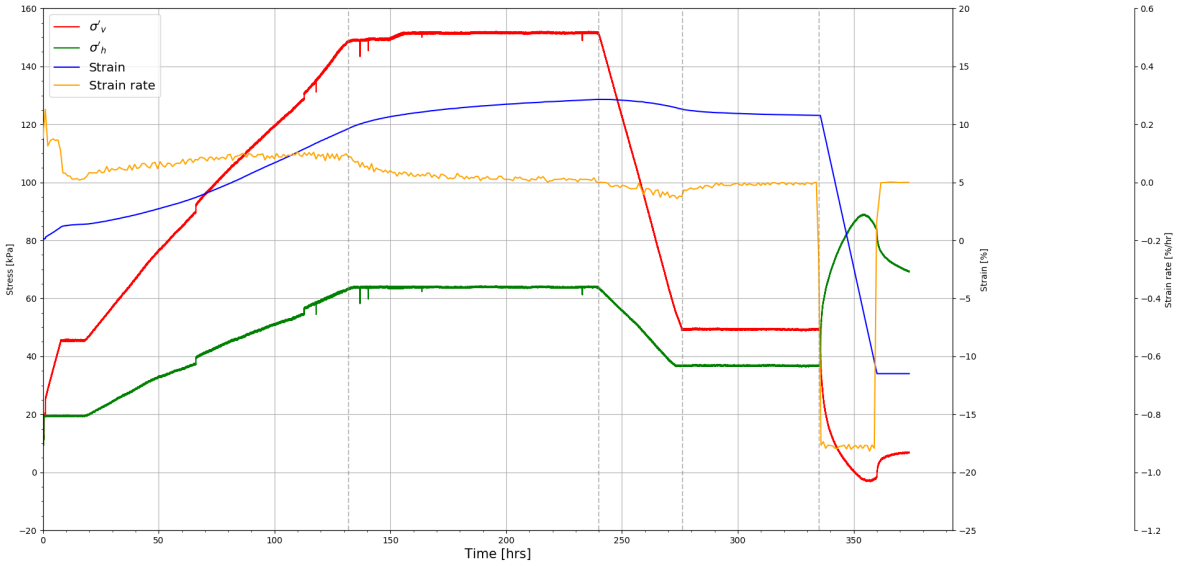
σ'_v
σ'_h
Strain
Strain rate
Stress [kPa]
Strain [%]
Strain rate [%/hr]
Time [hrs]

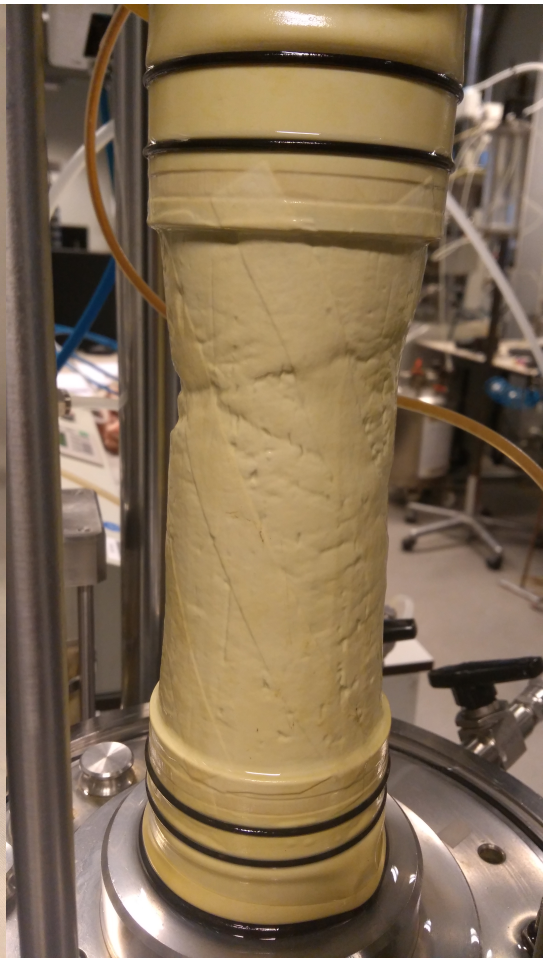

Sample name	**TRX8**
Type	Extension
Soil type	OVP clay
Soil classification	Silty clay
Before test	
Mass [g]	639.26
Height [mm]	129.4
Diameter [mm]	67.3
Void ratio [-]	2.35
Water content [%]	101.5
Particle density [kg/m^3]	2310
Bulk density [kg/m^3]	1389
B-factor	0.97
Backpressure [kPa]	400
Consolidation stage	
Vertical consolidation pressure [kPa]	12.5
Horizontal consolidation pressure [kPa]	27.5
Vertical pre-consolidation pressure [kPa]	150
Horizontal pre-consolidation pressure [kPa]	64.5
Creep rate [%/hr]	-0.01
Shearing stage	
Shearing rate [%/hr]	1
Peak strength	
Vertical effective stress [kPa]	110.3
Horizontal effective stress [kPa]	33.3
Undrained shear strength [kPa]	38.5
M_c[-]	-1.31
Max p'/q ratio	
Vertical effective stress [kPa]	104.3
Horizontal effective stress [kPa]	30.4
Undrained shear strength [kPa]	37.0
M_c [-]	-1.34
After test	
Mass [g]	593.9
Void ratio [-]	1.94
Water content [%]	84.0

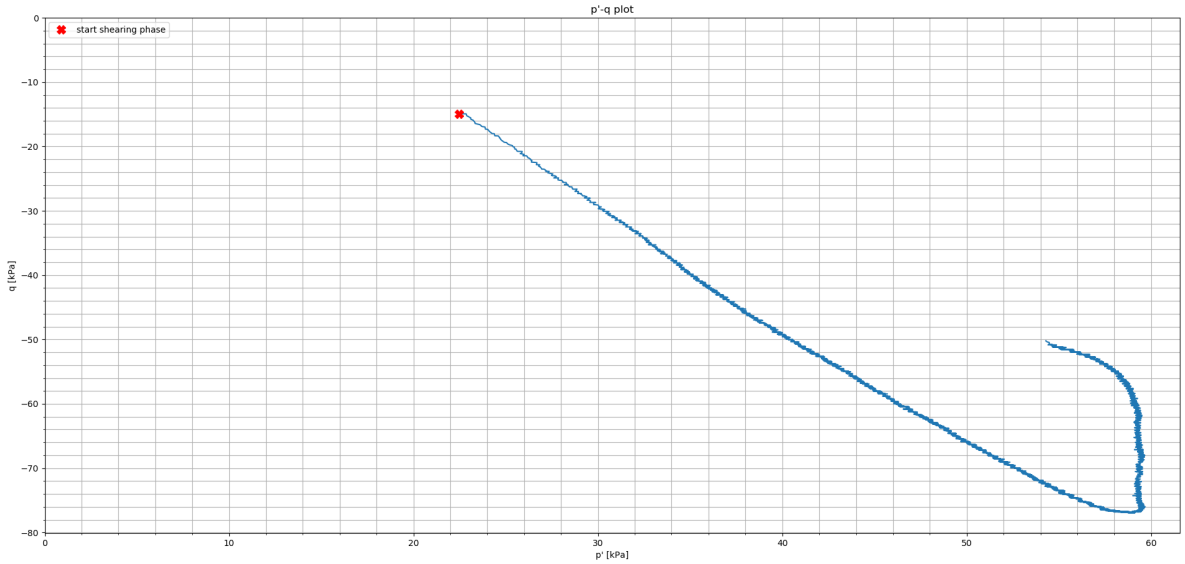
p'-q plot
start shearing phase
q [kPa]
p' [kPa]

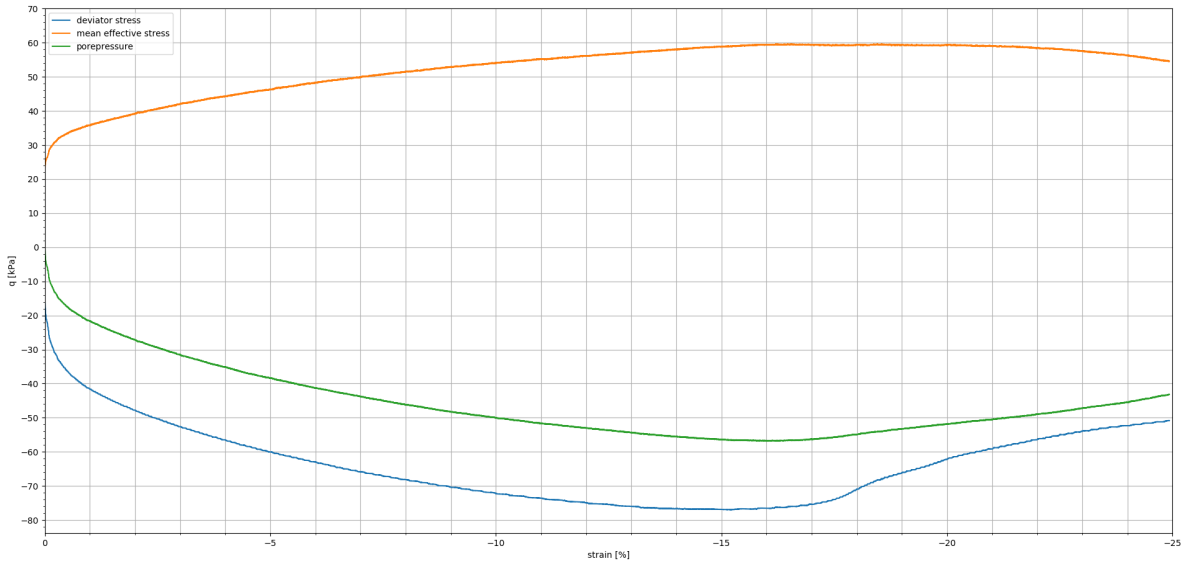
deviator stress
mean effective stress
porepressure
q [kPa]
strain [%]

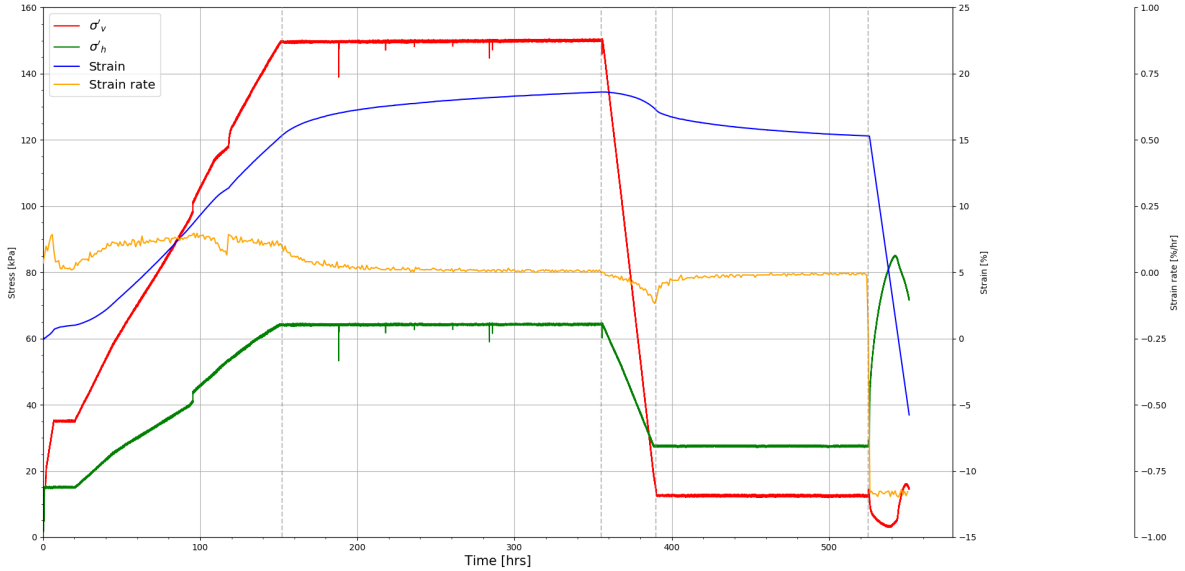
σ'_v
σ'_h
Strain
Strain rate
Stress [kPa]
Strain [%]
Strain rate [%/hr]
Time [hrs]

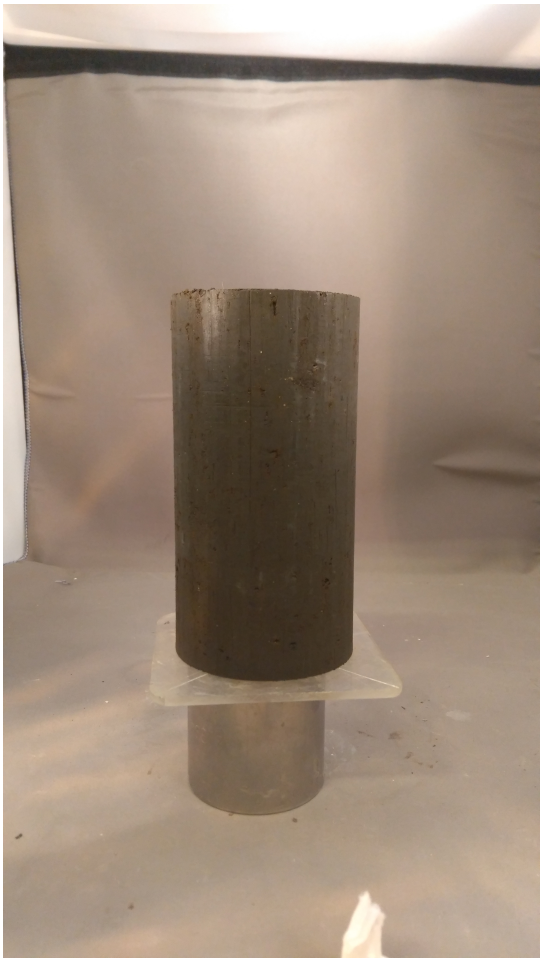

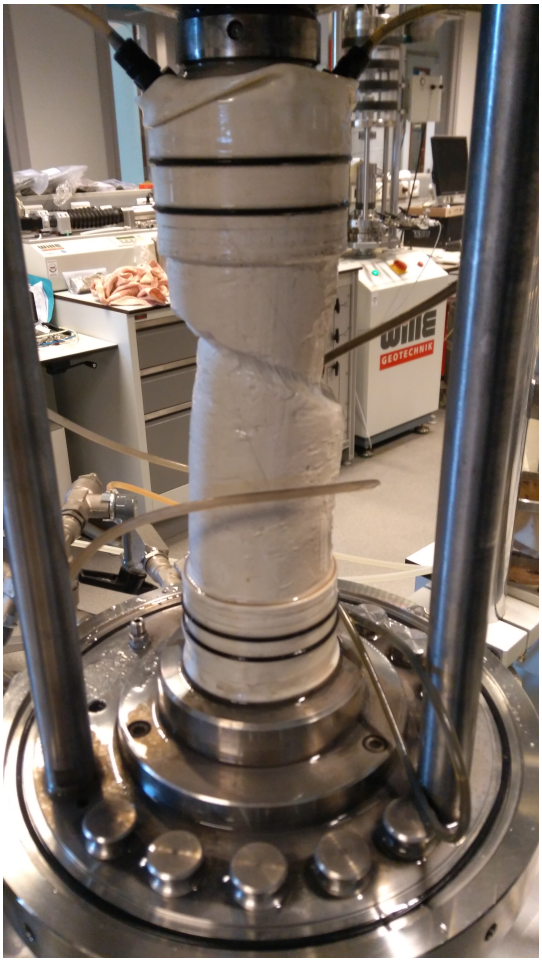
GEOTECHNIK

B

K_0-CRS tests

Sample name	**K_0-CRS 1**
Soil type	OVP clay
Soil classification	Silty clay
Before test	
Void ratio [-]	2.51
Water content [%]	108.5
Particle density [kg/m^3]	2310
Bulk density [kg/m^3]	1353
After test	
Void ratio [-]	1.99
Water content [%]	86.1

Test description					
Descriptions		rate		boundary condition	
0	start			0	kPa
1	loading phase	0.036	mm/hr	120	kPa
2	unloading phase	0.036	mm/hr	10	kPa
3	reloading phase	0.036	mm/hr	200	kPa
4	relaxation	48	hr	constant height	
5	unloading phase	0.036	mm/hr	10	kPa

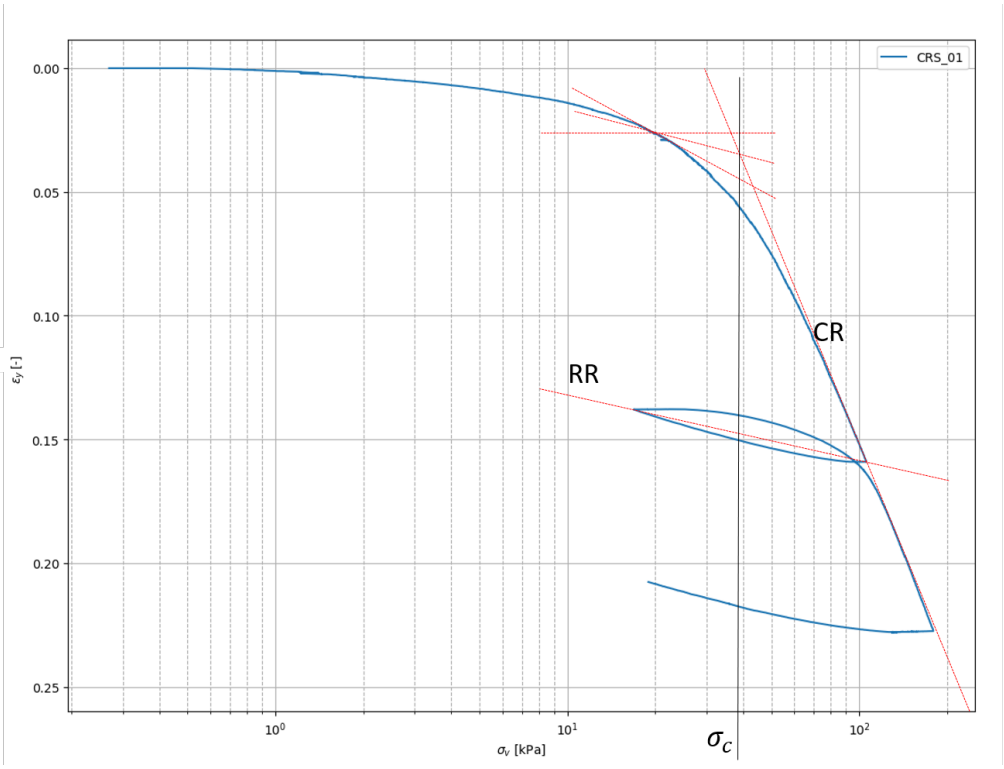

$CR = 0{,}29$
$RR = 0{,}038$
$\sigma_c = 39\ kPa$

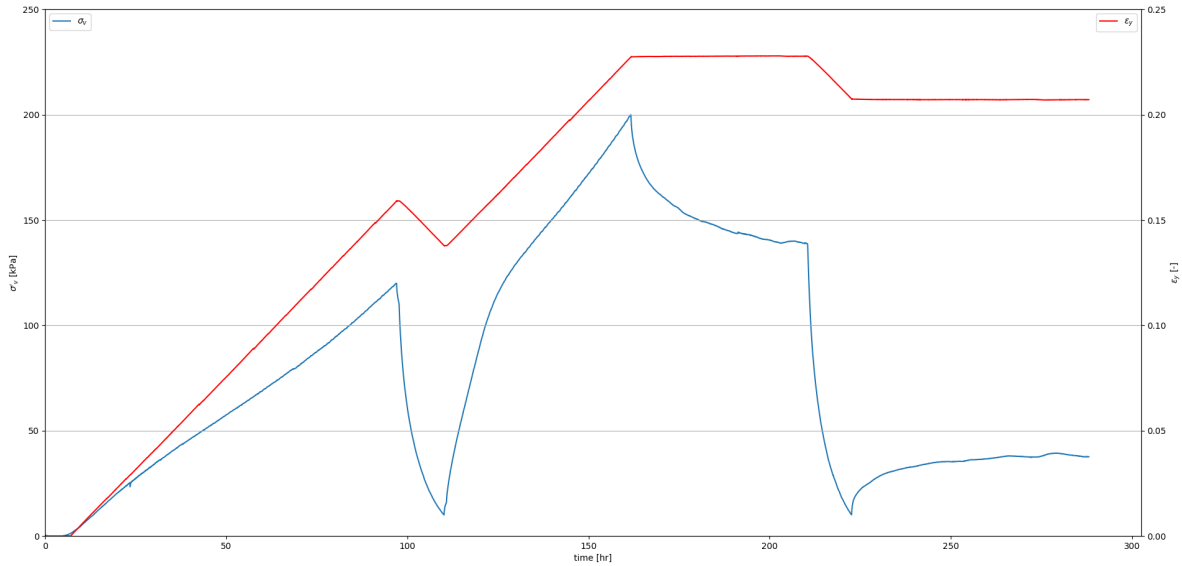

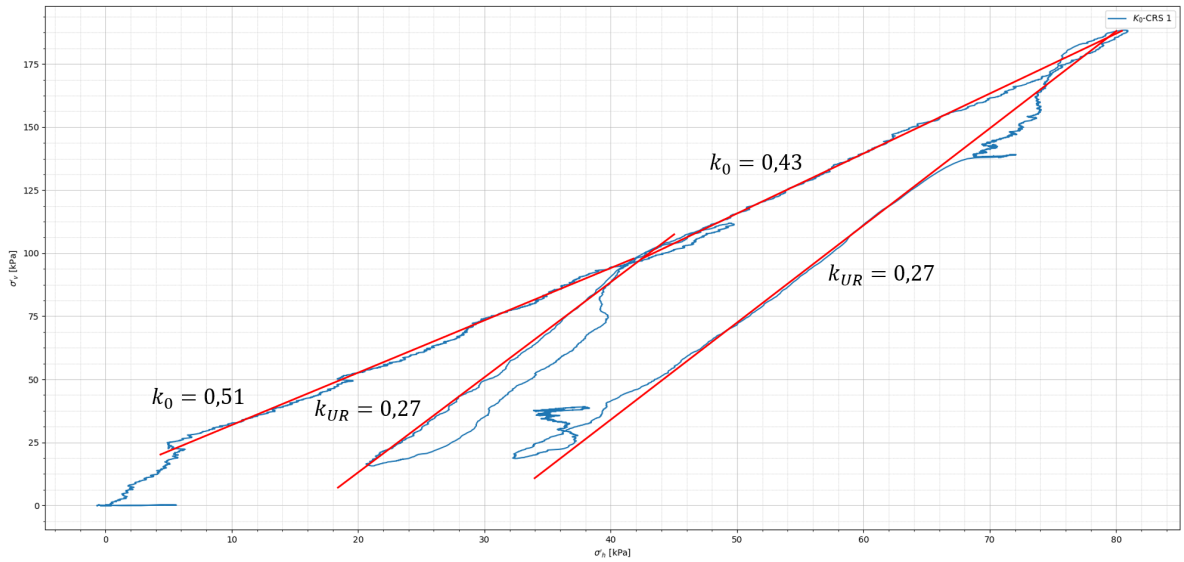

Sample name	**K_0-CRS 2**
Soil type	OVP clay
Soil classification	Silty clay
Before test	
Void ratio [-]	2.52
Water content [%]	108.7
Particle density [kg/m^3]	2310
Bulk density [kg/m^3]	1352
After test	
Void ratio [-]	1.95
Water content [%]	84.2

Test description					
Descriptions		rate		boundary condition	
0	start			0	kPa
1	loading phase	0.036	mm/hr	120	kPa
2	unloading phase	0.036	mm/hr	10	kPa
3	reloading phase	0.036	mm/hr	200	kPa
4	unloading phase	48	hr	200	kPa
5	unloading phase	0.036	mm/hr	10	kPa

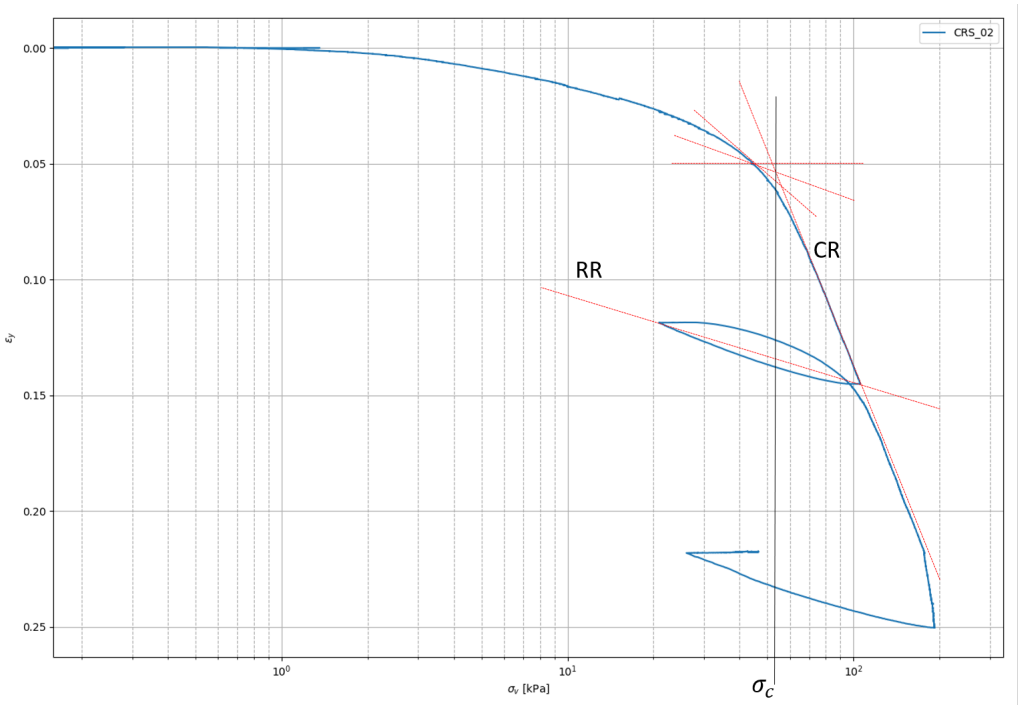

$CR = 0{,}30$
$RR = 0{,}043$
$\sigma_c = 53$ kPa

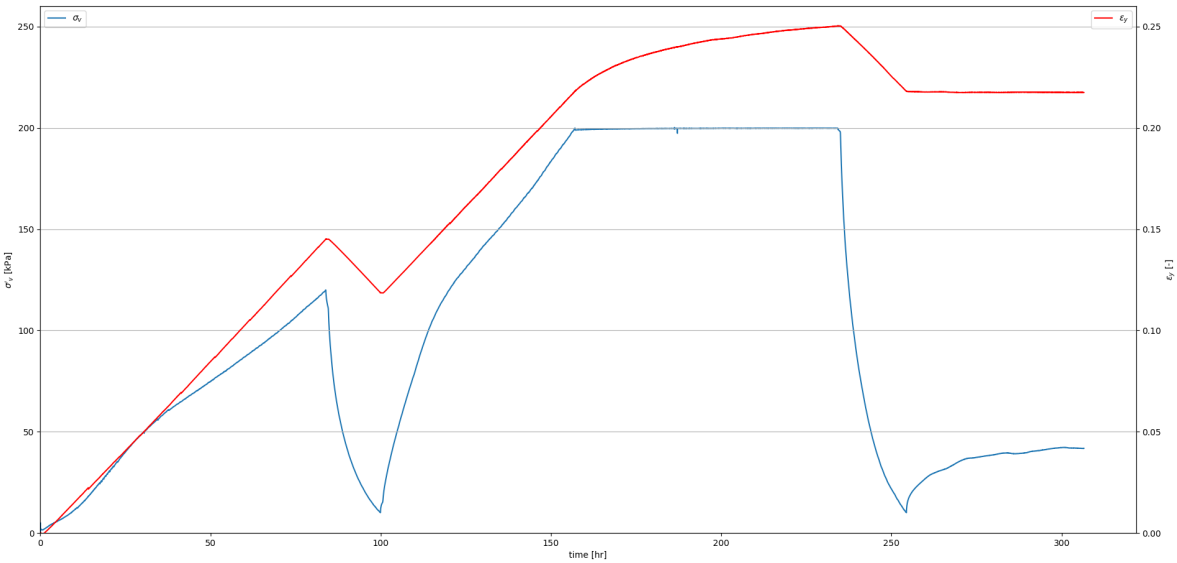

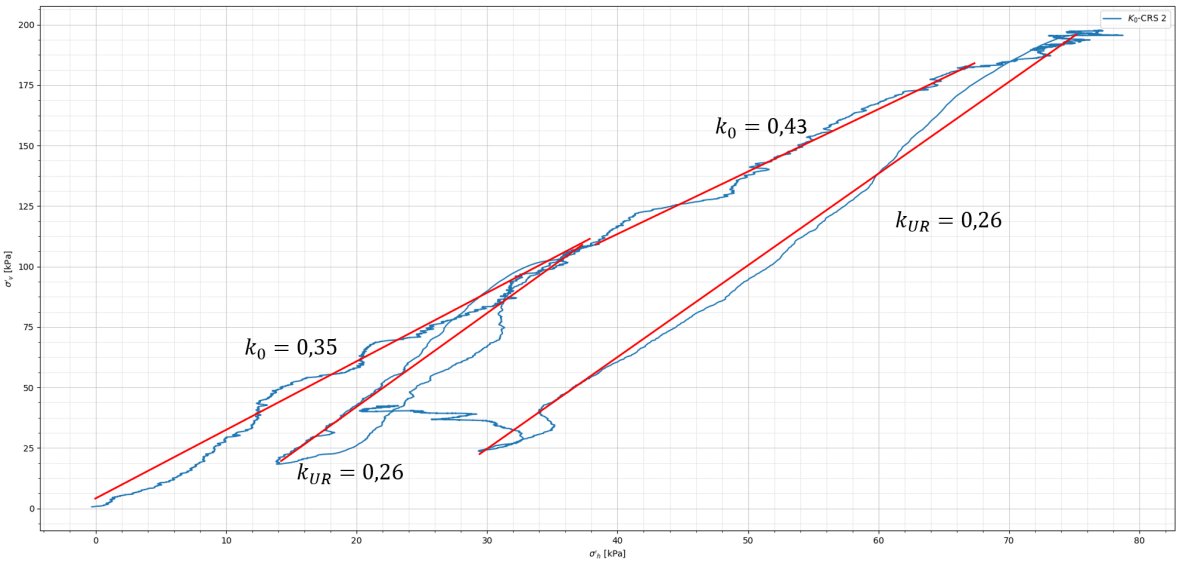

C

Isotropic compression test

Sample name	**Iso**
Soil type	OVP clay
Soil classification	Silty clay
Before test	
Void ratio [-]	2.56
Water content [%]	110.6
Particle density [kg/m^3]	2310
Bulk density [kg/m^3]	1377
After test	
Void ratio [-]	1.88
Water content [%]	81.0

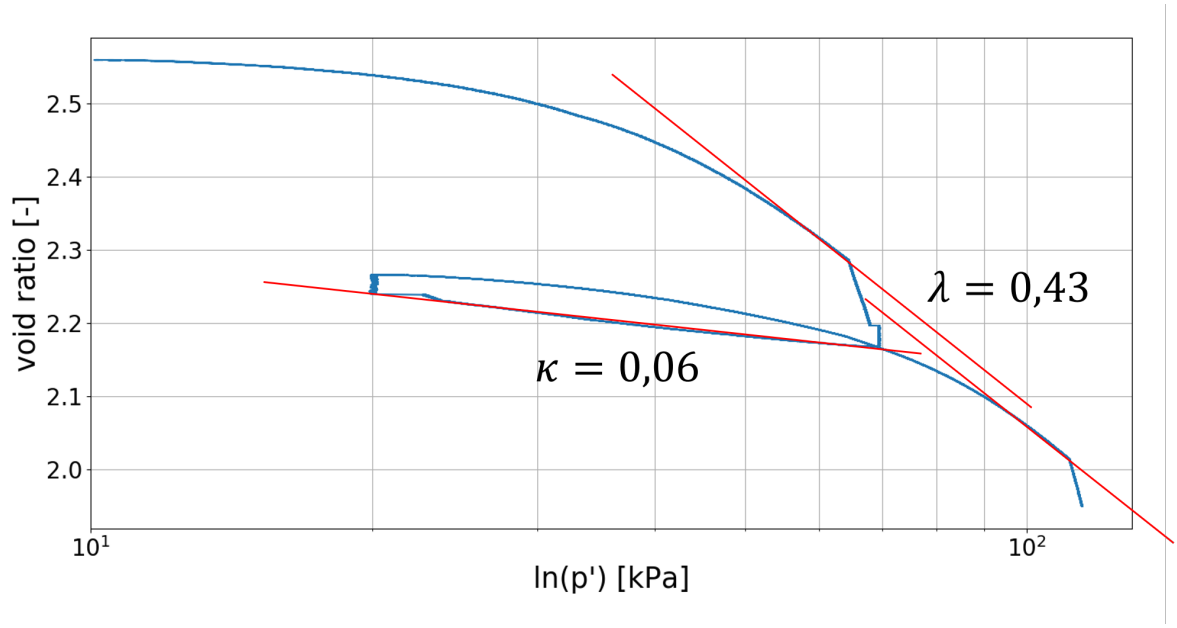
void ratio [-]
2.5
2.4
2.3
2.2
2.1
2.0
10^1
10^2
ln(p') [kPa]
$\lambda = 0{,}43$
$\kappa = 0{,}06$

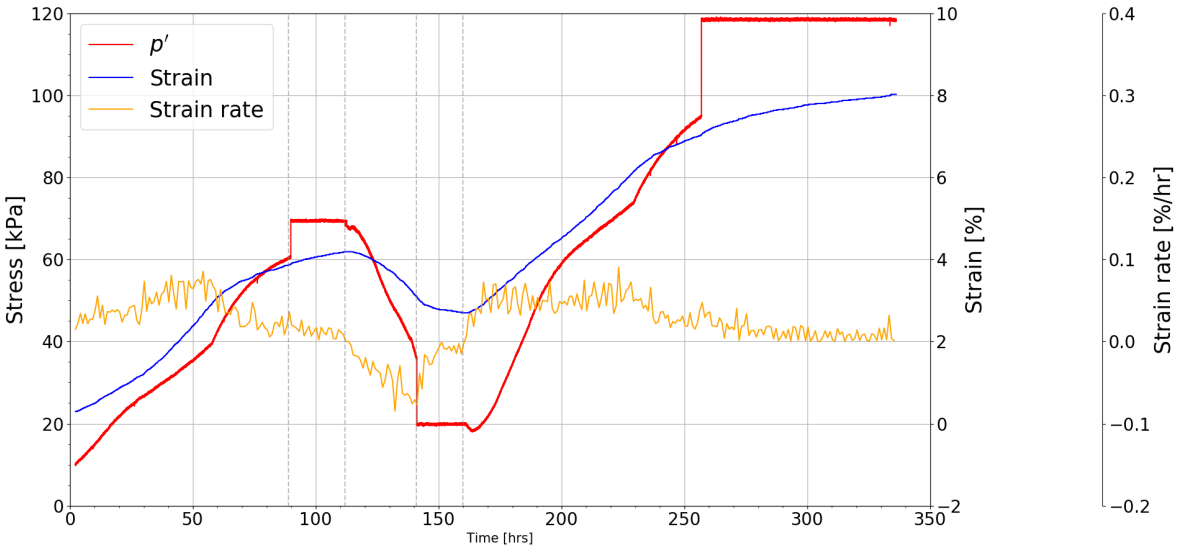
p'
Strain
Strain rate
Stress [kPa]
Strain [%]
Strain rate [%/hr]
Time [hrs]
0
20
40
60
80
100
120
−2
0
2
4
6
8
10
−0.2
−0.1
0.0
0.1
0.2
0.3
0.4
0
50
100
150
200
250
300
350

D

Derivation Equation 2.18

Adapted from [29]